OPTICAL LOCAL AREA NETWORKS NEW SOLUTIONS FOR FIBER-TO-THE-DESK APPLICATIONS

.

Twente University **Press**

Publisher:
Twente University Press,
P.O.Box 217, 7500AE Enschede, The Netherlands,
www.tup.utwente.nl

Print: Océ Facility Services, Enschede

ISBN 9036520029

OPTICAL LOCAL AREA NETWORKS:
NEW SOLUTIONS
FOR FIBER-TO-THE-DESK APPLICATIONS

PROEFSCHRIFT

ter verkrijging van
de graad van doctor aan de Universiteit Twente,
op gezag van de rector magnificus,
prof. dr. F.A. van Vught,
volgens besluit van het College voor Promoties,
in het openbaar te verdedigen
op donderdag 18 december 2003 om 13.15 uur

door

Igor Radovanović

geboren op 11 Augustus 1974

te Peć, Servië

Dit proefschrift is goedgekeurd door:
De promotor: Prof.dr.ir. Wim van Etten

Dit onderzoek is gesteund door de Technologiestichting STW als onderdeel van NWO en het technologieprograma van EZ.

Contents

Acknowledgments

Reminiscent of the winter of 1999 leads me to the beginning of my adventurous scientific journey into the World of Networks that seemed to be so exciting, challenging, full of variety and fun. It has been made possible by Prof.dr.ir. W. van Etten (Wim), my promoter and supervisor to whom I am very much indebted for his guidance through the unknown and help whenever I was in need. I thank him for numerous and lasting discussions, insightful comments and precious advices that helped me to scientifically evolve to what I am now. I would also like to thank his lovely wife Kitty for the most friendly support and understanding.

My appreciation goes to Wim Beuwer who helped me a lot, especially at the beginning when I was laying the foundation for the network to come.

A considerable part of my work has been done in the laboratory. It would certainly not be possible to obtain some practical results without unselfish support of Eduard. For the realization of the digital part of the network interface card I would like to express deep gratitude to a number of people. First of all I thank to Ronny, who stood along my side for almost two years struggling for the working system. Thanks to Jan-Rutger we had the first version of the PCB with FPGA. Finally, I acknowledge the generous support from my colleagues from the SAS group Henny, Geert-Jan and Johan.

For their strong contribution in filling up the chain of necessary equipment needed for testing our network I am indebted to colleagues from IOMS group,

Anton and Douwe. For supporting this cooperation I am very grateful to Chris. The last link in the equipment chain was built by the people from ICD group and I will never forget that.

It was so exciting and challenging working with number of students who enormously contributed to all the aspects of the network design, ranging from mathematical analyzes and calculations to complete PCB realization. I give them all gratitude for the joy they gave me, reminding me of the time when eagerness for knowledge drove me forward.

I have enjoyed a creative cooperation with Sami Musa, Els Kok and Albert Borreman who worked in the MOUSE project. I will always remember discussions we had and suggestions they gave me. I would like to express my gratitude to Prof. A. Driessen for his contribution in the research and valuable comments on the final draft of my thesis.

Everyday working atmosphere would not be so pleasureous without my colleagues from the TE group. Above all I would like to thank my dear officemates Arjan and Bo. I appreciate Arjan's willingness to help me with the Dutch language. I certainly benefit from our lively discussions about optical CDMA systems. Bo was there at the very beginning to give me support.

I am particularly indebted to my dear friend Diptish for his invaluable support in making tough decisions. Having worked with him was a privilege.

I am grateful to Geert, who I met the first from the TE group, for his collaboration on optical CDMA systems. I thank to Rajan for his help with LaTeX. I enjoyed our informal chatting. I appreciate advices I got from Frank Leferink about PCB fabrication and I will never forget his concern for continuing my future career. I thank Joe Tauritz for his willingness to read and correct my English.

I am grateful to the other members of my promotion committee B. Nauta, A. M. J. Koonen, A. C. Bochove, N. H. G. Baken, J. Vandewege and W. H. M. Zijm for taking time to read this dissertation and to evaluate my research.

For the relaxed atmosphere after long hours of heavy work I thank to all the 3HA3 (read NBA) superstars from the basketball courts: Boris, Dule, Zoki, Žika, Marko, Petko, Boki, Raša, Vojkan, Ljuba and all the members of the Arriba club.

I am strongly indebted to my dear friends Stanča and Vladana and their lovely daughter Anja. Together we have shared our experiences of the life abroad and endeavor to fill ourself at home. I acknowledge Vlada for his friendly support during the last four years. Without Boris, Jelena, Goran, Bilja, Saša,

Nataša, Rossano, Hélène, Dejana, Ruud, Katerina, Wilko, Kristin, Arie and many others, my life in Enschede would not be the same.

For their strong support from Serbia I am grateful to all my friends, especially Aca, who always found words that pushed me up when I was down. My appreciation goes to Duško for encouraging me to thrust further and Džoni for introducing me to The Netherlands.

There are no such words to express gratitude for my parents Tomo and Slavica who lived every single moment in anticipation for the news from me. I put their endless support and love sent from far away deep in my hart.

I enjoyed the privilege and honor of having my twin brother Saša doing his PhD work at the same faculty. From the bottom of my hart I express my eternal gratitude to him for all the advices and suggestions he gave me. I thank him for both technical and scientific cooperation we had about optical network design. I am grateful to my sister in low Vesna and their princess Sara for their constant support. For encouraging me when I was anxiously gearing up for the ever better performance, overwhelmed by ballast of problems and depressed by failures, I will be always grateful to them. Without family support and understanding I would never achieve my current position.

My final, and most heartfelt acknowledgment goes to my wife Jelena. Her support, encouragement, and companionship has turned my scientific journey into pleasure. For all she did for me she has my everlasting love.

Igor Radovanović
Enschede, The Netherlands
December 2003

Abstract

In this thesis we introduce optical local area networks for fiber-to-the-desk application. This in an attempt to bring the optical fiber ever closer to the individual user offering a huge information transmission bandwidth that will undoubtedly have a strong impact on future societies.

The research presented in this thesis is motivated from the viewpoints of both cost and innovation. The presented networks are based on multimode optical fiber and components, short wavelength lasers and detectors and the widely used Fast Ethernet protocol. These architectures are designed to lower the costs associated with passive optical LAN implementation. Further reduction in overall cost is achieved through decreased network downtime, lower maintenance cost, extended geometrical spans and larger headroom for future capacity increase. These networks represent a novel approach in bringing optical fiber all the way to the desk since this is for the first time that Fast Ethernet protocol is accommodated on the passive star-shaped optical network.

Two stumbling blocks, namely synchronization of bursty traffic and collision detection had to be resolved such that the presented architectures can accommodate the Fast Ethernet protocol. Synchronization of bursty traffic is solved by introducing a sinusoidal synchronization carrier that is sent through the fiber together with the data packet and switched on and off with it. The solution for collision detection is found in using the Directional Coupling method in combination with Average Power Sensing due to the simplicity of their imple-

mentation.

To facilitate realization of the network interface card a new physical layer device has been realized that can be attached to the already existing network interface card equipped with the medium independent interface. To design a physical layer device a transmitter and receiver are designed, which in turn consist of digital and analog circuitry. Measurements performed after realization of both the transmitter and receiver proved the correct functionality of the design.

Comparing our proposals with the other Fast Ethernet network proposals many advantages can be marked off. The variety of optical fiber advantages compared to the twisted pair wires that distinguish all the fiber-based network standards from the massively deployed twisted-pair ones holds for our proposals. What makes them prominent with respect to existing fiber standards is the lower overall cost, increased span, slightly improved performance and possibility for easy upgrade.

At the end of the thesis a spectrally encoded optical code division multiple access system based on cascades of Mach-Zehnder Interferometers that can be used in future local area and access networks is given. This system is also based on broadband optical sources, optical (de)coders and makes use of modulation in the electrical domain. Moreover, a generalized coherence multiplexing system is presented with a possibility to change the address of users by changing the phase shifts in particular stages of the cascaded system. It gives a strong contribution for practical implementation of the coherence multiplexing system.

Samenvatting

In dit proefschrift worden optische lokale computernetwerken voor fiber-to-the-desk toepassingen gentroduceerd. Dit in een poging om de optische vezel steeds dichter bij de eindgebruiker te brengen. Dit biedt een enorme transmissiebandbreedte voor informatieoverdracht, hetgeen ongetwijfeld een sterke invloed op de toekomstige maatschappij zal hebben.

Het onderzoek dat in dit proefschrift wordt gepresenteerd, kan zowel vanuit het oogpunt van kosten alsmede innovatie worden gemotiveerd. De voorgestelde netwerken zijn gebaseerd op multimode optische vezels en componenten, kortegolflengtelasers en -detectoren, en het alom gebruikte Fast Ethernet protocol. Deze architecturen zijn ontworpen ter verlaging van de kosten die gepaard gaan met de implementatie van een passief optisch LAN. Een verdere reducering van de kosten wordt bewerkstelligd door een afname van de "downtime" van het netwerk, lagere onderhoudskosten, vergroting van de spanwijdte en meer ruimte voor toekomstige uitbreiding van de capaciteit. Deze netwerken vertegenwoordigen een nieuwe aanpak om de optische vezel helemaal naar het bureau te brengen, want het Fast Ethernet protocol is hier voor het eerst toegepast in een passief stervormig netwerk.

Twee struikelblokken, namelijk de synchronisatie van bursty verkeer en de detectie van botsingen, moesten dusdanig worden opgelost dat het Fast Ethernet protocol in de voorgestelde architecturen kan worden toegepast. De synchronisatie van bursty verkeer is opgelost door een sinusvormige synchronisatiegolf

in te voeren, die samen met het datapakket door de vezel wordt gestuurd en samen met deze wordt aan- en uitgeschakeld. De oplossing voor de detectie van botsingen is gevonden in het gebruik van een richtingskoppelaar in combanitie met vermogensmonitoring, vanwege de eenvoud van hun implementatie.

Om de realisatie van een netwerkkaart te vergemakkelijken, is een nieuw circuit voor de fysische laag gerealiseerd dat aan een bestaande netwerkkaart met medium-onafhankelijke interface kan worden gekoppeld. Om een circuit voor de fysische laag te ontwerpen, zijn een zender en ontvanger ontworpen, die op hun beurt bestaan uit digitale en analoge schakelingen. Na realisatie is de correcte werking van het ontwerp door middel van metingen bewezen.

In vergelijking met andere voorstellen voor Fast Ethernet netwerken hebben de onze een groot aantal voordelen. De diverse voordelen van optische vezel ten opzichte van getwiste aderparen, die alle vezel-gebaseerde netwerkstandaarden onderscheiden van de reeds massaal genstalleerde netwerken gebaseerd op getwiste aderparen, spreken in ons voordeel. De belangrijkste voordelen van onze voorstellen ten opzichte van de reeds bestaande vezelstandaarden zijn de lagere totale kosten, de grotere spanwijdte, de enigszins hogere prestatie en de mogelijkheid tot eenvoudige uitbreiding.

Aan het eind van het proefschrift wordt een spectraal gecodeerd optisch code division multiple access systeem beschreven, dat gebaseerd is op het cascaderen van Mach-Zehnder Interferometers en kan worden gebruikt in toekomstige lokale computer- en aansluitnetwerken. Dit systeem is gebaseerd op breedbandige bronnen, optische (de)coders en modulatie in het elektrische domein. Bovendien wordt een gegeneraliseerd coherence multiplexing systeem gepresenteerd, dat de mogelijkheid biedt het adres van de gebruikers te veranderen door de fasedraaiingen in bepaalde secties van het gecascadeerde systeem aan te passen. Dit levert een belangrijke bijdrage aan de praktische implementatie van coherence multiplexing.

CHAPTER 1

Introduction

1.1 Motivation

The extensive growth of Internet traffic at the end of the last century contributed to the telecom industry boom, leading to massive deployment of optical fiber primarily in core and metropolitan networks. These networks are now connecting cities, states and continents. Unfortunately, huge amount of installed fiber created overcapacity in long-haul networks since applications that can fulfill terabits of capacity offered by fibers were missing.

This is the reason that focus of interest in the "telecom world" shifted towards optical access and Local Area Networks (LANs) that will run all the way to individual PCs, since bringing large capacity to the user can in turn create a necessity for the larger capacity in the long-haul networks. Moreover, user premises and computer rooms are the only places where optical fiber is still missing, making both in-building and in-home environments potentially huge market with great opportunity for investments.

Increased interest in using optical fiber all the way to individual PCs is manifest in larger companies where storage area networking, data back-up demands and sharing access to large databases are of great importance [1]. These firms

are willing to invest in optical fiber when upgrading their networks since fiber offers larger headroom for future bandwidth increase. Nevertheless, for as long as the overall cost of fiber networks remains high they will continue to use the copper medium. Furthermore, to exploit fiber running to the desktop in smaller offices and homes the overall cost of the computer network must be even lower. Especially the cost associated with the optical components and electro-optical and opto-electrical conversion.

High implementation cost is therefore the reason why copper interconnects continue to be more dominant. Nevertheless, network designers cannot rely on copper when computer networks have to operate in environments that are "polluted" by interfering electromagnetic radiation e.g. power plants, airport buildings, military facilities, etc. In these environments UTP transmission can be subject to long data packet delay and inherently low throughput. Optical fibers, on the other side, offer an excellent non-emissive transmission medium and at the same time are completely insensitive to incoming radiation.

Finding new solutions for the fiber-optic computer network that will be used in fiber-to-the-desk applications, which will bring the overall implementation cost down while offering better performance than copper-based network was a challenge that we have engaged. Our research is motivated from the viewpoints of both cost and innovation.

1.2 Research objectives

The first objective of the work presented in this thesis was to find a solution for affordable application of optical transmission in the local area network. Another objective was to bring the medium speed local area networks beyond the level of point-to-point connections and the last one was to give guidelines for easy upgrading possibility, such that the proposed solution can be used in the forseenable future.

1.3 Requirements for the new network

The requirements were to design and implement an optical LAN by combining the opto-electronic and optical components, fibers and network architecture such that new LANs can be realized at minimum cost and still offer a better performance than copper-based networks: better reliability, lower maintenance

cost, extended geometrical spans and most important, larger headroom for future capacity increase.

To meet these requirements we have used short wavelength optical components in combination with silica multimode fibers, we kept our network passive and we stick to the widely used protocols.

Many advantages of optical fiber with respect to copper-based wires, made it a preferable choice when deciding about the future transport medium in local area networks [2]. However, two types of optical fiber, namely single-mode an multimode offer different advantages and disadvantages, thus our choice has been determined from the LAN requirements.

The optical transmission in long-distance communication is based on long wavelengths (1300-1600 nm) and single-mode fiber, due to the optimal transmission parameters of the fiber in that region [3]. Both attenuation and dispersion are low such that signals can reach larger distances without the need for repeaters. However, the components for these wavelengths are very expensive for LAN application, mainly because of the light sources and the hybrid technology in the receiver module. In the latter, Si-based electronics has to be combined with the GaAsP photodiode. Therefore, the cost aspect forms a decisive argument regarding all the advantages of fiber-optic communication.

To achieve affordable transmission in the LAN environments we have decided to use silica multimode fiber due to its advantages in short-distance communication. It is less vulnerable for misalignment and dust particles and has easy and cheap connection capability [4]. Combining the multimode fiber with the short wavelength components will make our system more economically attractive. LDs and VCSELs operating at 850 nm are less expensive than lasers operating at 1300 nm and 1550 nm. They also open the possibility of integrating a Si photodiode with the receiver front-end using straightforward CMOS technology [5, 6]. The LDs that we have used in the network realization show relaxation oscillation at a frequency well beyond the information bandwidth. In this way the speckle pattern, that originates from the interference and which causes modal noise, will become “invisible” to the receiver. The modal noise can also be reduced by using broad-linewidth VCSELs which was taken into account when choosing the proper light sources for network realization. Integrated multimode optical devices based on polymers are used that have potential for low-cost realization [7, 8]. Moreover fiber-to-the-chip coupling is facilitated using those devices since they contain larger waveguides commensurate with the multimode fiber cores.

A very important issue in network design is to keep the network all passive [9]. The advantages of passive optical networks are manyfold: cutting the cost by sharing fiber, no electronics in outside plant reduces need for costly powering, improved reliability since reduced number of active components means less causes of failure, possibility for point-to-multipoint connection. Passive networks support any modulation format, protocol, bit-rate or wavelength and are easier to upgrade.

To facilitate transition from existing copper-based networks to future optical LANs the Ethernet protocol is chosen. It is the most used protocol to date and is expected to remain so in the coming years [2],[10]-[12]. The key features of Ethernet are low cost and simplicity. Simplicity has enabled Ethernet to evolve while maintaining compatibility with previous versions. This, in turn, has kept the deploying cost of Ethernet attractively small. Some studies have shown that by the time the new version of Ethernet becomes mature, the upgrading cost from one version to another increases only 2 times while the bandwidth increases 10-fold. Ethernet became so popular that according to Nortel 95 % of all LAN end nodes nowadays are Ethernet [2]. As the speed of Ethernet has increased, first to 10 Mbps, then to 100 Mbps and more recently to 1 Gbps and 10 Gbps more users have been accommodated. These users became so dependent on networks that these become a more central part of their world. What makes Ethernet so powerful technology is that new Ethernet standards are made for high speed MANs and WANs [13] which made the Ethernet protocol shifting from the traditional implementation in LANs towards high speed networks. Ethernet is also a standard in a wireless LAN [14] and people are already thinking about the 100 Gbps Ethernet.

1.4 The research project

This thesis and the research work has been accomplished within the framework of the MOUSE (Multimode Optical Upgrade of Star-shaped Ethernet) project, sponsored by the Dutch Technology Foundation. It was supposed to combine research efforts from two groups at the University of Twente, namely Telecommunication Engineering (TE) and Integrated Optical MicroSystems (IOMS).

The MOUSE project had two main research areas. The work of TE group, presented here, aimed towards the design of different Ethernet based network architectures that will bring a solution for fiber-to-the-desk networks. Moreover,

we concentrated on final realization of the network.

The IOMS group worked on realization of optical planar components including technology. They proposed a concept for developing multimode power splitters and (de)multiplexers, a few of the main building blocks of networks presented in this thesis.

1.5 Outline of the thesis

This thesis contains 9 chapters. It begins with the introductory chapter where motivation for the research and general requirements for the new optical local area networks are given. This chapter also describes how these requirements can be met by keeping the network passive, using the short-wavelength optical components and widely used protocols. The main contribution of the thesis is also given.

The second chapter gives general description of local area networks, network topologies and their technological characteristics. The idea was to give the reader a quick introduction to fiber-to-the-desk networks, their availability and prospectives. The advantages of using optical fiber in local area environments compared to twisted-pair wire is given to point out the necessity of optical LAN implementation. The implementation limitations are also presented.

The fundamentals of the most widely used protocol nowadays, Ethernet, are given in Chapter 3. Moreover, a variety of Ethernet protocols is shown that includes both Fast Ethernet and Gigabit Ethernet upgrades. The focus is on the Fast Ethernet networks, both twisted-pair and optical fiber, since these were the starting points in our research. Both advantages and disadvantages of different networks are given, as well as the possibility for their upgrade, using higher-speed Ethernet protocols and optical fibers. The perspectives of optical Ethernet networks in general are also given in this chapter.

In Chapter 4 several network architectures for fiber-to-the-desk application are given. They are all based on the passive star coupler and Fast Ethernet protocol. For each architectures both advantages and disadvantages are given and discussed. To compare the presented networks with the existing fiber-to-the-desk solutions, performance analysis of the networks are given with respect to both dispersion and attenuation limitations, throughput, maintenance and upgrade cost. The main problems to be solved in designing such networks are also given.

Implementing new architectures required the design of the new Physical layer responsible for data communication between computers through the optical fiber medium. The detailed transmitter design procedure is given in Chapter 5. Both analog and digital circuitry designs are given as well as the implementation of the proposed synchronization technique. Simulation and experimental results are also presented conforming the feasibility of the design.

In Chapter 6 the complete receiver design is given. Moreover, a practical solution for the collision detection problem is presented. Simulation and experimental results are given to confirm the design.

Chapters 7 and 8 deal with the subjects different from the optical Ethernet LAN design. They consider using the optical code division multiple access (OCDMA) method in local area networks and dispersion limitation analysis in optical systems based on broadband optical sources and multimode fibers. In Chapter 7 the special focus is on spectrally encoded OCDMA technique based on cascades of Mach-Zehnder interferometers. The analysis of the system in the frequency domain is given which provides both the maximum number of orthogonal codes and limitation of the system with respect to optical beat noise. Finally, a possible scenario for implementing this multiple access technique in LANs and access networks is presented. Analysis of dispersion limitation is given in Chapter 8.

The general conclusion of the thesis and recommendations are given in Chapter 9.

1.6 Main contribution of this thesis

The work presented here gives the original contributions for the optical LAN implementation in interconnecting personal computers and servers. We propose a new Fast Ethernet standard based on IEEE 802.3 specifications that offers better performance than the existing Fast Ethernet standards, promises low cost implementation and facilitates network upgrade. For the first time we have shown how the Fast Ethernet protocol can be accommodated on the passive star network.

CHAPTER 2

Local Area Network fundamentals

The simple understanding of the term network is a group of devices connected together via transceivers and a transmission medium. In the networks analyzed in this thesis we concentrate on devices like personal computers (PCs) and internetworking devices that are connecting different networks. The local area term refers to its short coverage range within the restricted area.

In design and development of the new local area network (LAN) it is important to understand the fundamental characteristics of those networks, benefits of using them and the differences with respect to the other network types, namely metropolitan and wide area networks.

2.1 Introduction to Local Area Networks

Local area networks first emerged in companies and their utilization was mainly associated with the office premises, but recent trends are pushing them more towards home environments. The main benefit of having a LAN is that it provides a possibility for sharing resources, like printers, drives and databases, and exchanging the information processed by individual computers. Resource sharing is important for enabling cost cutting since for example, fewer printers

are required, as every PC does not require its own printer.

LANs can be distinguished from the other network types by geographical area of coverage, data transmission rates, ownership, government regulation, data routing and the type of information transmitted over the network.

A LAN is a communication network that covers a relatively small area. This area can range in scope from the group located in an office building to the department located on several floors in the building, or to several buildings on the university campus [15]. The size of the coverage area will depend on the physical transmission limitations regarding cable distance between the devices connected to the LAN.

As far as transmission rate is concerned, LANs normally operate at a megabit-per-second rate, while MANs and WANs operate at gigabit-per-second and terabit-per-second rates, respectively. Although the latest LAN implementations already accommodate gigabit-per-second rates, data rates in MANs are still much higher, going to 10 Gbps (40 Gbps in the lab) per channel.

In difference with the other types of networks LANs are usually privately owned by the organization that installed it [16]. Since they cover a relatively small area, no special governmental regulations are necessary. Instead, building regulations determine the type of the wiring that can be installed in a building and whether the wiring must be run in a conduit.

Another important feature of the LANs is that data is routed along a path that defines the network. That path is usually a bus, ring or a star [17, 18]. More complex topologies like the mesh, commonly used in WANs, are not used.

The type of the information transported on the LAN is usually data. Voice and video transport is still mainly restricted to WANs [19].

2.2 Technological characteristics of the local area networks

The diversity of local area networks comes from different technological characteristics that lead their implementation. These characteristics comprise different network topologies, signaling methods, transmission media and access methods [10].

2.2.1 LAN topologies

The topology of a LAN refers to the shape of a network, or the network's layout. How different nodes in a network are connected to each other and how they communicate are determined by the network's topology. Topologies are either physical or logical. The most common topologies used in LANs are bus, ring, star and tree. They are illustrated in Figure 2.1.

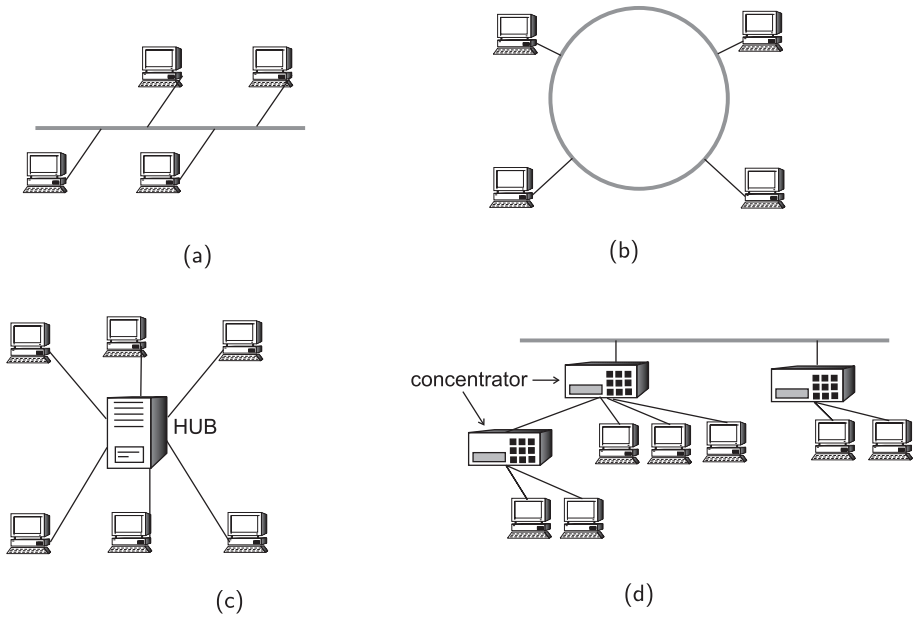

Figure 2.1: The four most common geometric layouts of local area network cabling from a bus (a), ring (b) , star (c) and a tree (d) structure.

Bus

In a bus topology, all the end stations are connected to a central cable (backbone), called the bus. When more end stations are connected to the central cable the increased network traffic can greatly reduce the performance and available bandwidth of the network. The main drawback of this topology when copper is used as the medium is that the entire network shuts down in case of backbone brake, due to reflections on the braking point. In case of the fiber backbone brake only the transmission on either side of the braking point can be supported.

Ring

In a ring topology the end stations are connected to one another in the shape of a closed loop, so that each device is connected directly to two other devices, one on either side of it. As in the bus topology a single brake can disable the whole network but protection methods like introducing an extra counter-rotating ring can be implemented. FDDI (Fiber Distributed Data Interface) is an example of a ring network.

Star

A star topology is one of the most used LAN topology within office premises. It became very popular because of the low cost and ease of troubleshooting. In this topology each end station is connected to a central node using a point-to-point connection. Access from any end station on the network to any other end station is accomplished through the central node. If the star central node is passive, the originating end station must be able to tolerate the reception of an echo of its own transmission. The networks presented in this thesis are also based on a passive star topology but suffer no echo problem due to a special construction of the star coupler and the access method used (CSMA/CD). The advantage of the star topology is that if one computer fails then only that computer is unable to send or receive data. The remainder of the network functions normally. The disadvantage of using this topology is that the entire network fails when the central node fails.

Tree

A tree network structure consists of a combination of bus and star topologies. In fact, groups of star-configured networks are connected to a linear bus backbone. Tree topologies allow for the expansion of an existing network. A disadvantage of this structure is the propagation delay since the two stations located at the opposite ends of the network require a signal to propagate twice the length of the longest network segment. A passive optical network (PON) is one of the examples of the tree topology networks.

2.2.2 Signaling methods

Signaling methods used in LANs describe the way the data is processed before transmission through the medium as well as the available bandwidth of the

medium [25, 31]. Data processing imply data encoding, pulse shaping and modulation such that the signal is adapted for transmission through the bandwidth limited medium.

Since the Ethernet protocol is an important issue discussed in this thesis, we will give distinction of LANs used in Ethernet terminology that is based on signaling methods. Using this terminology LANs are available as either broadband or baseband systems. A baseband network uses digital technology. No carrier signal is used to transmit data. The digital signals used for transmission of information occupy the entire frequency spectrum of the cable. An example of baseband signaling technique is Manchester encoding.

A broadband network is characterized by the use of analog technology. It uses a modem to introduce carrier signals onto the transmission media. The carrier signals are modulated by a digital signal. Broadband networks offer a possibility for multiple channel transmission of data, video and radio signals. An example of the broadband system is the 10BROAD-36 system that will be described in the next chapter.

The advantages of broadband networks are manyfold. They can support multiple simultaneous transmissions on separate channels and offer a possibility to use a tree topology that offers easy network expansion. The disadvantage is that broadband networks have shorter span compared to baseband networks due to the higher frequency range required for signal transmission. Most of the practically implemented networks are baseband.

2.2.3 Transmission media

The most commonly used media type in LAN environments are twisted-pair cables. Different categories of cables comprise of two, four and even six wires, depending on the bit-rates they have to support and the span they have to bridge. To adapt the signal for the transmission over different cable types inverse multiplexing is used, where high bit-rates are broken down to several low bit-rates. Two examples are 8B/6T and MLT-3 encoding. This is done due to the limited bandwidth of cables.

Coaxial cable is another medium, more related to early installed LANs. The latest trends go in favor of optical fibers that are gaining more and more popularity. As already mentioned, they support the highest bit-rates and the largest spans. Finally, wireless transmission, used in radio and infrared systems is expected to be another massively used medium, complementary to optical

fiber. Combination of fiber and ether media (hybrid networks) is most likely to penetrate the market in the near future.

2.2.4 Access methods

The access method can be defined as a set of rules that all the end stations connected to the same medium have to follow in order to communicate with each other. Without such rule it is quite possible for two messages sent by two different end stations to collide and neither will reach the destination. Two common access methods primarily employed in LANs are Carrier Sense Multiple Access with Collision Detection (CSMA/CD) and Token passing.

Carrier Sense Multiple Access with Collision Detection

The CSMA/CD can be categorized as a listen before send method. This is one of the earliest access techniques developed and is used in Ethernet networks [20]. The nice feature of this medium access protocol is that in average over certain time period, all the end stations have the same chance to access the medium.

When a station has data to send it first listens to determine if any other station on the network is transmitting data. The fact that the channel is idle (no transmissions) is determined in different ways depending on the signaling type and the medium. Only in the optical LANs there are many CSMA/CD techniques that can be implemented [21]. The condition when the channel is occupied is called carrier and denotes that traffic is on the line.

When the channel is busy, the station will wait until it becomes idle before transmitting data. This process is known as deferring to the passing traffic. As soon as the channel becomes idle, the station may commence transmission. When two stations discover an idle channel at the same time they both will transmit at the same time, provoking collision to appear. To avoid successive collisions to appear a special random delay scheme is embedded in the protocol.

Token passing

Token passing access mechanism is mostly used in the ring networks [25]. The token actually consists of a unique bit pattern. Every time an end station wishes to transmit a frame it waits for a free token. On receipt of the token its content changes to indicate that it is in use. Both information and the address of the intended recipient are added to produce a frame. This frame will travel all

around the network until it arrives at the sending end station again that will change the bit sequence into its original form releasing the token to be used by another station. During the time the token is in use the other end stations are not allowed to transmit to avoid packet collision in the network.

2.3 Passive optical LANs

The idea of passive optical local area networks came as a result of reducing the cost for optical fiber instalation all the way to the user, since optical networks that required active components were expensive.

Although the standard for such a network exists for many years already (10BASE-FP) [24], and some other proposals are given [26], passive optical LAN implementation never happened in practice. This is the reason we wanted to change the present situation and find a place on the market for passive optical LANs in the future.

The advantages of passive optical network (PON) are known from access environments. It offers point-to-multipoint optical connection with no active element in the signal path from the source to destination [27]-[29]. The only elements present between two network ends are passive splitters/combiners and couplers. These elements together with the optical fiber are shared among all the users attached to the network reducing the overall implementation cost. Moreover, the downstream laser transmitter is also shared.

Apart from decreased implementation cost there are other advantages of PONs, like improved reliability. Moreover, these networks are versatile, easy to upgrade and can change the business model [9]. Since no active components are installed in the communication link between the end users this means less causes of failure. Moreover, no extra costly power supply is necessary. Having E/O and O/E equipment installed only at the edges of the network allows high degree of freedom in selecting modulation format, protocol, bit-rate or wavelength. Lower cost per bit, lower operating cost and higher reliability give more options for business customers and create new markets. Decreased overall cost offers greater revenues for the operators and faster payback.

Network topologies subtable for passive optical LANs are bus, ring and star [30]. However, many LAN architectures are using combinations of those.

2.4 Comparing optical fiber to UTP wire

As the optical fiber medium is in the focus of interest in this thesis, it is significant to stress the advantages of its utilization in future LAN implementation compared to existing copper-based wires.

The twisted-pair wire is the most widely used medium in fiber-to-the-desk networks up to date but this is about to change in the future since optical fiber is gaining more and more popularity. There are many reasons for this and the most prominent is decrees in cost of optical components that appeared on the market.

Optical fiber brings many inherent benefits to LAN cabling. First of all, it has very high bandwidth and very low signal attenuation. These features enable fiber to support transmission over large distances, and offer fewer outages and less downtime. To cover the same distances using twisted-pair cables repeaters are needed that inevitably increase the costs.

The attenuation and dispersion limitations on signal propagation with respect to the signal bit-rate for both the fiber medium and Category 5 UTP cable are presented in Figure 2.2. Although there are different categories of UTP cables, ranging from Cat 3 to Cat 7 depending on the number of pairs of twisted-pair wires, thickness of wires and the distance between them, Category 5 was chosen since it is the most widely used cable in practice. Moreover, the price for higher categories is larger than the price of fiber, as the number of twisted-pair wires increases.

Because it is dielectric, optical fiber is immune to crosstalk and electromagnetic interference. This will contribute to increased reliability of the network in harsh environments like power plants and airport buildings. Moreover, lightening, one cause of failure in the transmission over copper-based medium, does not affect transmission in the optical fiber [9].

Optical fibers offer possibility for easier installation since there is no need for concern when installing cable near electrical machinery, heat sources and high voltage transmission systems.

Fiber provides flexibility to network designers when planning architectures because it supports high-speed data and different protocols. There is no need for expensive and time-consuming recabling. This is a nice feature of the optical fiber since data rates increased drastically over the past decade doubling the data speed every year. The trend of data increase is presented in Figure 2.3. Different letters from A to E denote different generations of fiber system.

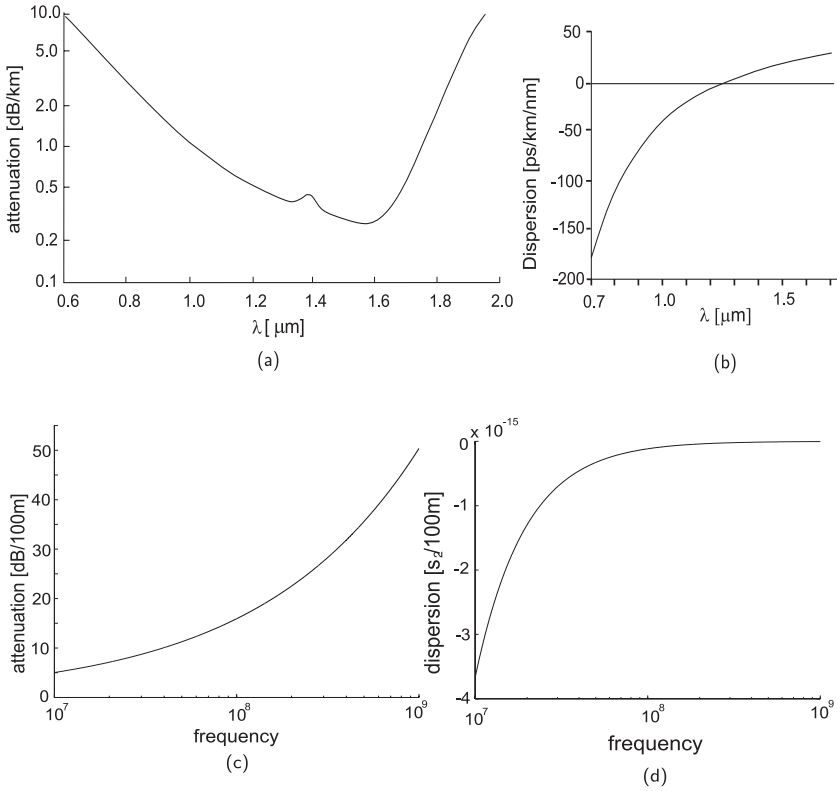

Figure 2.2: Attenuation and dispersion limitation on signal transmission in optical fiber (a), (b) and Category 5, UTP cable (c), (d).

Optical fiber is thin and lightweight. It requires only thin conduits for installation within the building. To increase the capacity by adding more fibers a little extra space in conduits is required. This in contrast to copper cables that are bulky and require much bigger cable ducts. Since fiber is much lighter than copper, there is no need for costly mechanical support systems that must be maintained.

Once installed, fiber is easy to test. There are many standardized testing procedures [23]. The most important parameters to test are attenuation and bandwidth. Attenuation measurement requires only a light source, power meter, test cord and an adapter. Fiber bandwidth is a parameter that is tested during the manufacturing process of the fiber and is therefore not required to test fiber bandwidth in the field.

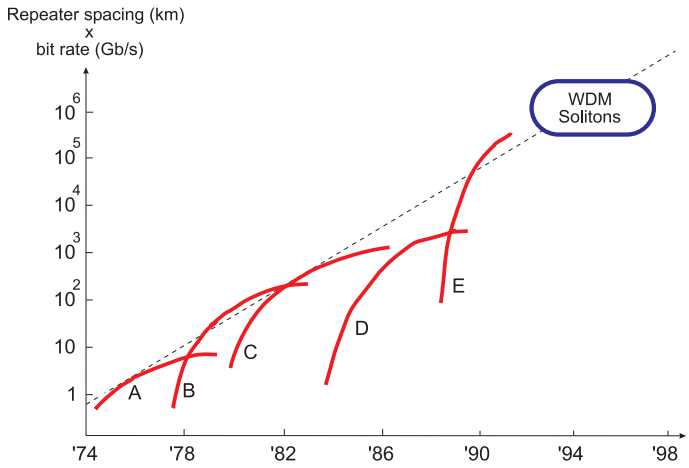

Figure 2.3: Data rates increase over years.

Security is another issue that places optical fiber in favor of copper-based twisted-pair wire. Since there are no radiated magnetic fields around optical fibers, tapping the signal being transmitted is almost impossible without cutting into the fiber or without reducing the received power.

Another nice feature that optical fiber offers in networks is low maintenance cost. Long-haul fiber networks typically cost less to maintain than copper-based networks because they exhibit less problems since they require less repeaters (active components).

Despite the many advantages of optical fiber, there are some disadvantages. Since it is relatively new technology compared to UTP, fiber optic components are expensive. Note that the fiber itself is not more expensive. Electro-optical (E/O) and opto-electrical (O/E) components in the transceivers are more expensive than electrical interfaces. Nevertheless, as the technology matures the use of fiber optics is expected to increase, since components cost will go down.

2.5 Optical sources

The choice of optical sources is crucial in designing affordable passive optical networks that will connect personal computers and servers, since these optical sources will be built in the network interface cards (NIC) mounted in those devices. Having expensive light sources will definitely make a complete NIC more expensive, and that is what network designers want to avoid. The choice

goes in favor of the short wavelength light sources that produce enough power to compensate for the losses in the transmission path. Such light sources are for example Fabry-Perot lasers and Vertical Cavity Surface Emitting lasers (VCSELs), producing short-wavelength light in the 850 nm region.

Fabry-Perot laser

The Fabry-Perot (F-P) laser contains a cavity that ends with two frequency selective and highly reflecting mirrors bouncing the light back and forth, forming a standing wave. This cavity is not very frequency selective, so light of different wavelengths can be produced as long as the mirrors are at the proper distance apart to form a standing wave. The only wavelength selectivity is from the wavelength dependence of the gain and resonant longitude modes.

The F-P lasers hop from one longitudinal mode to another as the current and/or temperature change. Most of them lase on several longitudinal modes simultaneously.

Vertical Cavity Surface Emitting laser

The Vertical Cavity Surface Emitting Laser, or VCSEL is a semiconductor laser diode that emits light in a cylindrical beam vertically to the surface of a fabricated wafer, and offers significant advantages when compared to the edge-emitting lasers currently used in the majority of fiber optic communications devices [16].

The VCSEL is cheaper to manufacture in large quantities, it is easier to test, and is more efficient. In addition, the VCSEL requires less electrical current to produce a certain amount of power than F-P LD. The VCSEL emits a narrow, more nearly circular beam than traditional edge emitters. This makes it easier to get the energy from the device into an optical fiber.

The VCSELs can be manufactured using standard microelectronic fabrication methods that allows integration of VCSELs on-board with other components without requiring pre-packaging. As an enabling technology, VCSELs allow superior new systems and products to be created at lower cost. Because the VCSELs are emitting at the top side, manufacturers can carry out on-wafer testing prior to dicing and packaging.

The first generation of VCSELs produced light at 850 nm, but with the latest technological improvements they can also produce light at 1300 nm.

CHAPTER 3

Ethernet networks and protocols

3.1 Ethernet protocol and OSI reference model

The main feature of the Ethernet protocol is allocating the use of a shared channel. The first concept of that dates back to early 1970s when Norman Abramson and his colleagues developed a radio network for communication among the Hawaiian Islands using the ether as a shared medium. The actual development of Ethernet occured in Xerox Palo Alto Research Center where Bob Metcalfe and his colleagues connected over 100 computers on a one kilometer cable [32]. They developed a collision detection mechanism, carrier sensing, in which stations listened for activity on the medium before transmitting and supported access to the shared medium. This is the reason for calling the Ethernet channel access mechanism Carrier Sense Multiple Access with Collision Detection (CSMA/CD).

The first 10 Mbps Ethernet standard is published in 1980 by the DEC-Intel-Xerox (DIX) vendor consortium. This was a vendor oriented standard that offered little possibility for world wide acceptance [10]. The IEEE on the other side, developed an open network standard published under the number 802.3, based on the original DIX standard avoiding the use of commercial names.

The IEEE standards are organized according to the Open System Interconnection (OSI) Reference Model. This model is a method of describing how networking hardware and software can function together in a highly structured way. To reduce design complexity the OSI reference model describes seven layers shown in Figure 3.1. The lower layers describe how bits are transported in the LAN system and the higher ones deal with more abstract notations such as the reliability of data transmission.

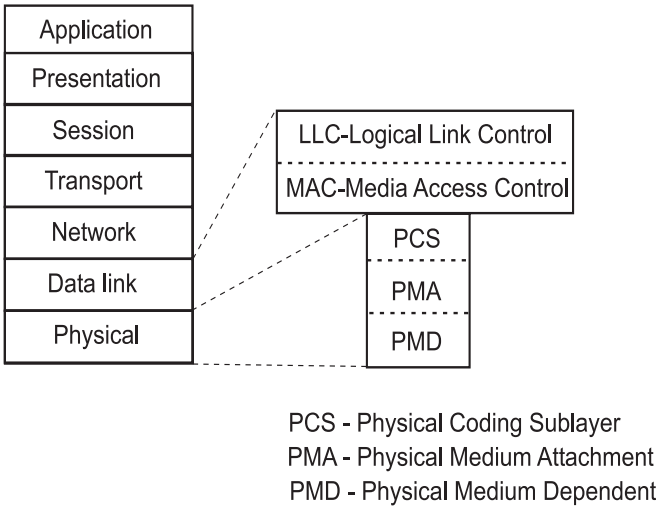

Figure 3.1: The OSI reference model.

The Physical layer standardizes the transmission media for actual transport of bits on different physical media e.g. air, copper cable, fiber etc.

The Data Link layer defines how a device or end user gets the access to the medium specified in the Physical layer. It defines data formats including the framing of data, recognizes link addresses and includes some procedures to correct transmission errors. The part of the standard that describes the Ethernet MAC format belongs to this layer.

The Network layer establishes logical connections between two end nodes that can comprise multiple data links. This includes addressing of the data packets, routing and switching. This layer works independent of the lower two layers, which means that the Ethernet protocol does not belong to this or any upper layers. An example of layer 3 protocol is the Internet Protocol (IP).

The Transport layer provides end to end control: it guarantees that the data transfer occurs correctly after a route has been established by the Network

layer. Examples of Transport layers protocols are Transmission Control Protocol (TCP) and User Datagram Protocol (UDP).

The Session layer provides mechanisms for establishing and terminating data streams between the nodes in a network.

The Presentation layer deals with data representation in applications e.g. converts transmitted data into a display format appropriate for a receiving device.

The Application layer supports end-user applications such as e-mail and file transfer using Hyper Text Transfer Protocol (HTTP), File Transfer Protocol (FTP) and Simple Mail Transfer Protocol (SMTP).

The layers that are of interest for Ethernet are the Physical layer and the Data Link layer which in turn contain several sublayers, shown in Figure 3.1. The sublayers are defined to help organizing the details in the Ethernet protocol. At the Data Link layer there are the Logical Link Control (LLC) sublayer and the Media Access Control (MAC) sublayer which are the same for all the Ethernet types. LLC sublayer is responsible for control and flow of data and perform recovery operations in the event of error. The MAC sublayer defines the protocol used to provide access to the Ethernet systems.

The LLC sublayer is independent of the IEEE 802.3 standard meaning that it does not vary no matter which type of LAN is used. All the sublayers below the LLC sublayer are specific to individual LAN technology.

The Physical layer is divided into three sublayers. The most upper physical sublayer is Physical Encoding Sublayer (PCS) that performs data encoding. The next one is the Physical Medium Attachment sublayer (PMA) that maps data from the PCS sublayer to the transmission medium. The Physical Medium Dependant (PMD) sublayer specifies the connector for the media used.

3.2 Ethernet based networks

The IEEE 802.3 standard is based on Ethernet and defines networks that were assigned names depending on the data rates they support, the type of signaling used and information about the transmission medium. Their names follow the following form "sTYPE-$t(l)$", where s is the speed in Mbps and TYPE denotes either broadband or baseband signaling. In the early media systems l was used to denote the cable distance in multiples of 100 m but the recent media system use t to refer to the media type used. The different networks defined in the

standard are:

10BASE-5 - the original Ethernet network standard based on a thick coaxial cable. The topology used is a bus with high-ohmic taps. The transmission speed was 10 Mbps and the maximum segment length was 500 m. To increase the network span multiple segments can be connected by repeaters. The maximum number of repeaters in any end-to-end path is four and the maximum number of users per segment is 100. The advantage of this network is its large span (2.5 km) but the disadvantage is that failure of the cable of the end node can cause the entire network to fail. This makes troubleshooting a failure difficult and time consuming.

10BASE-2 - defines using a thin coaxial cable as tranmission medium and the bus topology and is also known as the thin Ethernet system. The advantages of using thin coaxial cables are lower cost and easier utilization but it can not carry signals as far as the thick coaxial cable. The maximum segment length in this network is 185 m. The network shares the disadvantage of difficult troubleshooting with the 10BASE-5 networks and difficult reconfiguration.

10BROAD-36 - this is the only broadband network based on the CSMA/CD access method. It requires the use of radio frequency modems that modulate the input 10 Mbps NRZ encoded data signal for transmission on one TV channel. This system is constructed using coaxial cable and is supposed to cover large area up to 3.6 km. Nevertheless, the network designers nowadays rather rely on optical fiber when covering such large distances. The equipment for this broadband standard is scarce.

1BASE-5 - describes a 1 Mbps network based on unshielded twisted-pair (UTP) wiring in a star topology. It was not very popular and is very quickly replaced by the 10BASE-T standard.

10BASE-T - standard is developed to support an operating rate of 10 Mbps at the distance of 100 m using UTP cables. Here "T" denotes transmission over twisted-pair wire. A complete network comprises the NICs, UTP cable and one or more hubs. The network topology is a physical star, logical bus which offers better troubleshooting than the physical bus topology. The maximum number of hubs in the single LAN specified in the standard is equal to four. The maximum network span is thus 500 m.

10BASE-F - standard is based on the optical fiber medium, hence the letter "F" in the name of the standard. This standard provides network users ability to use fiber-optic hubs. Under the 10BASE-F standard, three types of segments for optical transmission are defined:

10BASE-FL - standard defines a fiber-optic link segment of 2000 m in length between two repeaters, two end stations or between the end station and a repeater port. It is based on the 62.5/125-μm multimode fiber and short wavelength light sources, around 850 nm.

10BASE-FB - standard, where "B" denotes a synchronous signaling backbone segment. It is made for extending a backbone system using fiber-optic repeaters that connect 2000 m length segments. A very few networks have been built in practice using this standard.

10BASE-FP - standard is made to connect the end stations via a common segment that can be up to 500 m in length. All the end stations are connected by means of a passive star coupler, hence the letter "P" in the name of the standard. The number of the end stations can be up to 33. This standard has not been implemented in practice.

100BASE-T - this is the standard for the high-speed Ethernet, commonly named as the Fast Ethernet. It contains, in general, four different physical layer specifications namely 100BASE-TX, 100BASE-FX, 100BASE-T4 and 100BASE-T2. All the Fast Ethernet standards are based on twisted-pair and fiber-optic media. Both 100BASE-TX and 100BASE-FX are generally denoted by 100BASE-X standard, since they are both based on the 4B/5B encoding.

100BASE-TX - operates over UTP wire at the data rate of 100 Mbps. The maximum network segment can be up to 100 m and the span of the network up to 200 m when repeaters are used. The "TX" in the name of this standard denotes that twisted-pair version of the 100BASE -X standard. Since this is the most widely used standard in practice, a detailed description will be given in Subsection 3.4.1.

100BASE-FX - defines Fast Ethernet baseband transmission over two optical fibers. Since this standard is of importance for the work to be presented in the following chapters more information will be given in Subsection 3.4.2.

100BASE-T4 - this is the Fast Ethernet standard based on the Category 3, 4 and 5 twisted-pair cables. It uses the 8B/6T coding technique where blocks of 8 input bits are mapped into the 6 ternary symbols. Since 3 wire pairs are used for transmission the total baud rate per wire pair is 25 Mbps. The 100BASE-T4 standard is not used much in practice and the availability of the 100BASE-T4 equipment on the market is scarce.

100BASE-T2 - this standard operates in a baseband mode and uses Category 3 cable for transmission. The number "2" in the name of standard denotes that 2 wire pairs are used for data transmission and the third one is used for

collision detection. This standard has never been implemented in practice.

1000BASE-X - Gigabit Ethernet standard describes 1 Gbps data transmission over both copper-based and optical fiber media. There are two fiber-optic standards, namely 1000BASE-LX and 1000BASE-SX and two copper-based, 1000BASE-CX and 1000BASE-T. Common for all the standards is 8B/10B encoding of the transmitted data.

1000BASE-LX - specifies the signal transmission via optical fibers using long wavelength light sources. Both single-mode and multimode fibers can be used for data transmission, putting different limitations in the total network span. The maximum span of the network when single-mode and multimode fibers are used are 3 km and 550 m, respectively.

1000BASE-SX - defines the short wavelength signal transmission via multimode optical fibers. Two different network spans are defined based on dimensions of the multimode fiber used. For 62.5/125-μm fiber the maximum span of the network is 260 m. The network span is more than twice as large when 50/125-μm fiber is used and is equal to 550 m.

1000BASE-CX - specifies the transmission over short shielded balanced copper (coax or shielded twisted-pair). The network span is limited to 25 m.

1000BASE-T - defines 1 Gbps transmission over Category 5 twisted-pair cable. The latest version of the standard includes Category 5e (enhanced) cable, made specifically to carry data at gigabit-per-second rate. The maximum network span is limited to 100 m.

3.3 The Ethernet system

The building blocks of the Ethernet system are the Ethernet packet (frame), media access control protocol, signaling components and physical medium.

3.3.1 Ethernet packet

All the bits carried in an Ethernet packet are collected in fields presented in Figure 3.2.

At the start of every Ethernet packet is a preamble of 7 bytes in length. This is a series of alternating ones and zeros that is used for acquiring synchronization at the receiving site. The preamble gives time to the Ethernet system at the start-up to recognize that the frame is being transmitted. This was originally built for the 10 Mbps systems, since the high-speed Ethernet systems (Fast

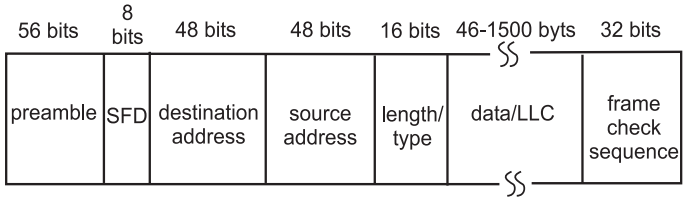

Figure 3.2: The Ethernet packet composed in the MAC sublayer.

Ethernet and Gigabit Ethernet) use constant signaling that avoids the need for a preamble. Nevertheless, it will be shown in Chapter 5 that the Fast Ethernet standard proposed in this thesis also makes use of the packet preamble.

To indicate the end of the synchronization sequence the Start of Frame Delimiter (SFD) was added. This is an alternating pattern of ones and zeros that ends with two consecutive ones and is used to acquire byte alignment. The SFD is not a unique code word and should only be indicated at the beginning of the packet. The destination address that follows the SFD indicates the address of the intended end station. If this field is set to all ones than the message is broadcast to all the end stations in the network. The source address is the 48 bit unique address of the sending end station given by the manufacturer of the interface to avoid the problem that two or more Ethernet interfaces in a network have the same address. This address is usually called the MAC address.

The field that comes after the address fields is the message length or the message type field. The reason for having two definitions of the field comes from the fact that the IEEE standard for Ethernet differs slightly from the original DIX standard. The latter did not need a length field because all the vendor protocols that used it had their own length fields.

The actual information sent over the Ethernet network is placed in the data field. This part of the frame is where an IP packet is carried. The minimum length of an Ethernet frame is 46 bytes of data together with the 26 bytes of overhead. This length ensures that every end station connected to the network can sense the frame within the correct time limits. However, this is a historical requirement derived for the bus topology with a coax cable (thick or thin) and a network with a two-byte address field. In the current hub topologies with the twisted-pair wires, collision detection is being done inside the hub, where the distance from the internal bus to the port is very short. Therefore, the data length could be much shorter, but the standard has not been modified. The maximum length of the Ethernet packet is 1500 bytes plus overhead. If the

data field is too long it can block other users from getting fair access.

The last field in the Ethernet frame is the Frame Check Sequence (FCS). It is just a cyclic redundancy check (CRC) that is used to control the correct transmission of bits in the packet. The preamble and SFD are excluded from this operation. In case the CRC indicates an error, the frame will be discarded by the MAC sublayer and the layers above will request retransmission.

The content of the address, the type and the FCS fields of the Ethernet MAC packet are of no direct importance to the Physical layer. In the Physical layer unaltered transmission is applied to the data packet in all the fields except that of the preamble (Subsection 3.3.6). Besides, the MAC sublayer has no interest in the value of the preamble bits, apart from the fact that it is waiting for a valid SFD to start transferring the data.

3.3.2 Media Access Control protocol

The media access control mechanism used in the Ethernet networks, based on half-duplex transmission, is CSMA/CD. It was already mentioned that it is the key feature of Ethernet.

Before transmitting the packet on the medium an end station connected to a half-duplex channel must wait until the channel is free, which means that no other end station is transmitting. After the channel becomes idle, the station has to wait for another period, called the InterFrameGap (IFG) time, before it may start to transmit a frame. After the IFG time has elapsed, the end station will not react to a detection of carrier any more. If a station wishes to transmit multiple frames, it must wait for a period equal to the IFG between two consecutive frames. The InterFrameGap timing in the [24] standard has been set to 96 bit times. It is intended to allow a very brief recovery time between reception of successive frames. Moreover, it also enables a fair transmission schedule, by allowing other stations to start sending their packets in this InterFrameGap.

A station that detects a collision during the transmission will continue to transmit 32 bits of data, called the collision enforcement Jam signal. If the collision is detected before the preamble of the packet has been transmitted then the end station will continue sending data until the preamble transmission is completed, after which it sends the 32 bits of Jam signal.

After sending the Jam signal, the station enters a state called backoff. In this state the end station waits a random period of time before it proceeds to transmit again. The backoff time takes care that colliding stations will choose

different delay times, preventing them to collide with one another again. If the frames collide in the next transmission attempt then the end station increases its collision counter. It enters the backoff procedure again, with the increased backoff time to decrease the probability of collision. This mechanism is very important in the networks with heavy traffic loads.

When an Ethernet end station has transmitted 512 bits of a frame without a collision, the station has acquired the channel. On a properly functioning Ethernet no collision should occur after channel acquisition. This 512 bit time is known as the Slot Time of the Ethernet channel and it is one of the determinants for the maximum Ethernet diameter. Once a station acquires the channel and transmits its frame, it also clears its collision counter, which was used to generate the backoff time.

All stations that participate in an Ethernet network are obliged to comply to the access mechanism stated above. This mechanism ensures that a collision will only affect the stations that are actively involved in the collision.

Slot Time

The Slot Time is defined as the worst-case time delay the end station must wait before it can reliably know a collision has occured [24]. It depends on both the propagation time of the packet through the Physical layer and the medium, and the maximum time required for collision enforcement. The latter implies the time to detect a collision and send a Jam signal.

The propagation time strongly depends on the network span. The larger the span the longer the time it takes for packets to travel from one end station in the network to another. To detect a collision a total round-trip time must be taken into account that includes twice the time a packet has to travel through the medium, plus the propagation time in the Physical layers of both transmitter at one side of the line and receiver at another. If repeaters are used in the network the delay in the repeater is also taken into account when determining the Slot Time.

The Slot Time in Ethernet protocol amounts to 512 bits. This is to ensure that even when the smallest legal frame is transmitted a transmitting end station will have enough time to detect that collision occured.

Ethernet parameter values

The most important parameter values for the Ethernet implementation are given in Table 3.1. All the values are given in bit times. The actual time durations of specific parameters will depend on the Ethernet type used. The higher the Ethernet speed accommodated, the shorter the parameter values with respect to actual time duration.

Table 3.1: Parameter values for Ethernet standard.

Parameters	Values
Slot Time	512 bit times
InterFrameGap	96 bit times
Attempt Limit	16
BackoffLimit	10
JamSize	32 bits
MaxFrameSize	1518 octets
MinFrameSize	512 bits
BurstLimit	not applicable

3.3.3 Ethernet signaling components

The signaling components are used to send and receive signals over the physical medium. They differ depending on the Ethernet type used but generally include Ethernet interface, transceivers and the cable connecting transceivers to the interface. The Ethernet interface is in fact a network interface card (NIC) containing electronics to send and receive Ethernet packets. A NIC can have a built-in transceiver or an external transceiver. Transceiver cable is used only in case of external transceiver utilization.

If the Ethernet system is using repeaters to extend the maximum span than these also belong to the signaling components. More about repeaters will be given in Section 3.5.

3.3.4 Ethernet media fundamentals

It was already shown that the Ethernet standard specifies data transmission using different media. But to transmit signals not only transmission media but also the connectors, and other components connected to the Ethernet system are equally important. Moreover different types of interfaces to connect the

end station to the medium have been specified, like attachment unit interface (AUI), medium attachment unit (MAU), medium independent interface (MII), gigabit medium independent interface (GMII), [24]. Here, an MII interface will be described in details due to its relevance to the work presented in this thesis.

The standardization of Fast Ethernet 100BASE-T came after the 10BASE-T Ethernet standard has become very popular. Increasing the speed tenfold required only minor changes to be made in the MAC sublayer since this operates independent of the data rate. Most of the changes had to be made in the Physical layer, which had to support three different media types, namely four wire pairs in 100BASE-T4, two wire pairs in 100BASE-TX and fiber optic media 100BASE-FX.

To accommodate multiple physical layers a Medium Independent Interface (MII) was introduced that supports both 10 Mbps and 100 Mbps data rates, keeping the compatibility with different Ethernet standards. The Physical layer that is below the MII is subdivided into three parts, as shown in Figure 3.1. The medium dependant interface (MDI) sublayer specifies the use of connectors. For the 100BASE-TX Fast Ethernet it is the RJ-45 connector and for the 100BASE-FX the subscriber connector (SC).

Medium Independent Interface

The Physical layer is connected to the MAC sublayer by means of the Medium Independent Interface, which is presented in Figure 3.3.

The MII can be built-in the Physical layer inside the complete NIC or it can be exposed, in which case an MII 40-pin connector is provided on the NIC to provide external Physical Layer Devices (PLDs) to be connected to the same NIC [24]. Different PLDs are made to support various media types like coaxial cable, twisted-pair wire and optical fiber. But no matter what medium type is used, the signals that are going through the MII are always the same, specified by the standard.

The MII accommodates two 4-bit data buses and several control signals to cater for the communication need between the MAC and the Physical layer. Table 3.2 shows the abbreviations of all MII signals and their notation. The signals over the MII have been subdivided into four subclasses.

Clock signals- The parallel data signals transported over the MII will be clocked with a frequency of 25 MHz, according to the standard [24]. Transmitted and received data patterns must change levels synchronously to their

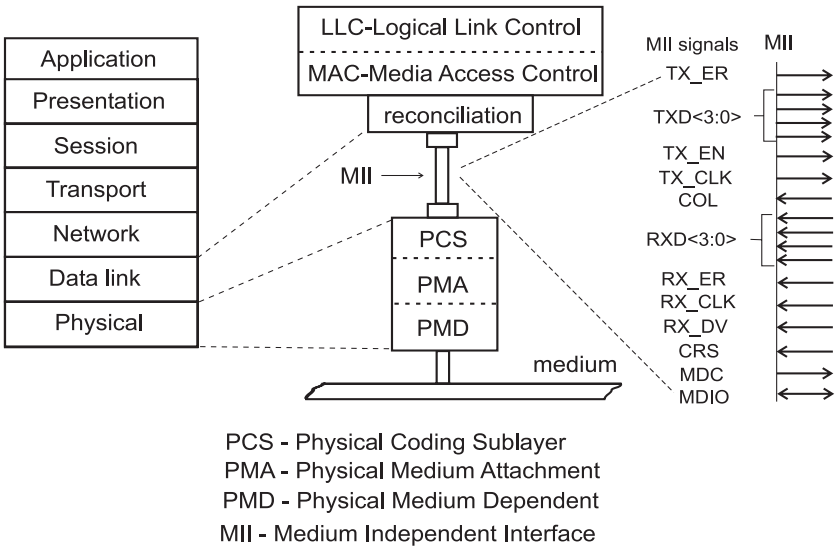

Figure 3.3: A Medium Independent Interface between the MAC sublayer and the Physical layer.

RX_CLK	Receive Clock
TX_CLK	Transmit Clock
RXD$\langle 3:0 \rangle$	Receive Data Bus
RX_DV	Receive Data Valid
RX_ER	Receive Error
CRD	Carrier Sense
COL	Collision Detection
TXD$\langle 3:0 \rangle$	Transmit Data Bus
TX_EN	Transmit Enable
TX_ER	Transmit Error
MDC	Management Data Clock
MDIO	Management Data Input/Output

Table 3.2: Signals over the Medium Independent Interface

accompanying clock signals, TX_CLK and RX_CLK respectively. Besides, all the clock signals are supposed to be generated by the Physical layer, for both transmission and reception of the signals.

Receive Signaling- The receive data valid signal, RX_DV, is driven by the Physical layer to indicate that it is presenting recovered and decoded data nibbles on the RXD$\langle 3:0 \rangle$ bus and that the data on this bus is synchronous to RX_CLK.

The RX_DV must change level synchronously with respect to the RX_CLK signal and must remain asserted continuously while the Physical layer is presenting decoded nibbles to the MAC sublayer. The RX_DV must encompass a frame, starting no later than the start of the SFD. Note that the completely formed SFD must be transferred over the MII in order to transfer a valid frame. Transfer of any preamble bits preceding the SFD can theoretically be omitted. In case any data preceding the SFD are being transferred, care must be taken that only words containing the preamble pattern are being used.

Transmit Signaling- A TX_EN signal shall become asserted synchronously to the first valid data-nibble (4 parallel bits from the MAC sublayer) the MAC sublayer presents to the TXD$\langle 3:0 \rangle$ bus and remains asserted as long as valid data is presented to the MII. Of course, invalid data on the TXD bus will not affect the Physical layer as long as TX_EN is de-asserted.

Management Data Clock- A management clock signal (MDC), which originates from the Station Management entity towards the Physical layer is aperiodic, asynchronous to the other clock signals and it can run on various rates.

Jabber Detect Operation

This operation is originally made for the Ethernet standard based on the shared medium and is avoided in the Fast Ethernet standards. In the latter, no really shared medium is used, readily a point-to-point connection is implemented. On the other side, the Fast Ethernet passive optical star networks proposed in the thesis are based on the shared medium and therefore the idea of a Jabber detect function can be reusable.

The Jabber is defined as the act of continuously sending data [24]. A jabbering station is one whose circuitry has failed, and which acquires the channel for a time longer than the maximum frame size prescribed in the standard. The Jabber detect function monitors the output signal from the transmitter by means of a jabber timer. It will check whether the physical transmitter attempts to transmit a longer packet than allowed. Transmission of an illegally sized packet would mean that the physical transmitter is broken, so that the MAC sublayer can no longer control it. Therefore, the jabber timer will disable transmission if the transmitter is active for more than a predefined time. This time is for the typical Ethernet network manufacturers approximately 26 ms.

The internal transmit enable signal has to become inactive for a certain time interval, the 'unjab' time, before the jabber function re-enables the transmit-

ter's outputs and de-asserts the COL signal. This time used is manufacturer dependent, but typically varies between 368 ms and 750 ms for 10 Mbps Ethernet networks. For 100 Mbps Fast Ethernet networks that are proposed in the thesis, a value of 40 ms will be implemented.

Both Jabber detect and Unjab signals directly control the driving current of the light source in the analog transmitting part of the Physical Layer Device. If Jabber is detected than the modulation signal is switched off. After Unjab time expires, the modulation signal will be switched on again.

3.3.5 Fast Ethernet signal encoding

The 100BASE-X encoding was originally developed for the ANSI Fiber Distributed Data Interface (FDDI) network standard. It is the 4B/5B block encoding that divides data into a 4-bit blocks. These blocks, so-called nibbles, are mapped onto 5-bit code words for transmission over the medium. The side effect of introducing 4B/5B encoding scheme is that the data rate increases from the originally 100 Mbps to 125 Mbps. The advantage of introducing 4B/5B encoding is that there are 32 possible 5-bit codes. With 4-bit nibbles there were only 16. A 5-bit code can be chosen such that each code has at least 2 data logical "1" bits, which can be used for synchronization, if constant signaling is used in the network. The use of 4B/5B encoding enables data and control information to be carried in each symbol represented by a five bit code group. It also enables IDLE signal used for synchronization and a special symbol used to force signaling errors.

The 4B/5B code groups from the 100BASE-X Fast Ethernet standard are presented in Table 3.3.

3.3.6 Fast Ethernet packet mapping from the MAC to the Physical layer

After a Fast Ethernet packet is generated in the MAC sublayer, the encapsulation of the packet into a physical layer stream is taking place in the PCS sublayer. Except for the two code groups SSD (SSD_J and SSD_K), data nibbles are not interpreted by the Physical layer. The conversion from a MAC packet to a physical layer stream and back to the MAC packet is transparent to the MAC sublayer. This conversion is depicted in Figure 3.4.

A physical layer stream has three components namely, Start of Stream De-

Table 3.3: 4B/5B code-groups

PCS code-group [4 : 0] 4 3 2 1 0	Name	MII (TXD/RXD) ⟨3 : 0⟩ 3 2 1 0	Interpretation
1 1 1 1 0	0	0 0 0 0	Data 0
0 1 0 0 1	1	0 0 0 1	Data 1
1 0 1 0 0	2	0 0 1 0	Data 2
1 0 1 0 1	3	0 0 1 1	Data 3
0 1 0 1 0	4	0 1 0 0	Data 4
0 1 0 1 1	5	0 1 0 1	Data 5
0 1 1 1 0	6	0 1 1 0	Data 6
0 1 1 1 1	7	0 1 1 1	Data 7
1 0 0 1 0	8	1 0 0 0	Data 8
1 0 0 1 1	9	1 0 0 1	Data 9
1 0 1 1 0	A	1 0 1 0	Data A
1 0 1 1 1	B	1 0 1 1	Data B
1 1 0 1 0	C	1 1 0 0	Data C
1 1 0 1 1	D	1 1 0 1	Data D
1 1 1 0 0	E	1 1 1 0	Data E
1 1 1 0 1	F	1 1 1 1	Data F
1 1 1 1 1	I	undefined	IDLE used as inter-stream fill code
1 1 0 0 0	J	0 1 0 1	Start of stream delimiter, part 1 of 2 always used in pairs with K
1 0 0 0 1	K	0 1 0 1	Start of stream delimiter, part 2 of 2 always used in pairs with J
0 1 1 0 1	T	undefined	End of stream delimiter, part 1 of 2 always used in pairs with R
0 0 1 1 1	R	undefined	End of stream delimiter, part 2 of 2 always used in pairs with T
0 0 1 0 0	H	undefined	Transmit Error; used to force signaling errors
0 0 0 0 0	V	undefined	Invalid code
0 0 0 0 1	V	undefined	Invalid code
0 0 0 1 0	V	undefined	Invalid code
0 0 0 1 1	V	undefined	Invalid code
0 0 1 0 1	V	undefined	Invalid code
0 0 1 1 0	V	undefined	Invalid code
0 1 0 0 0	V	undefined	Invalid code
0 1 1 0 0	V	undefined	Invalid code
1 0 0 0 0	V	undefined	Invalid code
1 1 0 0 1	V	undefined	Invalid code

limiter (SSD), Data Code-groups and End of Stream Delimiter (ESD). The SSD indicates the start of the physical layer stream, actually a data packet that is transmitted on the medium. It replaces the first octet of the preamble from the MAC sublayer. Data Code-groups are sent between two delimiters, which

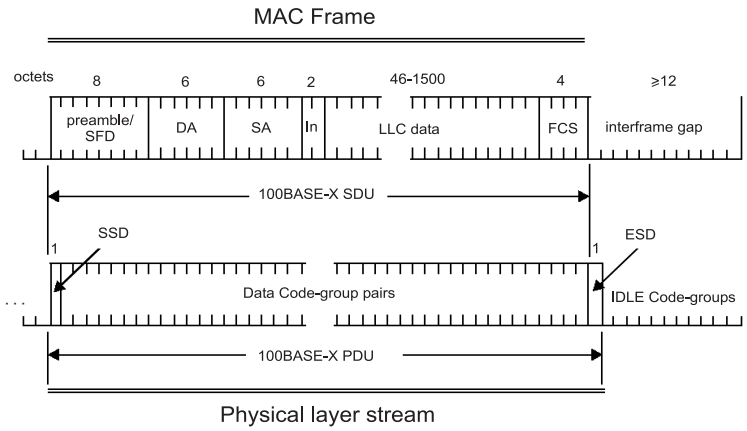

Figure 3.4: Fast Ethernet packet mapping between the MAC sublayer and the Physical layer.

convey data nibbles from the MAC sublayer that has been 4B/5B encoded, scrambled and MLT-3 encoded in 100BASE-TX standard. The ESD indicates the end of a properly received physical layer stream. It is transmitted by the PCS following the de-assertion of the transmit enable (`TX_EN`) signal on the MII. This deassertion takes place after the last data nibble composing the FCS has been sent from the MAC sublayer. The ESD is transmitted during the period considered by the MAC to be the InterFrameGap. On reception, ESD is interpreted by the PCS sublayer.

In between the Physical layer streams IDLE code groups are transmitted for synchronization purposes.

3.4 Fast Ethernet fiber-to-the-desk networks

In Section 3.2 different standards for Fast Ethernet networks are described. They all differ in the medium type used. The twisted-pair based standards are the most practically implemented ones and the fiber based standards are still struggling for their place in the fiber-to-the-desk application.

3.4.1 Twisted-pair networks

The 100BASE-TX twisted-pair network is the most widely used Fast Ethernet network up to date. It is based on two wire pairs, each used to transmit and

receive data signals, respectively. It was made as an extension to the existing 10BASE-T Ethernet standard. Some changes with respect to the maximum network span and the maximum distance between the end nodes and the hub had to be made to ensure proper collision detection. The total network span is decreased to 250 m, since the bit-rate increased for the factor of ten, to reduce potential propagation delay [24].

A 100BASE-TX NIC may be equipped with the Physical layer containing RJ-45 connector or with the 40-pin MII interface on which an external Physical Layer Device can be attached. The NIC support speeds of both 10 Mbps and 100 Mbps. At which speed the NIC will operate is determined by the Auto-Negotiation mechanism built in the Fast Ethernet standard. Moreover, with the Auto-Negotiation mechanism full-duplex or half-duplex transmission can be specified. Both functionalities of the mechanism enable gradual network upgrade. This will be elaborated in Sections 3.6 and 3.7.

The 100BASE-TX signaling system is based on 4B/5B encoding. The physical signaling used to transmit the five-bit symbols over twisted-pair cables is based on multilevel threshold (MLT-3) data encoding. This means that the line signal has one of the three possible levels at each clock transition. A change from one level to the next one takes place when a logical “1” is to be transmitted. The signal level stays unchanged when a logical “0” is transmitted. This reduces the total signaling rate on the wire. However, if a long sequence of logical zeros is transmitted a constant non-zero voltage level of the MLT-3 encoded signal will have significant power at very low frequencies, which can be problematic for the transmit an receive circuitry that is usually AC coupled.

Another problem is that a lot of high frequency signals have to be transmitted on the limited-bandwidth wire. This will increase the signal error rate causing packet loss and reduce network performance. This is the reason why a pseudo random data scrambling is introduced. It greatly reduces the average power of the harmonics above 32.5 MHz fairly smoothly distributing the power below 32.5 MHz.

3.4.2 Fiber optic networks

There are two types of fiber based standards released up to date, namely 100BASE-FX and 100BASE-SX, each having its advantages and disadvantages.

100BASE-FX

The 100BASE-FX fiber optic network is based on two optical fibers - one for transmission and one for reception. It uses the 4B/5B coding scheme identical to the one used in the 100BASE-TX network. The main advantage of this network is that it can support larger distances, especially if the single-mode fibers are used in combination with the full-duplex mode of operation. The coding scheme that is implemented on top of the 4B/5B is Non-Return-to-Zero, Invert-on-ones (NRZI). The system makes no change in the output signal level when a logical "0" is transmitted and inverts the signal from its previous value if a logical "1" is transmitted. In this way a certain number of logic transitions is made facilitating the clock extraction at the receiving site. Since there is no electromagnetic emission from the optical fiber, data scrambling can be omitted.

The optical transmitters in the Physical layer contain long wavelength lasers in the 1.35 μm region. This was chosen so that the standard would support a 2 km distance, as did the fiber optic Ethernet 10BASE-FL standard. However, the disadvantage of such a choice was that opto-electronics, implemented in the NICs, was not compatible with the previous fiber optic Ethernet standard, since the 10BASE-FL is based on a 850 nm optical components. The peak optical power transmitted is around 400 μW [24].

The whole system is based on a point-to-point connection between either two end stations or the end station and the repeater. The maximum segment length between any two end stations is limited to 412 m when half-duplex connection is used. For full-duplex connection this distance can go up to 2 km for multimode fibers and more than 20 km for single-mode ones, since the link segment is not restricted by the round-trip time limits of a shared Fast Ethernet channel. Instead, this link is limited by attenuation of transmitted optical power and dispersion in fiber.

100BASE-SX

This standard appeared after 100BASE-FX and is published in the TIA/EIA-568-B.1 [33]. For the first time it defined the strategy to migrate from Ethernet copper-based networks to Fast Ethernet fiber networks using a cable structure that is capable of Gigabit Ethernet speeds [34].

Everything above the Physical layer stays the same such that the new network can work along with the Ethernet/Fast Ethernet equipment.

The main improvement with respect to 100BASE-FX standard is that short

wavelength LEDs that work in the 850 nm region are used in contrast to the LEDs in the 100BASE-FX standard that work in the 1.3 μm region. The reason for choosing short wavelengths was twofold. Firstly, a compatibility with the 10BASE-FL standard can be achieved and secondly, using short wavelength light sources offer a lower cost implementation. Before 100BASE-SX was introduced, users with installed fiber could not use Auto-Negotiation mechanism since 10BASE-FL was based on short wavelength and 100BASE-FX on long wavelength components.

The drawback of introducing short wavelength components was reduced span of the network. Instead of 2 km, the maximum distance between any two end stations in the 100BASE-SX standard is limited to 300 m. The 100BASE-SX standard supports two types of multimode fiber, namely 62.5/125 μm and 50/125 μm and two connector types, SC and ST (Straight Tip) [33].

3.5 Ethernet internetworking devices

Understanding the functionality of the internetworking devices is an important issue, since these devices are the blocks upon which the networks are constructed. The devices that are used to both connect the end nodes to the LAN and interconnect different LANs are repeaters, hubs, bridges, switches and routers. They are usually interconnected by means of cables at different distances ranging from a few tens of meters to a few kilometers.

Repeaters

These devices are also known as the Ethernet repeater hubs. They work at the Physical layer and are used to connect different half-duplex Ethernet segments of any given media type. When linking segments together, repeaters regenerate the signal and restore the timing. Repeaters can either be used to extend the maximum segment length or to increase the maximum number of users that can be attached to the same segment by improving the signal quality. The total number of repeaters in the network link is limited due to the signal timing and quality. The signal timing must comply with the maximum Slot Time proposed in the standard, since all the different link segments connected by the repeater belong to the same collision domain. To separate collision domains, and in this way increase the total network span and available bandwidth, a bridge or a switch have to be used.

Hub

The hub can also be called multi-port repeater. It is a physical hardware device that is used to provide physical star topology. The hub is a central point where cables are put together. Having no intelligence it just forwards the incoming packets to all the output ports. It is typically used in star-shaped 10BASE-T Ethernet networks. A point-to-point connection is used between the end station and the hub. With respect to bandwidth utilization, the hub is a bottleneck since all the users connected to the hub belong to the same collision domain and they all compete for the available bandwidth.

Bridges

The bridges are devices that require software for proper functioning. They can be stand alone devices or they can be dedicated PCs with an extra NIC and bridging software. The bridges offer a possibility to build large Ethernet systems that stretch beyond a single collision domain. This is done by connecting different Ethernet LANs together. The Ethernet addresses of all the end nodes in networks connected by a bridge are stored in the bridge such that traffic from one network can be directed to the other one. This provides a bridge with the possibility to filter out the traffic that is not intended for a particular part of the network preventing it passing through. This filtering results in reducing the total traffic load in one LAN, thereby making more bandwidth available for use.

Switches

The switch is basically a multiport bridge that forwards packets from one port connected to a LAN to another port connected to a different LAN. Different LANs connected by a switch operate independently and simultaneously. The switch, like a bridge, filters out the traffic to different LAN segments but forwards only the traffic that is relevant to that segment. In this way it separates collision domains. The switch provides better performance than the bridge since it can forward more than a single frame at a time, increasing the overall bandwidth by many times that of a single shared LAN. The forwarding decision is based on the MAC address. This MAC address is Logical Link Control sublayer information, which means that a switch operates at the Data Link layer in the OSI reference model. This is in contrast to routers that operate at the Network layer. A nice feature of switches is that they can provide a simple way to in-

crease the total bandwidth without needing to rearrange the cabling structure or to replace the NICs at the user's site. The latter is due to the fact that users connected via switch are not sharing the available bandwidth. For example, if 10 users are sharing Ethernet channel, than each of them gets in average 1 Mbps. Introducing switches, data rates per user, can go up to 10 Mbps and there will still be no need for introducing new NICs. The disadvantage of introducing switches is that they require extra power supply and regular maintenance, both increasing the overall network implementation cost.

Routers

Routers are also filtering the traffic like bridges and switches, but since they work at the Network layer they can separate different protocols. An IP router can forward the traffic that is going to a certain network with a specific IP address. The major advantage of the router is that it reduces the traffic levels and performance problems caused by the excessive levels of the number of broadcast packets. Unlike switches and bridges a router does not automatically forward broadcast and multicast frames. In this way it protects a large system from high traffic rates.

Compared to bridges and switches, routers introduce more delay in the network, since filtering the protocol takes more time than filtering data packets. From the cost point of view routers are more expensive since packet forwarding is performed by the software running on an expensive high-performance processor, whereas both bridges and switches perform switching using integrated circuits.

3.6 Switched Ethernet topology

In this section a typical 100BASE-TX network topology is presented. This will bring a better understanding of the network topologies suggested in the thesis.

The 100BASE-TX technology is designed to support 10 Mbps, 100 Mbps and 10/100 Mbps transmission due to the compatibility among different Ethernet standards. Therefore, the Fast Ethernet topologies may combine different end stations and connect equipment that accommodates both Ethernet and Fast Ethernet protocols. This is known as the heterogeneous or mixed CSMA/CD network.

Network topologies can be developed within a single 100BASE-TX collision domain, or multiple collision domains. In the latter case a maximum flexibility

is achieved and the multiple segments are joined by bridges, switches and/or routers configured to provide a range of service levels to end stations. For example, a combined 100BASE-T/10BASE-T system built with repeaters and bridges can deliver dedicated 100 Mbps, shared 100 Mbps, dedicated 10 Mbps, and shared 10 Mbps service to end stations. Such a multibandwidth, multi-collision domain topology using multiport switches is presented in Figure 3.5, [24].

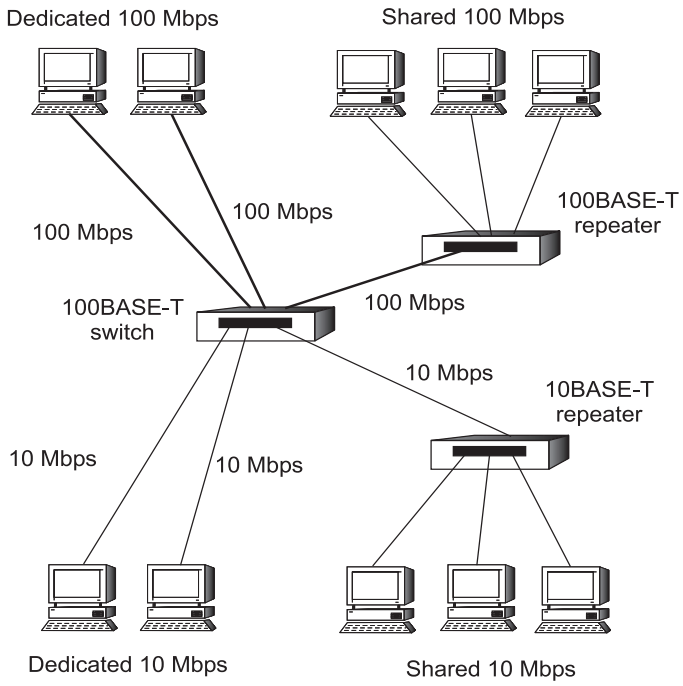

Figure 3.5: Multiple bandwidth, multiple collision domain topology using a multiport switch.

The effective bandwidth of shared services is determined by the number of end stations sharing the service. Connecting multiple 100BASE-T collision domains with switches maximizes flexibility. The switched topology shown in Figure 3.5, provides multiple bandwidth services since both 10 Mbps and 100 Mbps are supported.

3.7 Upgrading the twisted-pair network

Many companies installed the Ethernet 10BASE-T network in their buildings. Several years later there existed the need for upgrading the system. To do so, network designers can use the Auto-Negotiation mechanism built in the 100BASE-TX standard. The system upgrade may start by replacing a 10 Mbps hub in the wiring closet with a 10/100 Mbps bridge or a switch that provides a 100 Mbps connection to the critical end nodes. At the same time the end stations that may still operate with 10 Mbps connections will also be supported. In this way architectures like the one shown in Figure 3.5 are obtained. To upgrade the end stations operating at 10 Mbps in the future, an existing NIC has to be replaced by a 100 Mbps NIC.

Another possibility to upgrade the existing network based on twisted-pair wires and to increase the span is to install optical fibers. To do this the compatibility between 100BASE-X standards will be used. If the cost is the guiding factor in upgrading the existing network, the best solution is to use the 100BASE-SX standard. Media converters can be used that convert a 10BASE-T or 100BASE-TX signal into its fiber equivalent 10BASE-FL or 100BASE-SX and vice versa. The media converters use the Auto-Negotiation mechanism that allows gradual upgrade of the system such that most of the installed equipment can be retained. A typical upgrade scenario using media converters is presented in Figure 3.6, [34].

Here an existing NT server with a 10/100BASE-TX NIC is connected to a 10/100BASE-TX switch, which in turn is connected to a workstation with a 10BASE-T NIC. The link between the switch and the server is 100 Mbps, whereas the link between the server and the end station is 10 Mbps. The upgrading starts with optical fiber and media converter installations. Since the server costs are shared among all the users in the network replacing the NIC in the server with the new 100BASE-SX NIC can be afforded in the first phase.

The next phase would be to change the NIC in the end station. The end station is now directly connected to the media converter chassis in the main wiring closet by means of optical fiber, as shown in Figure 3.6(b). Finally, a 100BASE-TX switch can be replaced by a 100BASE-SX switch although this would not increase the performance of the network. Note that all the connections in the network are point-to-point.

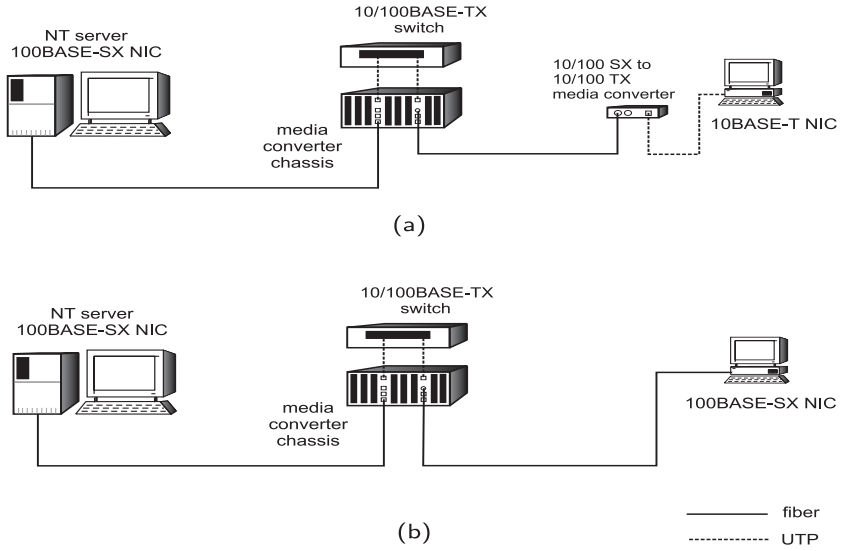

Figure 3.6: Typical scenario for upgrading the copper-based network accommodating the 10/100BASE-TX protocol into a network that accommodates the fiber optic 100BASE-SX protocol. (a) 10 Mbps Link, (b) 100 Mbps link.

3.8 Gigabit Ethernet

Gigabit Ethernet appeared as the extension to the existing Ethernet and Fast Ethernet standards. Interest in introducing this standard came from the fact that computer speed increased such that transferring the files among computers and servers became a bottleneck [2]. Moreover, video conferencing demands more bandwidth than the existing local area networks support.

The design objectives for Gigabit Ethernet were to offer 10-fold increase in bandwidth with respect to the Fast Ethernet standard, to support both full- and half-duplex operation and to be compatible with the previous Ethernet standards.

To achieve this most changes had to be made in the Physical layer. Three different standards were specified depending on the types of media used to transmit data, namely 1000BASE-SX, 1000BASE-LX and 1000BASE-CX. The specifications for all the standards are given in Section 3.2. The main difference with respect to the previous Ethernet standards are introducing carrier extension and frame bursting.

Carrier extension had to be introduced due to collision detection. Recall

that the minimum time to detect a collision is the time it takes the signal to propagate from one end station to another (Slot Time). But increasing the speed requires proportional decrease in the network span. Keeping in mind that the maximum network span for the Ethernet network is 2.5 km, increasing the speed 100 times would limit the span of Gigabit Ethernet network to about 25 m only.

The remedy to increase the network span was to increase the Slot Time and at the same time increase the minimum frame size. Nevertheless, in order to maintain compatibility with the previous Ethernet standards, the minimum frame size could not be increased. This particularly regards networks using half-duplex transmission and CSMA/CD at gigabit rates. For full-duplex transmission networks this is of no importance since the Slot Time does not limit the network span.

To increase the Slot Time keeping the minimum frame size unaltered a carrier extension technique is implemented. According to the standard, the use of this technique increases the Slot Time from 64 bytes to 512 bytes [24]. A composition of the Gigabit Ethernet MAC packet using the carrier extension technique is presented in Figure 3.7.

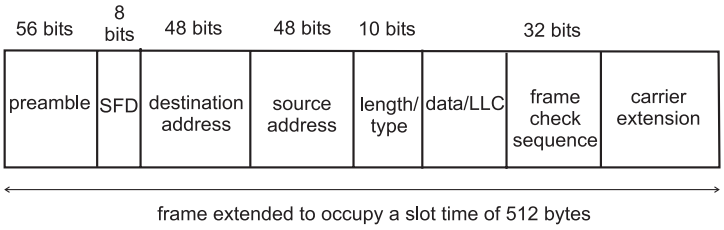

Figure 3.7: A Gigabit Ethernet packet composed using carrier extension technique.

Whenever the Gigabit Ethernet packet size is shorter than 512 bytes the packet is padded with the extension symbols that do not appear in the payload. The packet size increases, but as far as both transmitter and receiver are concerned the packets are normal Ethernet packets. Thus, the Frame Check Sequence (FCS) is calculated only on that part of the packet before padding. The LLC sublayer is not aware that carrier extension is being used.

The carrier extension is a technique that provides a simple solution to increase the network span when Gigabit Ethernet is accommodated but it has also a drawback. It is very bandwidth inefficient, especially for the short packets. For example, for the shortest Ethernet packet of 64 bytes, 448 bytes of padding

have to be added, resulting in a low throughput.

The solution for increasing the throughput is frame bursting. This is a feature that distinguishes Gigabit Ethernet from the other Ethernet standards. This technique allows stations to send a number of short packets such that full available bandwidth utilization can be achieved. If the end station has several short packets to send, the first packet is padded to 512 bytes and the other packets are just attached to the first one keeping the interframe gap between the two consecutive packets of 96 bits [24]. But instead of allowing the medium to go idle between frames, the transmitting station fills the interframe gaps with extension bits. Extension bits are "non data" symbols that maintain an active carrier, and are readily distinguished from data bits by receiving stations. The total burst length can be up to 1500 bytes, which is the maximum frame size defined in the Ethernet standard [24]. The frame bursting technique, shown in Figure 3.8, considerably increases the throughput [2].

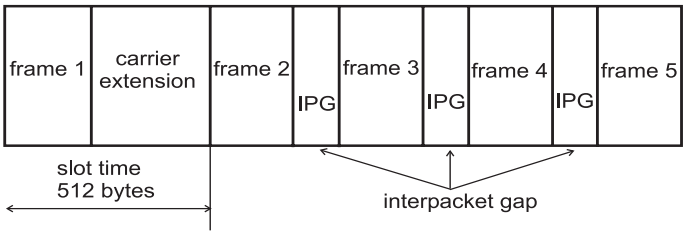

Figure 3.8: Frame bursting in Gigabit Ethernet.

Important to add about the Gigabit Ethernet is that it defines a gigabit media independent interface (GMII) that supports 10-, 100- and 1 000 Mbps data rates. It provides an 8 bit bus for both transmission and reception, so it can support both full-duplex and half-duplex modes of operation. The encoding scheme in Gigabit Ethernet is changed from 4B/5B to 8B/10B. Although this technique allows for good error detection and reliable synchronization of bits it is bandwidth inefficient, introducing 25 % of overhead. The actual signaling speed is thus increased from 1 Gbps to 1.25 Gbps.

3.9 Optical Ethernet networks perspectives

Although the Ethernet standard emerged as a LAN standard, over the last decade it evolved in both speed and span such that it now can be used in the metropolitan and wide area networks.

The original Ethernet standard has limited the network span by introducing half-duplex transmission and collision domains. This has changed when optical Ethernet bridges and switches emerged on the market that separated collision domains connecting several LAN networks together. This enabled an increase in size of the Ethernet LAN. Campus environments were very suitable for installing such networks since bridges connected LANs installed in different buildings together. The optical links between bridges were full-duplex increasing the total bandwidth of the link. The total span of the network was not limited by collision detection, but rather by the limited power emitted from the LED and dispersion in the multimode fiber. Several fiber optic Fast Ethernet standards were used like 100BASE-FX and 100BASE-SX.

Optical Gigabit Ethernet standards that appeared in 1999 specified transmission on both single-mode and multimode fibers. They specified half-duplex transmission and the CSMA/CD mechanism equivalent to the shared LANs of ordinary and Fast Ethernet. However, all of the Gigabit Ethernet networks implemented today utilize point-to-point, full-duplex connections.

As Ethernet was evolving fast, a 10 Gigabit Ethernet standard emerged recently that is based on the full-duplex, fiber-only technology. It uses neither CSMA/CD method nor the copper-based medium. This standard was specified for both local and wide area networks for which two different physical layer types were defined. With the release of the 10 Gigabit Ethernet standard, Ethernet implementation in WANs is expected to become reality. The main reasons are still the speed, cost and simplicity.

The main drawback of the Ethernet protocol is lack of quality of service (QoS). In contrast to other competing technologies like SDH/SONET and ATM that can guarantee quality of service, Ethernet is in essence a best-effort protocol, so no QoS can be provided. This is nevertheless inevitable if the real-time traffic is to be supported, since the users pay only for the guaranteed service. Home networks are one example when Ethernet is not a good candidate. Lack of QoS is the reason Ethernet is combined with technologies like SDH, and this combination gains more and more popularity in the telecom world. Another issue missing in Ethernet protocol is the priority of packets. In many automatically controlled processes some critical decisions must be carried in packets that should have a larger priority with respect to others.

3.10 Conclusions

Although optical fiber has many advantages over copper cable, fiber-to-the-desk network implementation did not reach its full scale. A few optical Ethernet links are implemented nowadays among personal computers within a computer room or small building. The environments where optical Ethernet found its practical implementations are the ones strongly affected by strong electromagnetic radiation.

The lack of optical Ethernet implementation is caused by the fact that the 100BASE-FX standard, which appeared long before 100BASE-SX, was not compatible with the 10BASE-FL fiber optic Ethernet standard. Upgrading the network would require replacing complete installations: every NIC, hub and switch used has to be changed. The only part of the network that would not require changes is the multimode fiber. Another reason is that wavelength sources that were specified for 10BASE-FL and 100BASE-FX standards were not operating in the same region. Moreover, the cost of the long wavelength sources required in 100BASE-FX is high and having them in the NIC at the users site would make the complete fiber-to-the-desk network very expensive.

On the other side, 100BASE-TX standard offered compatibility with the existing copper-based 10BASE-T Ethernet and easy network upgrade. To support network upgrade manufacturers brought 10/100 Mbps switches and NICs that can support both standards. Moreover, dual speed hubs were on the market that allowed both 10 Mbps and 100 Mbps transmission among the end nodes that shared the 100 Mbps available bandwidth, since they belong to the same collision domain.

Nevertheless, 100BASE-TX domination is likely to change once high bitrates have to be offered to the user at longer distances. This especially if Gigabit Ethernet is used, since the copper links that can support 1 Gbps tranmission cannot be more than 25 m long. To have a high-speed connection carried on the distances that exceed 200 m optical fibers have to be used. One example of such connection is the campus environments where optical fiber interconnects routers that on turn connect several LANs and provide WAN access. The aggregate traffic offered to these routers is transported through a high-speed 1 Gbps uplink from the Fast Ethernet switch to which routers and servers are connected.

CHAPTER 4

Optical Ethernet networks for FTTD application

4.1 Introduction

In this chapter different optical LAN architectures for FTTH applications that accommodate Fast Ethernet protocol are presented. The technology for their implementation is also suggested. The proposed networks have short downtime, low maintenance cost, extended geometrical spans compared to the network span specified in the short-wavelength optical LAN standard [33], and larger headroom for future capacity increase. These networks are novel because it is for the first time that the Fast Ethernet protocol runs on a passive optical star network. As a consequence, a few changes in the Physical layer of the IEEE 802.3 standard had to be implemented, since the newly designed networks share a common medium. These changes have to do with the collision detection method and the synchronization of bursty traffic. The fiber-optic Fast Ethernet protocols 100BASE-FX and 100BASE-SX can not be used, since we propose point-to-multipoint transmission in contrast to the point-to-point transmission in optical 100BASE-X networks.

All the architectures are based on short wavelength light sources (F-P lasers

and VCSEL), multimode fiber and multimode integrated optical components.

4.2 Ethernet based optical LAN architectures

To facilitate a smooth transition from existing copper-based networks to future optical LANs we have chosen Ethernet technology since it is the most successful networking technology to date and has been deployed in nearly every corporate and campus network [10]-[12]. The use of Ethernet technology provides low cost, high performance architectures.

A Carrier Sense Multiple Access with Collision Detect (CSMA/CD), on which Ethernet is based, provides equal-priority access to the users of the shared medium. The shared medium however, is not used in Fast Ethernet switched networks where collisions occur only in switches. Introducing switches has disadvantage that they require power supplies and regular maintenance, and a large number of switches can increase costs. Since copper based cables cannot reach more than 100 m, more switches have to be placed to connect larger distances. Another disadvantage of switched networks is delay in the switches. New switches developed and now available on the market overcome this problem, but some delay will always be present compared to passive star couplers, which in passive optical networks, introduce no extra delay. These reasons have led us to base our new network architectures on low-cost passive integrated multimode optical couplers that require neither an electrical supply nor extra maintenance and can be easily coupled to multimode fibers. Passive star couplers also offer us the possibility for point-to-multipoint connection. The firstly proposed optical LAN is the optically transparent network of Figure 4.1, [35, 36].

Network segmentation is done by means of coarse WDM. The network configuration is star formed and segmented in mini-stars, which offers geographical advantages. Each segment of the LAN uses its own assigned wavelength. A common signal transfer path to the router is created by inserting a multimode coarse WDM (de)multiplexer. In this way cabling length, which is determined by the maximum allowable signal delay prescribed by the standard, is reduced. The stability requirements for the lasers are not so stringent since multimode fibers are used and the wavelengths are not so densely packed as in PSTN applications.

The mini-stars comprise the end nodes that show an extensive mutual exchange of information. The geographical spread of these nodes is small, so that

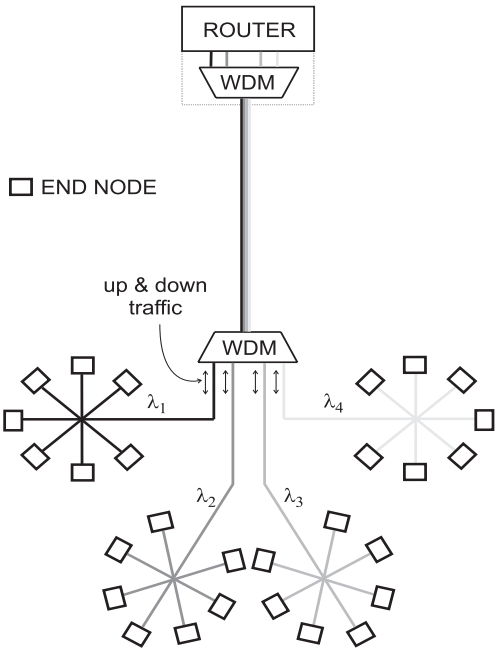

Figure 4.1: Optically transparent LAN for FTTD application based on multiple single-wavelength optical stars using a different wavelength for each mini-star.

a long common transmission line to the router is allowed. The stars are implemented using passive optical star couplers [8]. Electronic circuitry is required only in the router, which facilitates maintenance and reduces the cost.

Since the presented network is optically transparent it gives the opportunity for easy upgrade. Only electronics in devices connected to the network has to be replaced without replacing any part of the networks. There are no expensive bridges and switches in the data path that have to be replaced to accommodate gigabit speeds. This is a very important feature for companies that would like to have a network that can work for at least a decade requiring as little changes as possible, such that it can accommodate higher speeds.

To allow for upgrade, the Gigabit Ethernet protocol has to be implemented in presented architecture. Although no Gigabit Ethernet standard that run on a passive star coupler is specified up to date, it will be shown that solutions that we propose for accommodating the Fast Ethernet protocol on the passive star network can be scaled to work at gigabit-per-second speeds.

One disadvantage of this architecture is found in the fact that NICs in the

end nodes that belong to different mini-stars require different wavelength light sources. Another is the limited span of the network due to the fact that both the end nodes and the router belong to the same collision domain, limited in length by the IEEE 802.3 standard.

To overcome limitation in the network span retaining optical transparency, two alternative architectures are proposed. In those architectures data transmission methods in both LAN and access networks are combined. For up- and down-stream traffic between the end nodes and the router different wavelengths are used. The traffic among the end nodes in the mini-star stays unaltered with respect to the previous architecture. Introducing more wavelengths collision domains can be separated without introducing bridges and switches. The new collision domain comprises only the end nodes that belong to the same mini-star offering the possibility for increasing the network span. The first combined LAN/access network is presented in Figure 4.2.

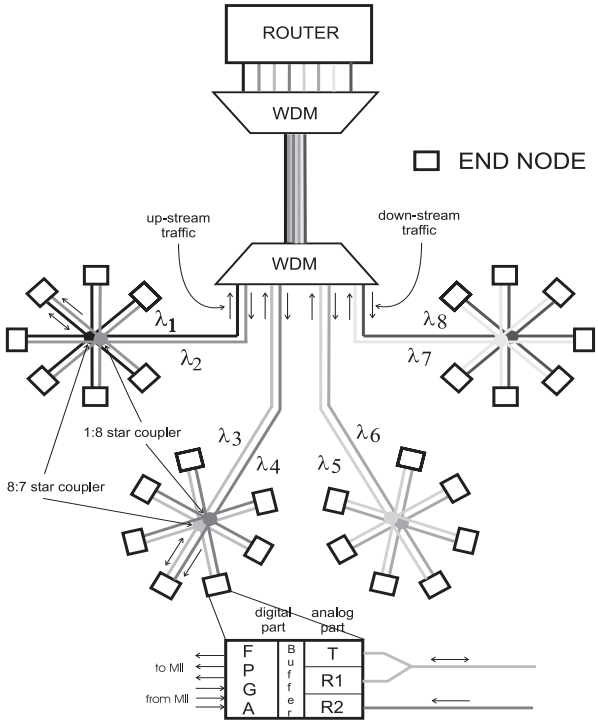

Figure 4.2: Optically transparent combined LAN/access network using different wavelengths for up- and down-stream traffic between the mini-star and the router. The total number of wavelengths in the network is twice the number of mini-stars.

Here an extra 1:N star splitter has been added per mini-star with an extra multimode optical fiber connecting this splitter with the end-nodes and WDM (de)multiplexer. N is the number of end nodes in the mini-star.

One advantage of this architecture with respect to the previous one is that the total bandwidth is shared only among the users within the same mini-star. The number of users is limited by the losses in the star coupler and it is typically about 16 to 32 users. Another is that the network can easily be upgraded to work with the Gigabit Ethernet protocol combining 10 Gigabit Ethernet protocol for the downlink from the router, since this is not a shared medium i.e. no collisions can take place during transmission. This is very important since 10 Gigabit Ethernet is not based on CSMA/CD in contrast to Fast and Gigabit Ethernet. Since Gigabit Ethernet is compatible with Fast Ethernet and moreover, it is essentially based on it, a gradual upgrade of the network is possible, which is a very important issue in the network design. If 10 Gbps is used in the down-stream traffic from the router the total network span is limited to 300 m and 10 km when multimode and single-mode fibers are used, respectively [2].

Further advantage of this architecture is that access network protocols can be used for the down-stream traffic from the router like EPON, [37, 38]. Since the signaling rate in EPON is 1 Gbps, the presented design can be adapted to support it and even offer tenfold increase in bandwidth with respect to EPON networks. This network architecture can be used for both Fiber-to-the-Home (FTTH) and Fiber-to-the-Desk (FTTD) applications.

The disadvantage of this network is that two wavelengths per mini-star are used which requires introducing more different light sources in the network. Moreover, an extra receiver in the end node has to be introduced compared to the first architecture. The total number of wavelengths used can be decreased if the downstream traffic is broadcasted to all mini-stars. In that case only one extra wavelength with respect to number of mini-stars need to be used.

Another way to overcome the drawback of introducing an extra wavelength per mini-star but to keep the downstream traffic broadcasted to individual mini-stars only, we have proposed the third optically transparent architecture where wavelengths for up- and down-stream traffic to (from) the router are reused, as shown in Figure 4.3. In this way we keep the total number of wavelengths equal to the total number of mini-stars. The losses will be lower since no extra WDM (de)multiplexer are introduced. The devices will have smaller dimensions and accordingly less on-chip propagation losses. The disadvantage is that this architecture requires one extra WDM multiplexer and demultiplexer and extra

fiber connecting these two. All the advantages mentioned for the first two architectures sustain.

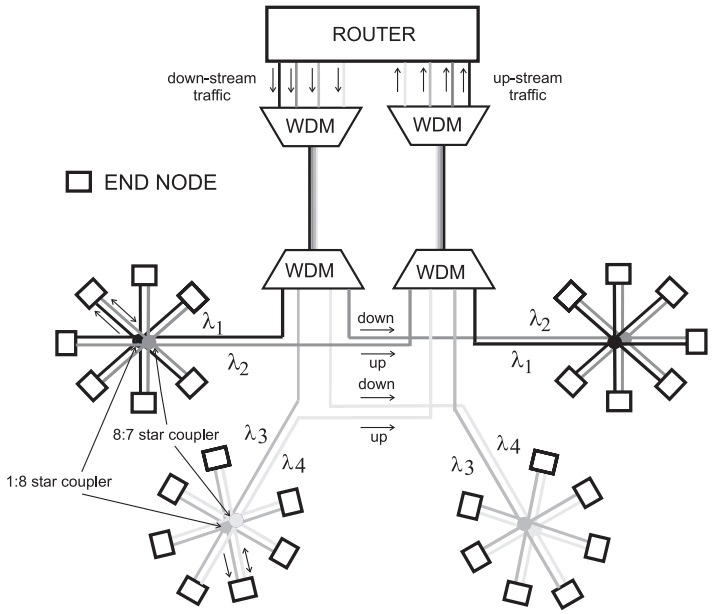

Figure 4.3: Optically transparent combined LAN/access network using different wavelengths for up- and down-stream traffic between the mini-stars and the router. The total number of wavelengths equals the number of the mini-stars.

Common for all presented optically transparent architectures is that up-stream traffic to the router originates from the users sharing the available bandwidth and the down-stream traffic uses a complete available bandwidth. This is in accordance to network traffic distribution where uploading requires much lower bandwidth than downloading.

The cost of NIC implementation can be reduced if all the NICs in the network use the same wavelengths. The best solution from the cost point of view would actually be to have an optically transparent network in which all the users use the NICs with the same light sources. One way to achieve this is to introduce a low-cost monolithically integrated all optical multimode wavelength converter between the passive star coupler and the WDM multiplexer. Nevertheless, no such converter for short wavelengths has been reported to date.

The simplest way to solve the problem of having the same NICs for all the users in the LAN is to introduce an electrical switch, as shown in Figure 4.4,

[36, 40].

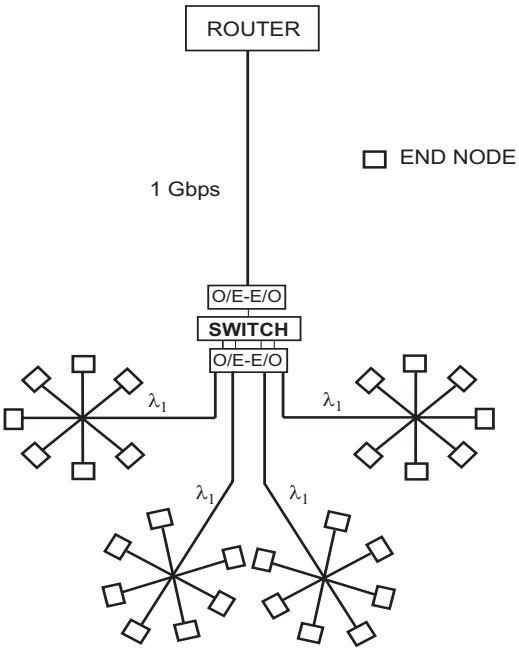

Figure 4.4: Optical LAN for FTTD application based on a switch and a single-wavelength star using the same wavelength for each mini-star.

In this architecture an electronic switch is introduced with a Gigabit Ethernet uplink on a single fiber pair to the router. The uplink can also be made using a single fiber at the cost of the power budget, since an extra splitter/coupler pair has to be introduced to split the up- and down-stream traffic. The cost is a critical factor when choosing a single-fiber or a fiber-pair solution, although this specific cost will be shared among all the users in the network.

The main advantage of this architecture is that the NICs can be identical for the end nodes all over the LAN since all the mini-stars use the same wavelength. The network span can be larger since no collisions can occur in the connection path between the router and the switch. Even larger span can be achieved using single-mode fibers with less attenuation and dispersion limitations.

The disadvantage is that electronic equipment, including the power supply, must be installed outside of the router cabinet, but there is only one switch that connects all the mini-stars whereas the end nodes are interconnected by means of the passive star coupler. Upgrading the network requires not only replacing the NIC at the user's site and NICs in the router but also replacing the switch.

Two other possibilities to overcome the problem of having different NICs in different mini-stars come to mind. One is the introduction of a Fast Ethernet switch that supports parallel switching with an extra coarse WDM (de)multiplexer between the switch and the router to support parallel transmission from and to different mini-stars. This is presented in Figure 4.5.

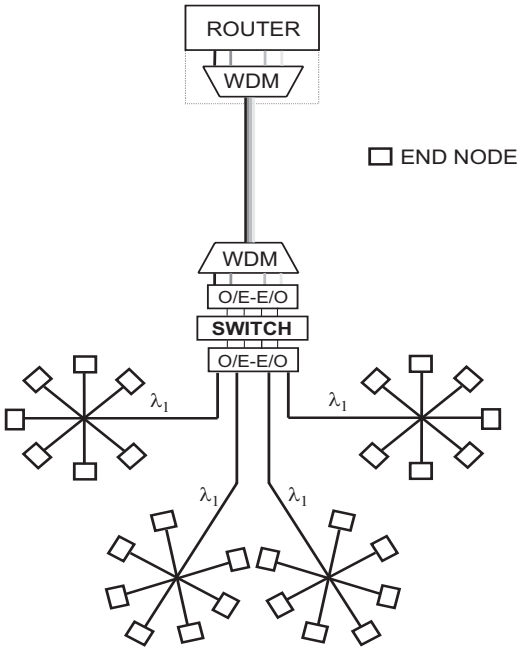

Figure 4.5: Optical LAN for FTTD application based on a switch, coarse WDM and a single-wavelength star using the same wavelength for each mini-star.

Another possibility is to introduce an electronic bridge instead of an electronic switch, as shown in Figure 4.6. This is a cheaper solution offering much smaller throughput since the total bandwidth is shared among all the users in the network.

The overall cost and specific application will guide users in choosing among the proposed architectures. The proposed architectures require changing the Physical layer implementation in the OSI reference model while the MAC sublayer and higher layers remain unaltered. We are actually proposing a new standard, having in mind that 100BASE-SX is also built by making changes only in the Physical layer.

Altering only the Physical layer facilitates network realization and lowers

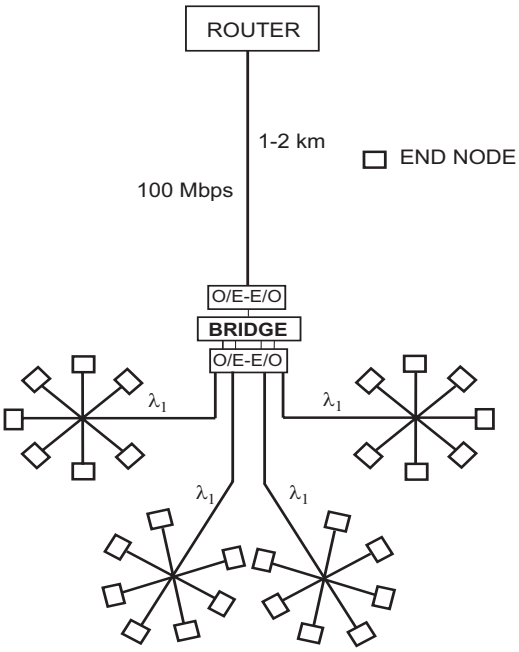

Figure 4.6: Optical LAN for FTTD application based on a bridge, coarse WDM and a single-wavelength star using the same wavelength for each mini-star.

the overall implementation cost. Such a realization is supported by the MII connector between the MAC and the Physical layer by means of which several different Physical Layer Devices (PLD) can work on the existing NIC. Although in the final realization cost consideration will lead to all the functionality of the NIC being integrated, we have concentrated on the realization of a separate PLD that can be attached to the existing NIC equipped with the MII interface to prove the feasibility of the design. Two stumbling blocks, namely synchronization of bursty traffic and collision detection had to be resolved.

4.3 Synchronization

Since all the presented architectures are based on passive star couplers, we have a common shared medium for the signal transmission, inherited from the original 10BASE-FP Ethernet standard. This is in contrast to all the other Fast Ethernet standards where each user has a separate path to a Fast Ethernet hub (bridge or a switch). In those standards synchronization is facilitated since continuous transmission between the end node and a bridge or a switch can be

maintained. When no packets are transmitted the IDLE signal is transmitted for synchronization and PLL technique is used for clock and data recovery. On the other hand, the use of a shared medium in our new architectures excludes this possibility since sending the IDLE signal would result in constant collision. In our architectures the end station is allowed to send only when it has a packet provided that the medium is free, so we had to find a solution for burst traffic synchronization in PON networks. this synchronization technique must be simple such that it can be realized with equipment available in our laboratory.

The synchronization techniques known at the beginning of our project could not satisfy the requirements to achieve synchronization on each incoming packet during the preamble period. For example, integrated circuits using PLL techniques available on the market had a long acquisition time (about 1 μs), which is much longer that the preamble duration (480 ns). Thus, we had to find another solution for synchronization. The Clock Phase Alignment (CPA), nowadays popular in EPONs, was not known yet to us at that time.

The most simplest solution of the synchronization problem is to use a multiplexing technique allowing simultaneous transmission of clock and data signals, for example use WDM introducing an extra wavelength for clock transmission, sub-carrier multiplexing or even spectrally encoded OCDMA [41]. Although these solutions might have been simple to realize, they would most certainly have led to an increase in overall network cost, something that we wished to avoid.

To keep the design simple we decided to use the embedded clock transport (ECT) technique where an analog sinusoidal signal is simultaneously sent in addition to the data signal during the whole packet duration. Provided that the clock signal in the PLD at the transmitting side has been generated using this sinusoidal signal, we can recover data at the receiving side. Separation of the encoded data signal, sent in packets, and the synchronization signal can be performed by using simple filtering, given that the frequency content of the signals do not overlap. Introducing the extra synchronization signal improves detection at the cost of increased power consumption. The ECT technique is simple and effective and it scales very well with bit rate so this synchronization technique can also be used when upgrading the networks introduced here so that they can accommodate the Gigabit Ethernet protocol.

The actual bit-rate of the signal transmitted through the fiber when using the Fast Ethernet protocol is 125 Mbps. To generate these data a 125 MHz clock is used. Since the data signal is NRZI encoded after 4B/5B coding [24], its power

spectral density will have a quadratic Sinc shape with the first spectral null appearing at 125 MHz. This offers us an opportunity to insert a synchronization signal at this frequency as shown in Figure 4.7.

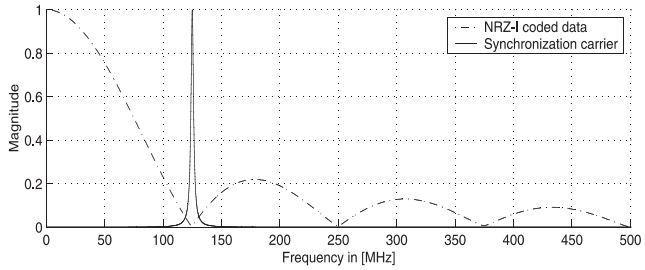

Figure 4.7: Power spectral densities of the NRZI encoded data signal and synchronization signal.

As can be seen from Figure 4.7, a narrow-band 125 MHz synchronization signal cannot seriously affect received data signals keeping in mind that 95 % of the data signal power is contained in the spectrum between the frequencies of 0 and 0.75 times the data rate. This means that we can easily separate the signals by using two filters: a bandpass filter with a center frequency of 125 MHz for the synchronization signal and a low-pass filter with the cut-off frequency of about 95 MHz, for the data signal. This concept is illustrated in Figure 4.8. Noticeable is that sinusoidal carrier introduces increase in bandwidth of the transimpedance amplifier in the receiver. This increase amounts to 30 %, which is one of the disadvantages of using ECT technique.

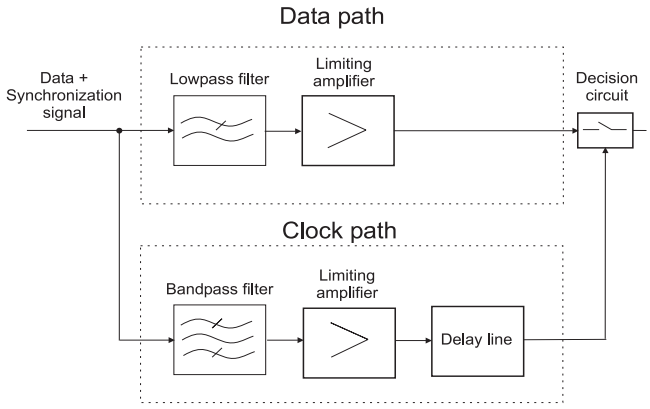

Figure 4.8: A block scheme of the clock and data recovery circuit in the receiver.

Since the synchronization sinusoidal signal has been made from the clock signal, both signals will have the same frequency and a well defined, fixed phase relation. The phase synchronization is performed by introducing a delay in the receiver (clock path). The amount of delay between the clock and data signal is always fixed and depends only on the delay in the Physical layers of both transmitter and receiver. The delay in the fiber for both signals is the same. Thus, by introducing a proper delay in the receiver phase synchronization can be achieved. The disadvantage of the receiver presented in Figure 4.8 is that the clock path is feedforward so it is difficult to control delays with temperature variation.

The recovery time of the synchronization signal will depend on the type of bandpass filter used and its response time. The best choice can be found by studying the tradeoff between quality factor and filter response. On one hand we would like to have a filter with a rather narrow passband to eliminate the presence of the data signal and on the other hand, we need a short response time of the filter to achieve fast synchronization. The amplifiers placed after the filters serve to make a clock signal out of the synchronization sinusoidal signal in the clock path and amplify the signal amplitude in the data path. A decision circuit is used for data recovery.

Note that for synchronization purpose we really need the preamble at the beginning of the data packet in contrast to existing Fast Ethernet standards that do not require a preamble of the packet due to the constant signaling technique they use. This is one of the differences between our architectures and existing ones.

4.4 Collision detection

Collision detection is a mechanism that has been added to CSMA/CD, which has been implemented in the MAC sublayer. This mechanism assures that a given station will not start sending packets as long as another station in the same collision domain is occupying the shared transmission medium. Furthermore, it will discontinue transmission in case an incoming signal from another station is detected. To detect that shared transmission medium is occupied the end station is "listening" to the medium. This is called carrier sensing.

Several collision detection methods have been proposed for fiber optic CSMA/CD networks [21]. We chose to use a Directional Coupling method

in combination with Average Power Sensing due to the simplicity of implementation. The Directional Coupling method uses a special coupling, or interconnection technique, which assures that the transmitting station can listen to all stations but itself. Collision detection in this system is straightforward. If a station senses data at its receiver while it is transmitting, it means that some other station is also transmitting and thus a collision has occured. But, at the beginning of the receiving process, synchronization has not been achieved, thus no data bits can be recovered. To detect a collision we have to combine another method, namely Average Power Sensing, in which detection of the incoming signal is determined based on the average power carried.

To implement this type of collision detection a special reflective type star coupler has to be used. The idea for implementing such a coupler has been proposed in [42]-[44], but we want to realize it as a low cost multimode polymer based integrated-optic component [45]. Depending on the optical star design one or two fibers can be used per user for signal transmission. In the case of one fiber system, fiber cost is lower but an additional 2x2 coupler must be placed before the transceiver in the NIC to split up- and down-stream traffic.

Another condition for this type of collision detection is that all the sources in a given mini-star use laser diodes of identical wavelength, which is exactly the case in our architectures. This is due to the wavelength dependent loss of the star coupler that for two different wavelengths of 800 nm and 850 nm can have a loss difference of 2 dB. In order to predict a link budget that fits all the hosts, the output power of laser diodes in each of the hosts should be nearly identical. Fluctuations in the transmitting lasers will always occur and must be reflected in the threshold level for carrier sensing.

To implement the collision detection mechanism we have to calculate the optical power level at the photodetector in all the architectures. It is obvious from Figure 4.1 to Figure 4.6 that the optical signals in every mini-star are physically separated from the signals in other mini-stars, so collisions will occur only within a single mini-star. To calculate power levels we have to take into account losses in the fiber, connectors, star coupler and in the first architecture the WDM (de)multiplexer. The main signal attenuation will be in the passive star coupler [8], especially if more users are connected to the same mini-star. Laser output power must be sufficiently large to compensate for the losses. In the firstly proposed architecture, lasers that are built in the router NICs must supply a larger output power to compensate for the WDM losses such that the signal received from the router does not differ much in power level with respect

to the signals received from another end node within the same mini-star. To include degradation of the components with aging some margin must also be taken into account.

In an ideal case when a signal is received that is larger than a certain noise level the carrier from another end station will be sensed. An appropriate signal (`CRD`) that goes to the MAC sublayer will be set high to indicate that an other end station is already occupying the transmission medium. In the case that no other end station is transmitting, no signal on the line will be detected. On the other hand, if the level of the received signal in case a packet is transmitted is high enough, carrier sensing will be simple. The digital part of the PLD now checks whether the end station is transmitting at the same time, and if that is the case, activates the collision mechanism in the MAC sublayer. In case the end station is not transmitting, it defers transmission according to the CSMA/CD protocol.

But, sending the synchronization signal requires that the light source in the transmitter works in its linear regime, which means that there will always be some light transmitted, even when no data packet is sent. This will be elaborated in Chapter 5. Although the received power level is low, it has to be taken into account when more users are connected to the same mini-star. To sense the carrier we must have signal level difference in the case that no packet is transmitted and in the case that the signal is transmitted. Taking into account all the variations in signal levels caused by the lasers and passive optical components we have to place a threshold between the two levels such that the carrier sense signal is high when the threshold is crossed. This is presented in Figure 4.9. The threshold level will mainly depend on the type of lasers used in the system and the number of end nodes in the mini-star.

Since the data packet is accompanied by the synchronization signal there are three possibilities for measuring the received signal level which will be used to determine the threshold. We can either separately measure the average value of the data and the synchronization signal after filtering or the level of the combination of both before that.

Provided that the signal is encoded and possibly scrambled, it is very difficult to measure the mean of the data signal, for example after integration, since the value varies depending on the integration constant. The larger the integration constant the more accurate the result is, but the time for the carrier sense is longer and that will cause a decrease in throughput. On the other side, if we want to measure the mean value of the synchronization signal in the absence

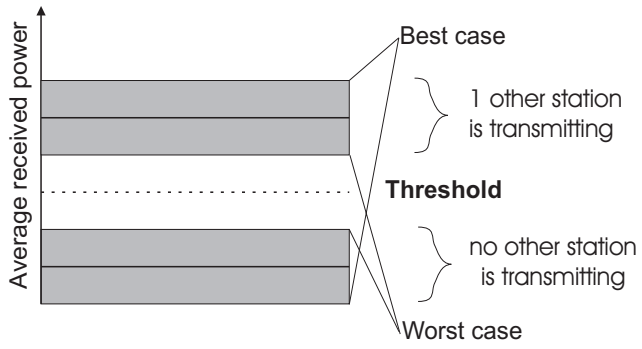

Figure 4.9: Threshold level determination for the carrier sense.

of the data signal, since it should yield a more constant value after a shorter integration time, we will get zero since the DC component is eliminated by means of a bandpass filter. Some methods can be used to overcome this problem but this would only complicate the design. The simplest method for determining the received signal level is to measure it before the signals are split into data and synchronization paths (Figure 4.8). Tapping a part of the signal in the receiver and bringing it to the integrator is the best way to determine the received signal level. Although the value obtained varies with the integration constant due to changes in the data, we can set the threshold based on the level obtained from the synchronization signal only and the mean data value will only contribute to exceed that threshold in the case that the data signal is unipolar. If the threshold is reached, then the carrier is sensed. Based on this signal we can detect a collision by sensing the simultaneous presence of the transmitted signal.

4.5 Performance analysis

The performance analysis of networks is made with respect to both attenuation and dispersion limitations as well as the signal delays in the transceivers and fiber.

4.5.1 Performance analysis with respect to attenuation and dispersion

The design of an optical system is a balancing act. The top two technical considerations are power budget and transmission capacity, or bandwidth. The power budget calculation is needed to assure that enough optical power reaches the receiver to give adequate performance. The calculation should leave some extra margin above the minimum receiver sensitivity to encounter system aging, temperature fluctuations and repairs. However, the received power should not overload the receiver. The transmission capacity of an optical fiber system is the highest digital bit-rate it can carry [16]. In order to determine the transmission capacity we have to determine the dispersion effect in the system to assure the system can handle signals at the speeds we want to transmit.

To determine the effect of both dispersion and attenuation on the performance of presented systems both analytical calculations and simulations using the program package MATLAB have been made.

We built our simulator such that it either gives the maximum number of users in the mini-star and the number of mini-stars in the optically transparent architectures, given the maximum bit-rate of the signal it has to support, or the fiber length limitation due to dispersion and attenuation given the maximum bit-rate of the signal transmitted on the fiber, number of users per mini-star and the losses in WDM (de)multiplexer. These losses are taken into account only in the optically transparent architectures.

To simulate the effect of attenuation on system performance, a calculation of the received power, based on minimum transmitted power and losses in the system, has to be done. Based on this received power a maximum bit-rate that a system can support can be calculated for a given sensitivity of the receiver (Equation (4.1)). Moreover, calculation of the maximum bit-rate the system can support based on dispersion has to be done to determine dispersion limitations of the system. Finally, based on the maximum bit-rate a system can support a fiber length limitation can be calculated from the bit-rate-distance product.

To calculate the maximum bit rate B_0 that can be transmitted over a link with length of L with a given BER the sensitivity of the receiver has to be specified. This is defined as the minimum number of photons per bit necessary to guarantee that the BER is smaller than the prescribed rate. In our case BER=10^{-9}. A sensitivity of n_0 photons corresponds to optical energy $h\nu n_0$ per bit and optical power [4]

$$P_p = 10.5\frac{h\nu n_0 B_0}{\eta} \tag{4.1}$$

where we assumed Poisson statistic of the photon arrivals. In Equation (4.1) η is the quantum efficiency of the photodetector, which is for simulation purposes taken to be $\eta = 0.9$. For the receivers operating at λ_0=0.87 μm n_0 is approximately 300 photons per bit and this is the number we have used in our calculations.

If the received power calculated from the power budget is larger than the receiver sensitivity, the difference can contribute to increase either the fiber length or the number of users per mini-star. It can be seen from Equation (4.1) that by varying the maximum bit-rate of the data signal in the network, different receiver sensitivities are obtained. For each of them a difference with respect to received power obtained from the power budget can be calculated and based on that the maximum fiber length L can be determined.

Calculations of the received power in presented optically transparent architectures must include WDM (de)multiplexer losses. This means that the presented architectures containing a bridge or a switch can support more users per mini-star or that they can have a larger span. It is obvious that most of the losses in both architectures will be introduced by the passive star coupler. For simulation purposes we have used the expression for attenuation of the multimode integrated-optic polymer-based star coupler since such a coupler has been used in the experiments [45]:

$$A_c = 10\log(N-1) + 4 \quad [\text{dB}] \tag{4.2}$$

where N is the total number of users in the mini-star interconnected by the star coupler. We have encountered in Equation (4.2) measured propagation losses of 1.3 dB, fiber-chip coupling losses of 0.7 dB and mode dependent losses that are less than 2 dB. Note that $N-1$ is used in the expression due to a special construction of the star coupler in which user that transmits does not receive its own signal.

The losses of WDM (de)multiplexers used in simulations of the first architectures are based on measurements [7]. Extra losses in the system that are included in the simulations are connector and splicing losses. Connector losses

are taken to be 0.4 dB at maximum and splicing losses about 0.2 dB, which is a typical value obtained from measurements. Calculations comprise typical multimode fiber losses of 2.5 dB/km for wavelengths of optical light around 850 nm. The power from the light source is taken to be 1 mW, although this value can go to 2 mW in F-P lasers and VCSELs used in our experiments (Subsection 5.5.1).

To calculate the system dispersion limitation the procedure given in [3] is used. Since the modal dispersion is the main limiting factor in our system, calculation of chromatic dispersion is avoided. If the width of the received pulse that increases as the fiber length L increases exceeds the bit time interval $T = 1/B_0$, the performance begins to deteriorate as a result of intersymbol interference. Thus, to calculate the maximum fiber length that the pulse of a width T can travel along the fiber of length L that is used in the system, we will use the expression for the bit-rate-distance product in the graded-index multimode fiber [3]

$$L \cdot B_0 = \frac{2c_1}{\Delta^2} \tag{4.3}$$

where c_1 is the speed of light in the fiber and Δ is the fractional difference in refractive index between core and cladding in an optical fiber. For the fiber used in the systems $\Delta \approx 0.01$.

The simulation results for the first architecture with 4 mini-stars and 16 users per mini-star is shown in Figure 4.10. The emitted power was 0 dBm and receiver sensitivity -38 dBm. Power margin is taken to be 3 dB.

It can be seen from the curve (a) in the Figure 4.10 that the maximum fiber length between any two computers in the system can be about L=1.3 km for the bit-rate B_0 of 125 Mbps. As predicted, the main limitation in the system comes from attenuation. The obtained maximum fiber length is much larger than the length specified by the protocol [24, 33]. Nevertheless, fiber length in the implemented network will be limited by the protocol and not by dispersion or attenuation. The results of simulation for the architectures that contain a bridge or a switch is presented as curve (b) in Figure 4.10.

We see that the total fiber length can be larger in the architectures where the router is outside of the collision domain comprising the end nodes in the mini-star, since there are no WDM (de)multiplexer losses. Another possibility is to have more users per mini-star for the same fiber length.

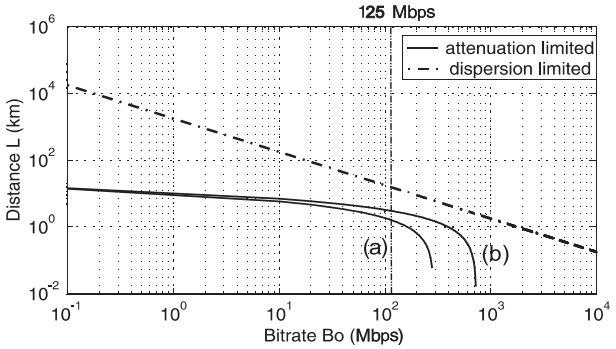

Figure 4.10: Maximum fiber length versus bit rate for the system with 4 mini-stars and 16 computers in the mini-star with (a) and without (b) WDM (de)multiplexer. Both attenuation in the system and dispersion in the fiber are taken into account.

4.5.2 Performance analysis with respect to delays

To determine maximum network span remind that the maximum propagation delay is the maximum round-trip time taken by any two stations in the network and is defined to be 464 bit times [24]. Slot Time, which corresponds to 512 bits, determines the upper bound on the acquisition time of the network and should be no longer than the sum of propagation time and the Jam time. It also restricts the length of the network. Since we do not use the Jam time (Section 5.2) we can afford to have longer propagation time, (512 bit times instead of 464), which results in a larger network span, since we already showed that restriction on the total network span comes from the protocol and not from attenuation or dispersion in the fiber.

The maximum delay caused by the cables and the other components in the signal path should not exceed the Slot Time. Keeping this in mind the total delay is given by [10]:

$$\text{PDV} = \text{link delays} + \text{repeater delays} + \text{ end station delay} + \text{safety margin} \tag{4.4}$$

The end station is the first factor in determining the round-trip delay. The measured delays in the new PLD showed that these are well within the limits of the specified value of the delay in the end station of 50 bit times [24]. The measured delays in the digital part of the PLD are presented in Table 4.1.

Table 4.1: Bit delay constraints: MDI to MII delay constraints (exposed MII, half duplex mode).

Sublayer measurement points	Event	Max (bits)	Standard specified values (bits)
MII ⇔ MDI	`TX_EN` sampled to MDI output	8	14
	MDI input to `CRD` assert	17	20
	MDI input to `CRD` de-assert (aligned)	22	24
	MDI input to `CRD` de-asserted (unaligned)	17	24
	MDI input to `COL` assert	17	20
	MDI input to `COL` de-assert (aligned)	22	24
	MDI input to `COL` de-asserted (unaligned)	17	24

It can be seen from this table that all the delay constraints from [24] are satisfied. In making calculations to determine the maximum network span, the worst case total delay in the end station (50 bit times) will be taken into account.

After subtracting the sum of delays in both transmitter and receiver from the Slot Time, 412 bit times will left over. This 412 bit times can be considered as the maximum bound in calculating the span of proposed networks, since we do not have a repeater delay. Keeping in mind the bit time of 10 ns in the Fast Ethernet networks and the light propagation speed in fiber ($0.67 \cdot c$) we have calculated that a maximum network span is 412 m. This value outperforms the existing 100BASE-SX network, standardized by TIA/EIA as it can have a maximum span of 300 m [33].

Apart from increasing the network span, having no repeaters in the network and avoiding using the Jam signal can slightly increase the throughput with respect to the 100BASE-X network [24]. In the existing Fast Ethernet networks the backoff algorithm starts by the transmitting stations after at least 64 bits of the preamble and 32 bits of the Jam time. Thus, it takes at least 96 bit times. In our proposed scheme carrier sensing can be done well within the preamble time,

so collision detection can also be detected faster, causing the backoff algorithm to start earlier. The theoretical increase in throughput will be proportional to the product of the total number of collisions, e.g. backoff times, and the 32-bit Jam time.

4.6 Comparison with the existing Fast Ethernet networks

Based on the analysis given in this chapter and description of the existing Fast Ethernet networks given in the previous one, comparison among different standards is made. The key factors are the cost and upgrading possibility and the total network span. The Table 4.2 summarizes characteristics of different standards. The advantages of the proposed networks with respect to existing ones are with respect to cost, reliability and the possibility for future upgrade. The disadvantage is that they are not compatible with Ethernet networks.

Table 4.2: Comparison among different Fast Ethernet standards.

Description	100BASE-TX	100BASE-FX	100BASE-SX	MOUSE
max. unrepeated segment length [m]	100	412 2000	300	412
Cabling type	UTP	multimode fiber single-mode fiber	multimode fiber	multimode fiber
connection type	point-to-point	point-to-point	point-to-point	point-to-multipoint
NIC cost	low	high	medium	medium
upgrade	high	medium	medium	high
reliability	low	medium	medium	high
maximum number of end stations per collision segment	high	high	high	low
interoperability with previous standards	yes	no	yes	no

4.7 Conclusions

In this chapter several network architectures for FTTD and FTTH applications are presented. They are all suited for lowering the cost of bringing optical fiber all the way to the user. To achieve this the designs are primarily based on the

most widely used Ethernet protocol. Moreover, multimode fibers are used together with multimode polymer-based integrated star couplers and coarse WDM (de)multiplexers and short wavelength lasers and detectors. Further decrease in costs is achieved through the lower downtime of the network, lower maintenance cost and the possibility for future upgrade. The last feature especially applies to the optically transparent architectures.

The main problems to be solved in making the new PLD for presented architectures, such that they accommodate the Fast Ethernet protocol, were synchronization and collision detection. Collision detection has been solved by using a special construction of the multimode star coupler and synchronization of bursty traffic is solved by introducing a sinusoidal synchronization carrier that is sent through the fiber together with the data packet and switched on and off with it. This implies using the packet preamble which distinguishes our networks from all the other Fast Ethernet networks that do not make use of the packet preamble due to the constant signaling technique implemented among the end stations.

The architectures presented can also accommodate the Gigabit Ethernet protocol. To achieve this only NICs at the user's site and NICs in the router have to be replaced. It would appear that solutions for synchronization of bursty traffic and collision detection, presented in Sections 4.3 and 4.4 respectively, can be scaled to the Gigabit Ethernet signaling rate of 1.25 Gbps facilitating a new Gigabit Ethernet NIC realization.

The presented performance analysis shows that the presented architectures may offer slightly better throughput performance with respect to 100BASE-X networks. With respect to its short wavelength counterpart Fast Ethernet standard 100BASE-SX, presented optically transparent networks are more reliable and can have a more than 100 m larger span. Moreover, they potentially can be realized and upgraded at lower cost due to their all-passive nature.

CHAPTER 5

Transmitter design and implementation

5.1 Introduction

The Physical Layer Device for suggested architectures, which is made to show the feasibility of the proposed networks, comprises the transmitter and receiver which in turn contain analog and digital circuitry.

This chapter describes the functionality and design of both the digital and the analog part of the transmitter. The design takes into account the two most important issues, namely synchronization of bursty traffic and collision detection.

Based on the configuration presented in Figure 3.3, it is required that the transmitter must accommodate data packets coming from the MAC sublayer via the MII interface. The delay constraints in both the analog and digital part of the transmitter must comply with the standard. Looking from the medium side, the output of the transmitter is not standardized e.g. there is no Fast Ethernet protocol that specifies transmission in the passive-star based optical network and we used this fact to adapt the signals for transmission in the proposed optical networks. A block scheme of the transmitter is given in Figure 5.1.

The digital circuitry is connected to the MII connector of the NIC. The data

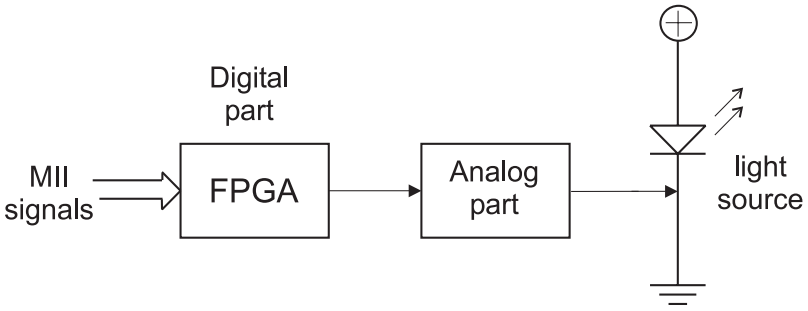

Figure 5.1: A block scheme of the transmitter.

coming from the MAC sublayer in the NIC is processed in the digital part of the transmitter and brought to the analog part circuitry where it is processed further for the transmission through the optical fiber.

5.2 Digital part of the transmitter

There are several differences between the standardized PLD for optical fiber NIC and our proposed PLD. First of all we do not use an IDLE signal for synchronization to avoid constant collisions. Moreover, we do not require the Jam signal, which is used by the Ethernet hub to denote that some other station is transmitting, commencing the collision detection process. This is due to the fact that we have here a point-to-multipoint connection where all the end stations are sensing the shared medium at the same time. Data scrambling can be avoided due to high transmission bandwidth of optical fiber. The preamble of the data packet is slightly changed due to the synchronization problem. Since the synchronization will not be established during the first several bytes of the data packet, we cannot place a Start of Stream Delimiter (SSD) at the beginning of the preamble, since it will not be detected. In the original standard this has been used to distinguish data packets from the IDLE signal. Thus, to detect the beginning of the packet the safest way is to put the SSD just in front of the Start of Frame Delimiter (SFD), so we can be sure that the synchronization is achieved at that point in time and that packet can be recognized. This is illustrated in Figure 5.2.

Another extra feature that we have inherited from the original 10BASE-T Ethernet is the Jabber Detection. This is important for disconnecting an end station that is continuously transmitting, leading to a constant collision. After

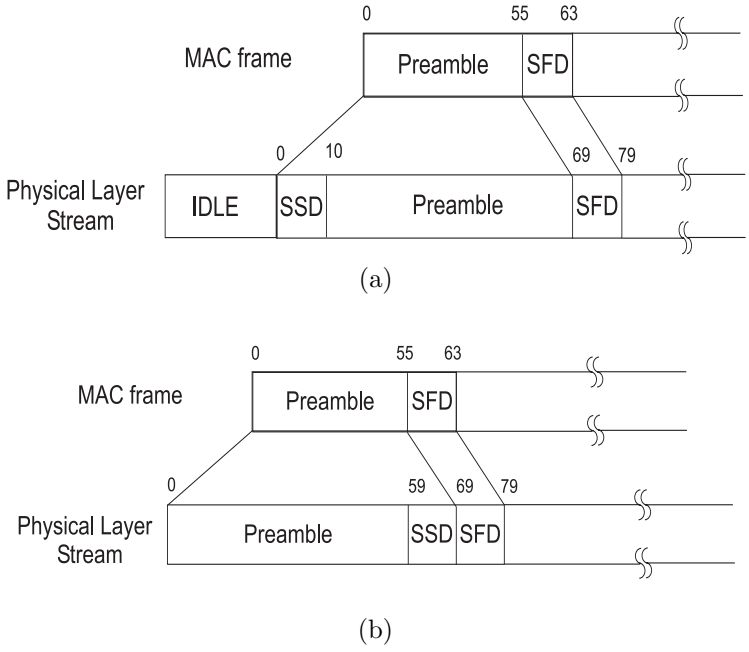

Figure 5.2: (a) The IDLE signal and the Fast Ethernet packet in the 100BASE-X standard, (b) Modified Fast Ethernet packet: Start of Stream Delimiter is inserted just in front of the Start of Frame Delimiter to make sure that synchronization is achieved. The IDLE signal is removed due to the use of shared medium.

some predefined time, Unjab time, a station can be connected again. To disconnect a station a special signal is used that switches off the laser by decreasing its bias current. All the other functions stay the same. We have to stress that PLDs must have an internal clock running at 125 MHz that can be switched from free-running frequency to the frequency determined by the incoming synchronization signal, which is specified by standard. This is important since we have a synchronization signal only during data packet duration.

According to description of the line coding given in the Chapter 3, parallel data coming from the MAC sublayer in nibbles of 4 bits will be 4B/5B encoded, since such scheme provides control codes in addition to the ordinary data codes. Particularly the SSD control code is necessary to provide frame and byte alignment. Moreover in combination with NRZI encoding it smoothes the power spectral density of the data (Chapter 3). This is the reason we have decided to keep the 4B/5B and NRZI encoding in our scheme. Due to less bandwidth

limitation we do not need to use scrambling, but this is implemented in the design as an optional feature.

5.2.1 Transmitter block scheme

The block scheme of the transmitter is given in Figure 5.3. Presented sub-modules run in two clock domains, namely 25 MHz and 125 MHz.

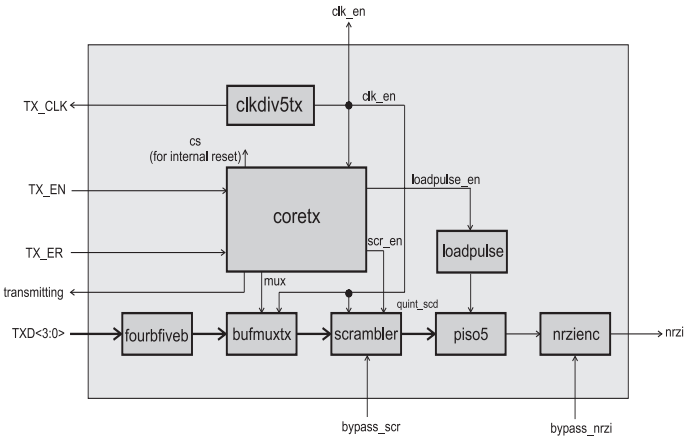

Figure 5.3: The transmitter block diagram.

Apart from the standardized MII signals between the Physical layer the MAC sublayer as inputs to the transmitter we have introduced two more:

`-bypass_nrzi`: Active-high static input signal to bypass NRZI encoding/decoding;

`-bypass_scr`: Active-high static input signal to bypass scrambling

The presented output signals are standardized [24].
The sub-modules, presented in Figure 5.3 that run at 25 MHz are:

- **clkdiv5tx** - divides the 125 MHz nominal clock into 25 MHz. The output is connected to the `TX_CLK` output. It also provides a clock enable signal `clk_en`, which is used by **coretx**, **bufmuxtx** and **scrambler**. This signal is also used by the Jab counter and the Unjab counter in the Jabber detection that is implemented as a part of the transceiver.
- **fourbfiveb** - serves as the 4B/5B encoder. It encodes the `TXD`$\langle 3:0 \rangle$ into the 5-bit code-groups.

- **bufmuxtx** - is a frame composer. It is controlled by the **coretx** via the `mux` signal. It puts the SSD, ESD and transmit-error 5-bit code-groups into the frame when **coretx** signals it to do so. Otherwise, it will just pass the frame (which is already encoded by **fourbfiveb**). In case of no transmission, the output of this block is a low level signal (logical "0").

- **coretx** - controller of other sub-modules. As such, it is a state machine. It takes `TX_EN` and `TX_ER` input signals, along with the `pre_count` signal, which is internal to this sub-module (from internal counter), as the condition signals. The state machine runs by using the clock enable signal from the **clkdiv5tx** sub-module.

- **scrambler** - performs parallel Frame-Synchronous Scrambling on the data stream under **coretx** control. However, if the `bypass_scr` is asserted, it will not perform scrambling. It will just pass the data stream instead. Although it runs at 25 MHz its linear feedback shift register runs at 125 MHz.

The following sub-modules run at 125 MHz:

- **loadpulse** - produces a load signal that is used by **piso5** to load the parallel data stream into its shift registers. The **coretx** signals the **loadpulse** when to start producing the signal with the `loadpulse_en` signal.

- **piso5** - is parallel-to-serial converter realized with a shift register. The parallel data stream is loaded when the load signal is high and the serial data stream is sent out.

- **nrzienc** - encodes the serial NRZ data stream into NRZI format. The output of this block is `nrzi` signal. However, if the `bypass_nrzi` is asserted, it will not perform NRZI encoding. It will just pass the data stream instead.

The output signal `transmitting` is set high when a data packet is transmitted and is used in combination with `receiving` signal in the receiver for collision detection.

5.3 Digital part design and simulation results

To realize the digital part of the PLD implementing the blocks described in the previous section a piece of hardware is required. The simplest way is to use an

Application Specific Integrated Circuit (ASIC) or to combine different ASICs together to achieve the functionality. In lack of such components on the market a different solution is needed.

One solution is to use a Field Programmable Gate Array (FPGA) chip placed on a printed circuit board (PCB). In this FPGA chip the complete digital part functionality can be programmed. Since the chip can be programmed many times it is very suitable for prototyping. To choose the appropriate FPGA chip for the digital part of PLD implementation, the following requirements must be fullfiled:

1. The FPGA chip must be able to process data at speed of 125 Mbps.

2. The number of logic elements must be large enough to support full design. The FPGA chip has to allow future extensions and modifications.

3. The software for developing complete digital circuitry must be available, as well as the design knowledge of the laboratory personnel.

To support high data rates a good choice is to use a differential signaling type since it is less sensitive to environmental influences. One of such a signaling type is Low Voltage Differential Signaling (LVDS); an IEEE standard designed for low electromagnetic interference. If the analog circuitry in the transceiver uses an other signaling type an appropriate level translator chip has to be implemented.

The extension feature of the FPGA is important if additional functionalities in the Physical layer are required. This will inevitably increase the cost of the FPGA chip. The best choice can be found from the tradeoff between the chip size and complexity on one side and cost on the other side.

Having knowledge and experience with Altera FPGA chip design, the choice is made for the Altera EP20K1500EBC652-1x chip from the 20KE family. Based on previous implementations [46] it was proven that this chip can support data rates of 155 Mbps, which is already higher than 125 Mbps required in our system. Our laboratory was already equipped with the necessary software tool for digital circuitry development.

5.3.1 Design steps

To realize the digital circuitry three design steps are taken. First of all, a VHDL description of the transmitter functionality is written without knowledge of the

FPGA chip available for implementing the design. VHDL is an abstract language that can be used to model a digital system at many levels of abstraction, ranging from the algorithmic level to the gate level. To verify the expected behavior of the VHDL code a functional simulation has to be made. To do this the input signals have to be defined in a file called the testbench. Based on input signals and the VHDL code the simulator calculates the output signals. For this the ModelSim software from ModelTech is used.

Secondly, a netlist with the necessary hardware components with connections among them is made such that functionality of the transmitter can be realized in the chosen FPGA chip. This netlist is created from the VHDL code with the synthesis tool Leonardo Spectrum software from Mentor Graphics.

Once the netlist has been created, the place and route software Quartus from Altera is used to map the netlist onto the available logic resources inside the FPGA. This is done in such a way that proper timing is satisfied for the required processing speed. The output of Quartus is a file that can be downloaded into the FPGA chip. Quartus also makes a VHDL file that can be used for simulating the final behavior of the FPGA at gate level, taking into account the used logic resources in the FPGA chip. Simulation is done using the ModelSim software. Obtained results should match the ones obtained in the simulation at the algorithmic level (first step).

The simulation results at the gate level, obtained after processing the MAC packet, are presented in Figure 5.4. The beginning of the packet is shown only for the sake of clarity of representation. The signals marked with "G" are generated by the testbench file and are used as the input for the VHDL code. Other signals represent the output.

From the output signal `NRZI_OUT` at Figure 5.4 it can be seen that input signals `TXD_G(0..3)` are 4B/5B encoded and serialized. Both NRZI encoding and scrambling are bypassed for the sake of simplicity of presentation. The SSD is inserted just in front of the SFD as required for synchronization.

Apart from the functional simulation that shows the output waveforms, Quartus software contains also a static timing analyzer. This analyzer reports the delay of every design path in the FPGA after placing logical resources and routing paths among them, and reports the performance of the design in terms of maximum clock speed. Reported delays represent the worst case. The timing parameters calculated in the static timing analyzer for the transmitter are given in Table 5.1.

All the parameters given are satisfying the requirements. The setup times

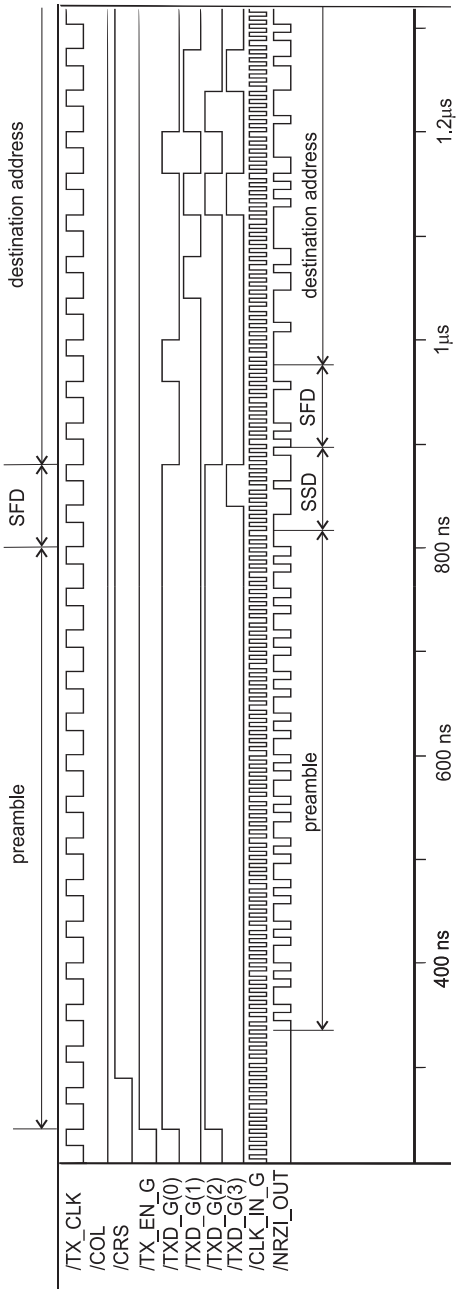

Figure 5.4: Simulation results of processing the Fast Ethernet MAC packet obtained from the VHDL file generated by the Quartus software.

Table 5.1: Timing parameters from the static timing analyzer.

Transmitter		
Timing	Signal	Value
Setup time	TXD[0]	11.9 ns
Setup time	TXD[1]	11.6 ns
Setup time	TXD[2]	12.0 ns
Setup time	TXD[3]	13.5 ns
Setup time	TX_EN	11.8 ns
Setup time	TX_ER	11.6 ns
Clock to Output time	TX_CLK	10.6 ns
Clock to Output time	NRZI_OUT	2.2 ns

are much shorter than the period of data signal at the input of the digital part of the transmitter (40 ns). The Clock to Output time for the NRZI_OUT signal should be less than 8 ns and for the TX_CLK less than 40 ns. Obtained results showed that this is also satisfied.

If both static timing analysis and the functional simulation of the FPGA when available hardware components are taken into account are giving correct results, the design is expected to be correct. To finally test the design measurements have to be performed on hardware implementation of the digital part.

5.4 Experimental results of the digital part

The digital part of the transmitter has been experimentally demonstrated to verify the ability of the new PLD to process the data packets together with management signals according to the requirements. The setup comprised both digital and analog circuitry, but the results obtained from testing the analog circuitry will be given later on in this chapter.

To test the complete system the PING program is used. This is an application that makes use of the ICMP (Internet Control Message Protocol) protocol, and allows user of one end station to test the accessibility of another one. The ICMP messages are encapsulated in IP packets. When a PING message is received by the receiving end station (PC), it sends back an echo reply message (PONG). If the reply message appears on the screen of the sending PC, the functionality of the system is correct. The experimental setup for complete transmitter is shown in Figure 5.5.

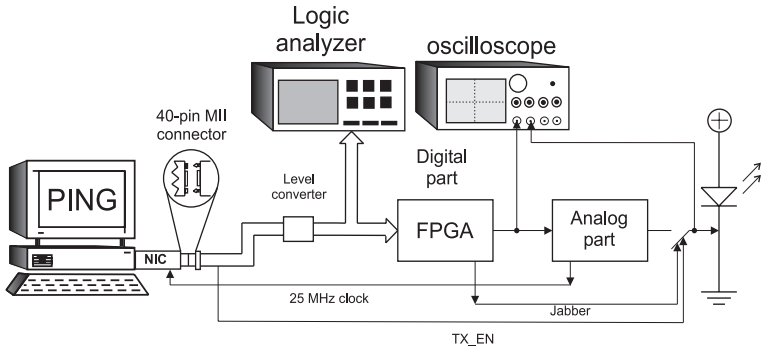

Figure 5.5: The experimental setup for the transmitting part of a new PLD in FTTD network.

The digital data that is to be transmitted through the network in the form of the Fast Ethernet packet is applied via a 40-pin MII connector to the input of the PCB with the FPGA chip. The cable length between the MII connector and this PCB must be short enough to avoid extra delays in the transmitter. A logical level converter is placed in between to convert the TTL signals from the MAC sublayer to Low Voltage TTL (LVTTL) signals that are brought to the Altera FPGA chip mounted on the PCB. This PCB is shown in Figure 5.6.

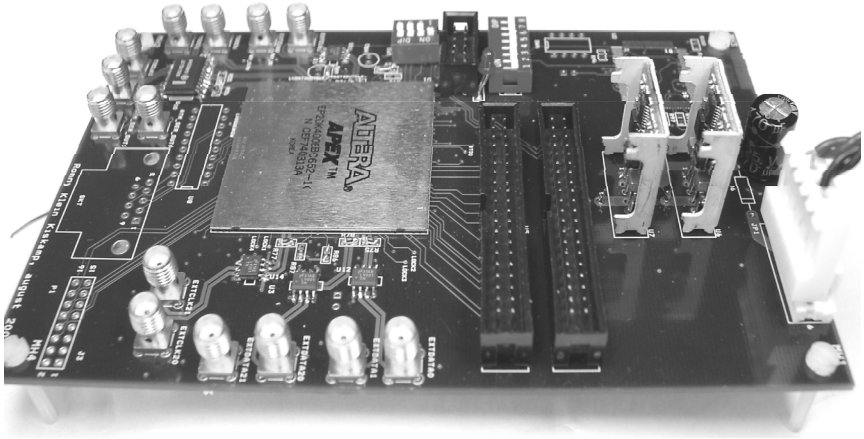

Figure 5.6: The PCB with complete digital circuitry of the Physical Layer Device.

For proper functioning of the NIC the analog part of the PLD provides a 125 MHz clock, since the digital part uses this clock for processing the serial

data stream that is going to (coming from) the analog part.

The parallel input signals are processed in the FPGA according to specifications given in Section 5.2. After data has been 4B/5B encoded, the SSD (10 bits) is added to the MAC packet. The packet is then scrambled (can be switched off), converted to a serial form with the data rate of 125 Mbps and NRZI encoded. The processed data stream proceeds towards the analog PCB circuitry for conversion to an optical signal. This data is monitored using an oscilloscope. Figure 5.7 depicts the measurement results.

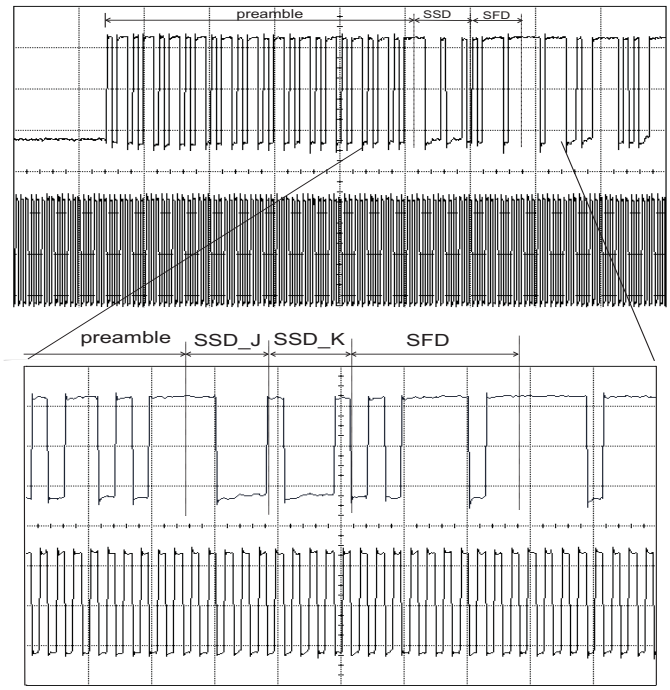

Figure 5.7: The serial data output from the FPGA chip.

Presented results confirm the correct functioning of FPGA chip. The other situations, like collision situation and error transmission are also tested and the outcome again showed that the FPGA design was correct.

5.5 Analog part of the transmitter

The analog part of transmitter has to be designed such that it can transmit mixed signals. Due to the presence of the analog synchronization carrier, the

complete system, including the receiver, should be linear. Sending a sinusoidal synchronization signal requires that the laser operating point always lays in the linear part of the P-I curve, which is presented in Figure 5.8.

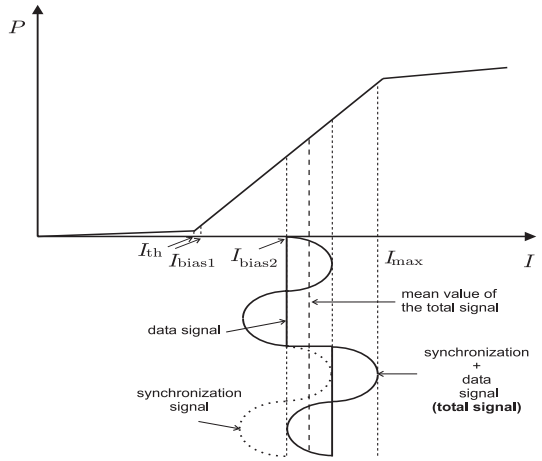

Figure 5.8: Direct modulation of the laser with combined data and synchronization signals.

To simplify the implementation the laser is usually directly modulated using the On/Off Keying (OOK) modulation format with various modulation depths. In order to facilitate carrier sensing and eventually collision detection, the difference in transmitted power in case the data packet is transmitted or is not, must be as large as possible. If the bias current of the laser is chosen such that the operating point is in the middle of the linear part of the P-I curve we will have substantial light power even when there is no data packet to be transmitted and the difference between the signal levels with and without data would be very small. This would make it very difficult to set up a threshold level for carrier sensing. The threshold level must be kept as low as possible when the data is not transmitted in order to facilitate carrier sensing and eventually collision detection.

A solution to this problem has been found in using two bias currents. One will set up the operating point when there is no data to be transmitted (I_{bias1}), and the other, (I_{bias2}), when data is transmitted, as shown in Figure 5.8.

The first bias current will be slightly larger than the threshold current I_{th}. Emitted power will be very low and the laser can respond to quick changes in operating point when necessary, since it has already been turned on. Due to

this small emitted power, we will receive the summed powers from all the other end stations in the mini-star, even when the end stations are not transmitting data packets. If the received power level is much smaller than the power level received from an end station transmitting a data packet, added to the power from the other end stations that are not transmitting data packets, we can easily set up the threshold level to sense the carrier. When the end station is ready to transmit the packet, the bias current has to be changed such that the sinusoidal synchronization signal can be sent without distortion. The condition to be met is that there is no clipping even in the presence of the data signal. This means that the total signal amplitude must remain within the linear part of the P-I curve. This leads to a tradeoff between the signal amplitude and the bias current. In order to facilitate detection it is better to have a larger difference between the logical levels of the data signal. On the other hand, since we use only the sum of the zero mean value synchronization signal and the bias current for carrier sensing (Section 4.4), a larger bias current would facilitate collision detection. The schematic representation of the analog part of the transmitter is given in Figure 5.9.

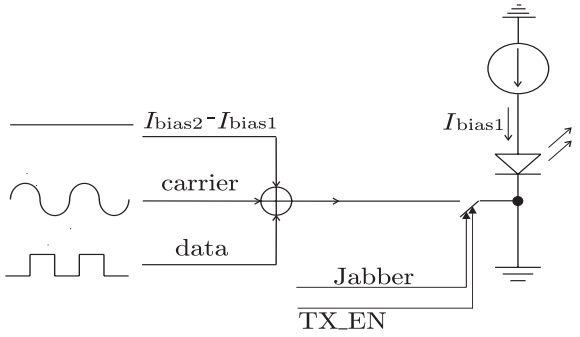

Figure 5.9: Schematic representation of the analog part of the transmitter.

The data signal, processed in the digital part of the transmitter, is added to the synchronization signal and the bias current $I_{\text{bias2}} - I_{\text{bias1}}$. When data is to be transmitted a `TX_EN` signal coming from the MAC sublayer becomes high and closes the switch. The outgoing signal from the analog part, added to I_{bias1}, is finally modulating the light source. We can see from Figure 5.9 that there is one more signal controlling the switch. This is the Jabber signal that becomes low when Jab time is exceeded, putting the switch in open position, detaching the transmitting station from the mini-star until the Unjab time expires.

5.5.1 Designing the transmitter for mixed signal transmission

When interfacing laser driver circuits with laser diodes at high data rates two issues must be taken into account: the electrical characteristics of the laser diode and laser driver circuit design.

Laser diode electrical characteristics

As mentioned before, for fast switching operation a laser must be biased slightly above the threshold to avoid turn-on delay. The laser optical output power depends on the driving current amplitude and the current-to-light conversion efficiency or slope efficiency of the laser diode. Both the threshold current and the slope efficiency are strongly related to laser structure, fabrication process, materials and operating temperature. The slope efficiency and the threshold current variation for the typical laser diode are shown in Figure 5.10 for two different temperatures.

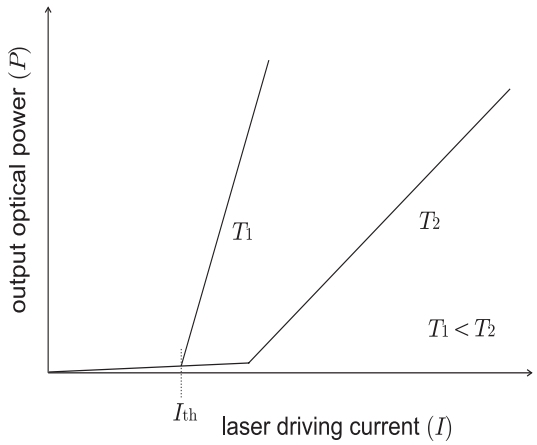

Figure 5.10: Typical laser P-I curve dependency with temperature.

As the temperature increases, the threshold current (I_{th}) goes up in an amount exponentially proportional to the working temperature. If this current is larger than nominal, due to temperature changes, as given in Figure 5.10, the laser will operate below threshold. This will introduce erroneous system operation and has to be taken into account in the design.

The laser slope efficiency is the ratio of the increment of the optical output

power to the increment of the input current and is given in mW/mA. Increase in temperature causes the slope efficiency to decrease (Figure 5.10). If the laser slope efficiency is reduced, the maximum, minimum and average optical power output levels will be lower than the intended set-up levels. The system will remain usable but the signal-to-noise ratio and bit-error-rate are degraded.

To overcome the problems of slope and threshold current variations with temperature an Automatic Power Control (APC) circuit should be added using the monitoring photodiode. For the sake of simplicity of the design we have avoided this circuit. Instead, we have designed the laser driving circuit taking the worst case scenario into account. This scenario assumes the largest threshold current and the smallest maximum driving current for which the laser still operates in its linear regime. In all the other cases the difference between the smallest and the largest driving current can only be larger which facilitates both signal detection and carrier sensing. All the current values can be determined either by measurements or from the specs provided by manufacturers of the lasers.

Laser driver

The function of the laser driver is to provide appropriate currents for bias and modulation of the laser diode as shown in Figure 5.9. The bias is a constant current that pushes the laser diode operating range beyond its threshold value and into the linear region. Ideally the bias current should track the changes in the threshold current and the modulation current should track the changes in slope efficiency.

To set-up the bias, a current mirror can be used. It has a high output impedance (20 kOhms), much higher than the serial resistance of the laser that is typically about 20 to 30 Ohms. The design of the current mirror must provide a tunable output current that can be changed by means of a variable resistor, since different light sources are required for optically transparent architectures (Figures 4.1-4.3).

The modulation current, on the other hand, is provided by a transconductance amplifier that converts the input voltages into currents. These currents must be set-up according to the laser's P-I characteristics.

To add the input signals a summing amplifier can be used. As shown in Figure 5.9 these signals are a sinusoidal analog carrier, a data signal and a DC signal to provide increase in bias currents when data packets are transmitted.

Another possibility is to add synchronization and data signals only using a summing amplifier and then add extra bias current using a transconductance amplifier, since there are transconductance amplifiers available where the output DC current can be set up by changing an appropriate resistor at the input (OPA660).

The composite signal at the output of the transconductance amplifier is used to modulate the laser. The switch that controls the modulating current is closed during the duration of data packets. It is controlled by the `TX_EN` signal from the MAC sublayer. When the end station has a data packet to be transmitted on the line the `TX_EN` signal will be set high, otherwise it will stay low. The timing is very important and has to be taken into account since there will always be delay present in the digital part of the transmitter. This means that the signal that controls the switch will be set high before the data arrives from the transconductance amplifier and the switching time must be shorter than the delay in the digital part such that no data is distorted. Ideally this switching time must be zero. Besides, the delay in the digital part must be taken into account such that the `TX_EN` signal is delayed when the MAC sublayer completes packet transmission. The reason is that on completing the packet transmission `TX_EN` will be set low. This will open the switch before the complete packet has been transmitted from the PLD causing a fault in the transmission. To avoid this the `TX_EN` signal must be delayed for as long as the data is processed in the digital part of the PLD plus the delay in the analog circuitry from the FPGA output to the output of the transconductance amplifier. Delaying the `TX_EN` signal will cause a decrease in the total network throughput but this has already been taken into account when calculating the throughput (Section 4.5.2). According to the standard [24] this delay should not exceed 25 bit times.

To switch the composite signal “on” and “off” a fast switch has to be used that does not affect transmission. The simplest solution is to use a JFET transistor in which the drain current is controlled by the gate-source voltage. The transistor specifications must be such that this drain current is large enough to bias and modulate the laser.

Light sources

The light sources used in the realization of the transmitter are LDs and VCSELs operating in the short wavelength region (around 850 nm). The LDs are of the Fabry-Perot type with the output light of a wavelength around 800 nm. The

VCSELs are used since the firstly presented architecture requires light sources of wavelengths different from 800 nm, but still in the region around 850 nm. The advantages of VCSELs compared to LDs are given in Section 2.5. The P-I curves of both types of light sources are presented in Figure 5.11.

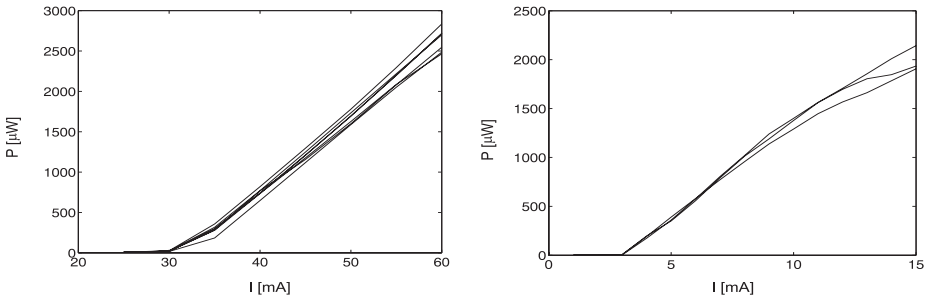

(a) (b)

Figure 5.11: (a) The P-I curves for 7 different F-P lasers of the same type RC010-RC, (b) P-I curves for 3 different VCSELs of the type VD910469.

Although these two light sources use different driving currents the power of light they produce has similar levels. An important property of both lasers is a linear P-I curve within a certain region, which is very important for sending analog signals without distortion. It can be seen from Figure 5.11 that the linear operating region for LDs is achieved using driving currents ranging from I=35 mA to I=55 mA. The output powers are large enough to satisfy the specifications. The operating region for VCSELs is for driving currents between I=3.5 mA and I=13 mA.

The linearity of both P-I curves will make the design of the system easier, since no extra linearity compensation circuit is required in the design. Another important property derived from measurements is that linearity of both curves stays unchanged irrespective of temperature variations.

To further simplify the transmitter design no Automatic Power Control circuit has been implemented to stabilize the output power that varies in time with the temperature of the laser. Nevertheless this variation in power has to be taken into account when determining the threshold level for the carrier sense circuit. Power deviation with temperature is given by the producers and is used later in both simulations and realization of the analog part of the receiver.

Reducing the modal noise effect

One of the serious problems that can deteriorate the performance of the optical communication system based on multimode fibers is the modal noise. The light of the laser traveling through a multimode fiber can take multiple paths of slightly different lengths due to a differential mode delay. At a certain cross-section or the end-face of the multimode fiber the light comprises contributions from the lights in all paths (modes), [4]. Depending on the relative phases of the modes at each point, constructive or destructive interference occurs. This will cause special filtering of moving speckles and mode selective loss.

The light at the certain cross-section of the fiber with the fringes is also called the speckle pattern that depends on the laser coherence time and fiber length. The smaller the coherence time of the source and the larger the length of the fiber the smaller the visibility of the speckle pattern. What we are interested in are the actions we have to take to avoid its appearance, since it reduces SNR [4]. As an example, a speckle pattern at the silica multimode graded-index fiber end-face when excited by a highly coherent HeNe laser is presented in Figure 5.12. Since this laser emits highly coherent light the speckle pattern is clearly visible.

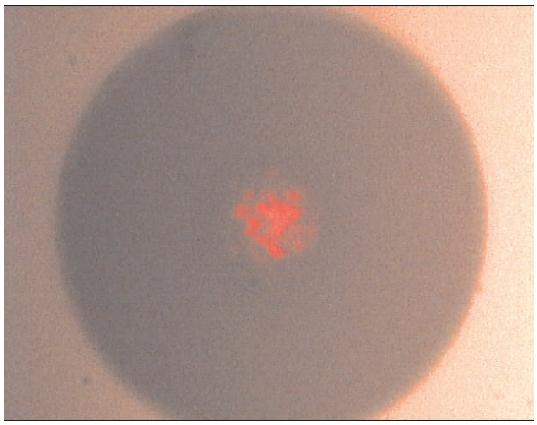

Figure 5.12: The speckle pattern at a silica multimode graded-index fiber end-face when excited by a highly coherent HeNe laser.

What is important is that moving speckle pattern acts as a noise source in devices such as connectors, splices, mode mixers and coupling to a photodiode where a part of the speckle pattern is spatially filtered due to mode-dependent losses. The speckle pattern appears when following conditions are fulfilled at

the same time [4]:

1. a coherent source;
2. multimode fiber and devices;
3. mode selective loss.

When one of these conditions is absent, there can be no modal noise. Since we made a choice for multimode fiber and devices, the second condition is automatically fulfilled. The third condition also exists since the connector losses are not negligible. However, the most important countermeasure we took to eliminate the speckle pattern consisted of the selection of incoherent laser sources in order to negate the first condition. Since the F-P lasers that we have used in the experiments show a relaxation oscillation at a frequency well beyond the information bandwidth, the speckle pattern that originates from the interference and which causes the modal noise will become "invisible" to the receiver. These relaxation oscillations are shown in Figure 5.13.

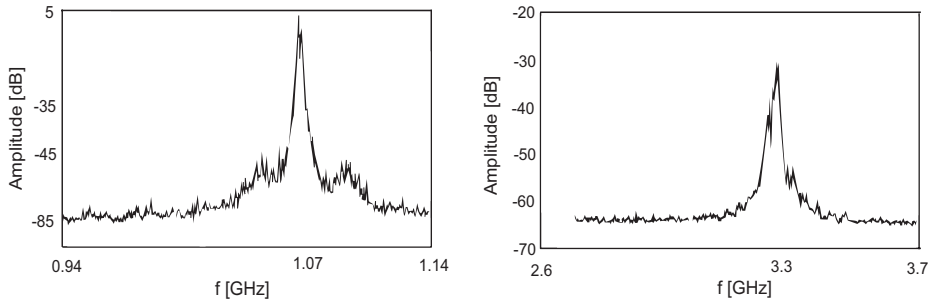

Figure 5.13: Relaxation oscillation frequency for the F-P laser RC010C-BS for the driving current a) I=35 mA; b) I=55 mA.

Moreover, both F-P lasers and VCSELs that we have used in the experiments have broad spectral linewidths i.e. short coherence time, so once the time delay between several modes that propagate through the multimode fiber exceeds the coherence time of a F-P laser or a VCSEL, the contrast between the light and dark spots at the output of the fiber is reduced. This means that the speckle contrast is harder to distinguish so the effect of modal noise decreases. The linewidth of the spectrum for both light sources used in our experiments are presented in Figure 5.14. Broad linewidths of the sources will increase the

chromatic dispersion limitation in fiber lengths, but the penalty will not be considerable due to the relatively short fiber lengths (limited by the standard) used in our networks.

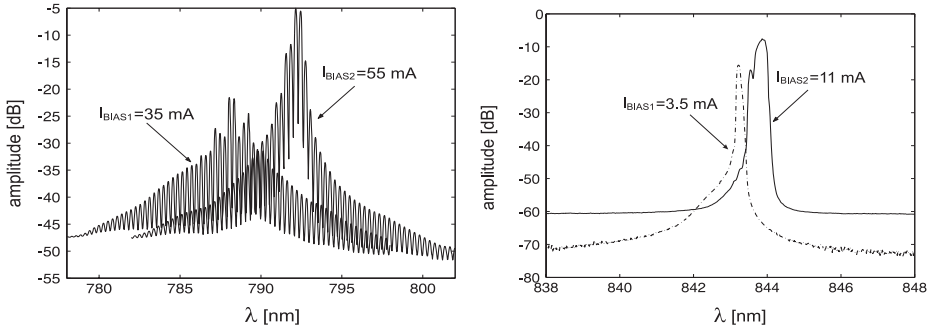

(a) (b)

Figure 5.14: (a) The spectra of the output light from the (a) F-P laser RC0101C_BS for two different driving currents I=35 mA and I=55 mA and (b) VCSEL of type VD910469, for two different driving currents I=3.5 mA and I=11 mA. For low driving currents both lasers emit light at shorter wavelengths and have a longer coherence time.

We have finally observed the light in the fiber end-face for both LD and VCSEL excitation, to confirm that speckle pattern will not deteriorate performance of our system. The light is captured by a CCD camera and the result is shown in Figure 5.15.

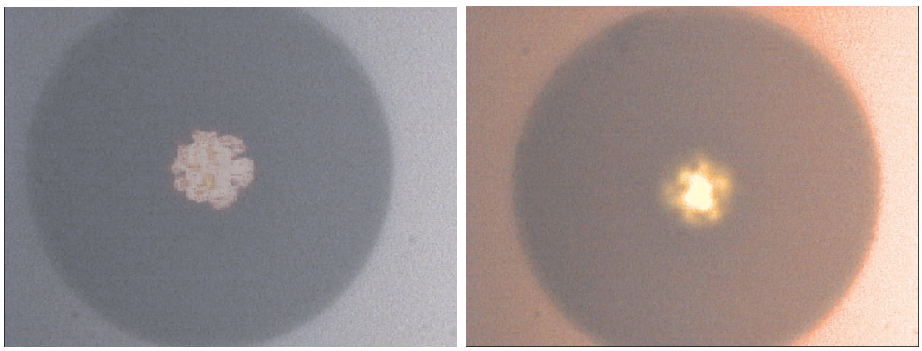

(a) (b)

Figure 5.15: The speckle pattern at a silica multimode graded-index fiber end-face when the optical signal is excited by (a) F-P laser diode and (b) VCSEL.

Both photos presented in Figure 5.15 show smooth light distribution across the fiber core indicating the absence of modal noise.

5.6 Simulation results of the analog part

To simulate the transmitter analog circuitry OrCAD PSPice software is used. The models of components used are either found in libraries provided in the software package or obtained directly from the producers of particular integrated circuits.

A summation circuit based on a transconductance amplifier OP660 is used for making the composite signal. In the path of the signal that controls the switch an inverter has been introduced to adapt the signal levels. The switch is an N-channel JFET, 2N555, with a typical switching time of about 10 ns. To simulate the circuit when a signal is transmitted and when is not, a `TX_EN` signal is set for half a period to be low and half a period high. The total simulation time was 180 ns. The output current waveform obtained from the simulation is presented in Figure 5.16.

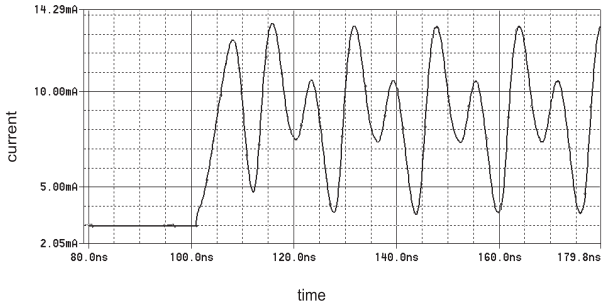

Figure 5.16: The composite current waveform used to modulate the VCSEL.

Based on measurements of the P-I characteristics of both the VCSEL and F-P laser, different bias and modulation currents must be used for proper transmitter functioning. Since the operational principle is the same for both types of light sources, only the result obtained using the VCSEL is presented.

The peak-to-peak amplitude of the composite signal is around 9 mA, which corresponds to requirements that this amplitude should fill the complete driving current range such that operating point still lies in the linear part of the P-I curve of the laser, since this provides maximum SNR, [4]. The switching “on” and “off” times are both around 10 ns, which also comply with requirements. The

maximum output current amplitude is just above 13 mA, preventing destroying of the VCSEL. The minimum VCSEL driving current is $I_{\text{bias1}} = 3.3$ mA avoiding the operation of the VCSEL in the non-linear region. This constant current is slightly larger than the threshold current (3 mA).

5.7 Experimental results

To confirm the functional principle of the transmitter analog circuitry we have designed a printed circuit board using OrCAD Layout. All the components used in transmitter implementation are commercially available. The final PCB realization is presented in Figure 5.17.

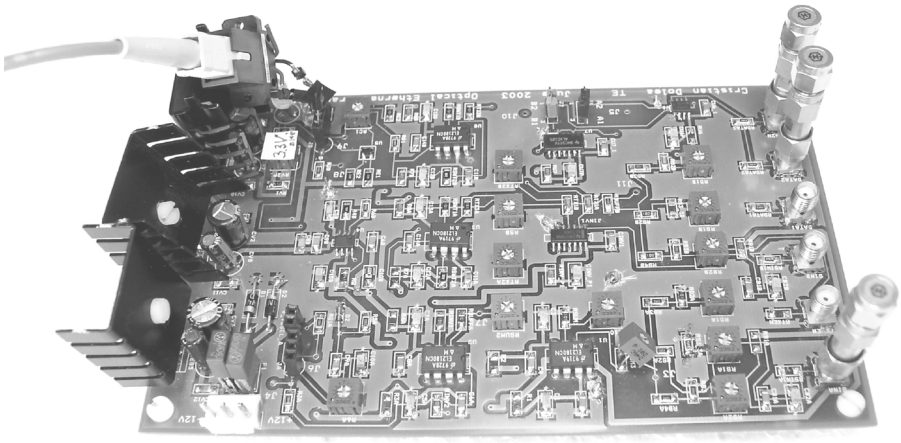

Figure 5.17: The printed circuit board of the analog part of the transmitter.

The processed Fast Ethernet packet is in the form of a serial Low Voltage TTL (LVTTL) signal brought to the input of the analog PCB. After summing the signal with the sinusoidal carrier and the bias in the transconductance amplifier OPA660X1, the combined signal will modulate the VCSEL. The waveform of the combined signal is presented in Figure 5.18.

The first part of the upper signal is the measured voltage on the anode of the VCSEL diode when I_{bias1} is driving the VCSEL. The lower signal is `TX_EN`, and is low when there is no data to be transmitted. Once the signal is transmitted, `TX_EN` becomes high, the switch is closed and the composite current is driving the VCSEL. The measured anode voltage is presented in the second part of the upper signal. The amplitudes of both data and synchronization signal are taken

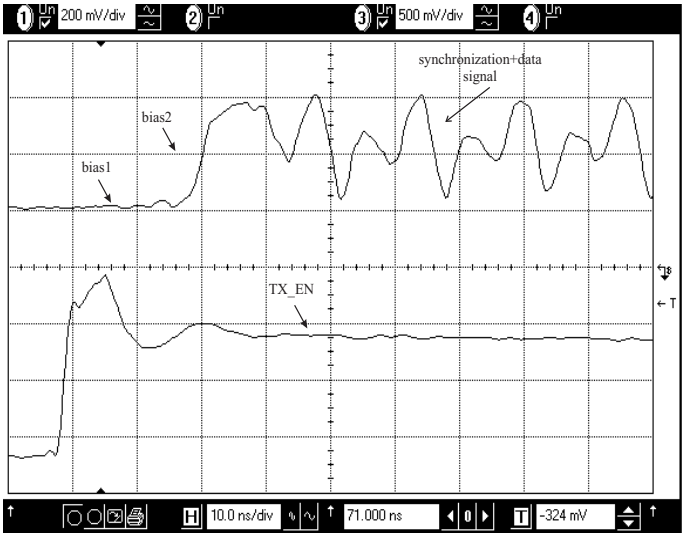

Figure 5.18: The measured composite waveform used to modulate the laser. The upper signal depicts two bias levels, synchronization signal and data (Fast Ethernet packet preamble) at the output of the transmitter. The lower signal TX_EN activates the transmission.

to achieve maximum SNR. It is obvious that the obtained measured modulating output signal satisfies the requirements and corresponds to the simulated value.

5.8 Conclusions

Both the analog and digital circuitry design of the transmitter are presented in this chapter. The analog circuitry design is done using OrCAD software and the digital circuitry design is done by using VHDL programming. Both circuitries are fabricated using PCBs. To implement the digital design an Altera FPGA is used. Both designs are made to show functional feasibility of the transmitter, but in the final realization this has to be integrated and combined with the receiver.

The digital circuitry design was made such that new features can be implemented. These features are in fact the differences with respect to existing standards that mainly were made to support the ECT synchronization technique. The eliminated IDLE signal and shifted SSD are just some of them. Some extra functionalities, like Jabber detection and avoiding Jam signal enforcement are consequences of using a passive star coupler for end station interconnection.

Both timing analysis and functionality of the FPGA design are confirmed to be correct. Ultimately, the final fabrication of the FPGA on a PCB proved that signals from the MAC sublayer can be processed correctly before transmission onto the fiber medium.

The analog circuitry is designed to support the ECT synchronization technique with the combined data packet and analog carrier (mixed signal). To avoid distortion of the analog carrier, modulation currents are chosen such that the operating point always lays in the linear part of the P-I curve of the light source. A tradeoff had to be made with respect to both carrier and data amplitudes on one side and carrier sensing on the other. An optimal solution is chosen such that amplitude values of both sinusoidal carrier and data signal are the same such that the peak-to-peak amplitude of the combined signal spans the full range of the light source driving current when the light source works in the linear regime [4].

Both simulated and experimental results confirm that requirements for transmitter design can be met such that the ECT synchronization technique can be used.

CHAPTER 6

Receiver design and implementation

6.1 Introduction

To complete the PLD design and eventually build an entire computer communication system a receiver had to be designed based on both synchronization and collision detection requirements. The receiver, like transmitter, consists of analog and digital circuitry. The same software packages are used for their design as in case of the transmitter. The block scheme of the receiver is shown in Figure 6.1.

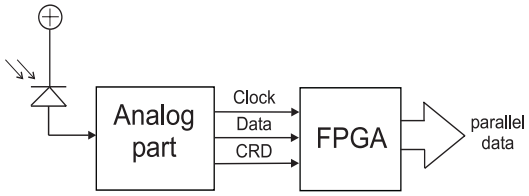

Figure 6.1: The block scheme of the receiver in the PLD.

6.2 Receiver analog part

The analog part of the receiver in the PLD comprises two parts, namely clock and data recovery and carrier sense circuits. Due to the analog carrier transmission the voltage representing combined data and carrier must linearly depend on the current obtained from the photodiode, which in turn linearly depends on the power of the light impinging on the photodiode. This linearity is achievable for small values of the signals. The analog circuitry schematic is presented in Figure 6.2.

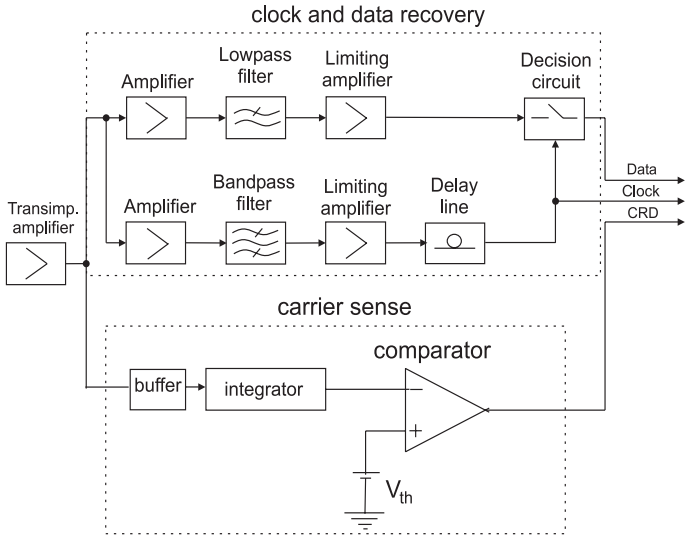

Figure 6.2: The schematic diagram of the analog part of the receiver.

The photodiode current is converted to a voltage by means of a feedback resistance. This voltage is amplified further since most of the time one amplifier stage is not able to boost the signal of interest to a useful level. Typically, a limiting amplifier is used as a post amplifier but we cannot implement this in our design since we have to provide transparency of the input signal for the clock recovery and the carrier sense circuit. The limiting amplifier would only clip the sinusoidal synchronization signal. Consequently, the spectrum of the clipped signal will overlap the spectrum of the data signal. The two signals could not be separated by means of filtering making the clock extraction impossible.

The DC level of the total input signal will be used by the carrier sense circuit and the AC signal for clock and data extraction. To achieve linearity both transimpedance amplifier and post amplifier must have linear amplification

to provide transparency of both the synchronization signal and the mean value of the total signal. After the postamplifier the received signal will be split into clock and data and carrier sense circuits.

6.2.1 Carrier sense circuit

Remind that the signal used for carrier sensing is the DC signal obtained from the driving current I_{bias2}. In the carrier sense circuit a mean value of the total received signal is determined and such a value is then compared to the threshold level based on the average power of the received signal (Chapter 4). A straightforward way of finding the mean value of the received signal in practical implementation is to use an integrator. The simplest way is to use a passive RC network with a time constant that depends on the application.

The mean value of the synchronization signal is equal to zero and will not contribute to the mean value of the total signal. The integration time of this signal can ideally be set to one period (8 ns) but in order to minimize the noise effect it is best to integrate the signal over several periods. The mean value of a 4B/5B encoded and possibly scrambled data signal varies depending on the integration constant. Although encoding performed at the transmitting side makes the number of logical ones and zeros in the data signal equal on average, this is only true after a large number of bits. For a shorter integration time, e.g. smaller number of bits, we have to take into account that those numbers significantly vary. That will be the reason for level variation of the total received signal. Nevertheless, the signal level obtained after the integrator will always be larger than the level determined from the worst case transmission when only logical zeros are transmitted (Section 4.4).

To determine the integration constant $\tau = RC$ we must take into account the delay that is introduced by complete carrier sense circuit. Here a tradeoff between the total delay in the carrier sense circuit on one side and the noise effect on the other side, must be taken into account. To increase the throughput and eventually provide better network performance the total delay must be as short as possible i.e. the integration constant must be short. On the other side, to minimize the noise effect, the integration constant must long.

If the mean value of the input signal, obtained after integration, surpasses the predetermined threshold the carrier will be sensed. The output of the comparator will become high reporting detection of the data packet. An appropriate signal (`CRD`) is then transmitted from the output of the carrier sense circuit to

the digital part of the receiver. In this way the end station detects that someone else is occupying the medium. Finally, the `CRD` signal is used for collision detection.

6.2.2 Clock and data recovery circuit

To separate data and synchronization signals two filters are used: one bandpass filter with a center frequency of 125 MHz for the synchronization signal and another one, lowpass with cutoff frequency of 95 MHz, for the data signal, since most of the data signal power is concentrated below this frequency. Figure 6.2 depicts this idea.

The recovery time of the synchronization signal will depend on the type of the bandpass filter used and its response time. The best choice can be found from the tradeoff between the quality factor and the filter response. On one side we would like to have the filter with a rather narrow passband to eliminate the presence of the data signal and on the other side, we need a short response time of the filter to achieve fast synchronization. The amplifiers placed after the filters will serve to make a clock signal out of the synchronization sinusoidal signal in the clock path and amplify the signal amplitude in the data path. The delays in both paths might be different and this is the reason we have added extra delay lines to synchronize the phases of data and clock signals. This delay is fixed and equals the sum of delays in the transmitter and receiver. There is no delay between two signals in transmission through the fiber. Finally, a decision circuit is used for data recovery.

6.3 Receiver digital part

The main consideration in the digital circuitry design was that processed signals obtained from the analog part of the receiver must be in accordance with the standard, since the output of the digital part proceeds to the MAC sublayer via the MII interface.

A block scheme of the receiver is given in Figure 6.3. Like in the transmitter, presented sub-modules run at two clock domains.

The sub-modules that are presented in Figure 6.3 are:

- **clkdiv5rx** - divides the 125 MHz nominal clock into 25 MHz. The output is connected to the `RX_CLK` output port. The **corerx** provides additional

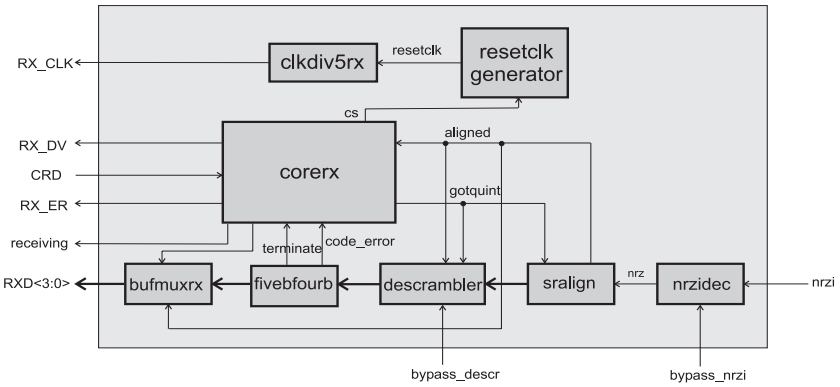

Figure 6.3: Block diagram of the digital part of the receiver.

reset to this module via the **resetclk generator** to assure that the rising edge of `RX_CLK` is in the middle of $\texttt{RXD}\langle 3:0\rangle$.

- **sralign** - composed of a 10-bit shift register and a simple state machine. The function is to perform serial-to-parallel operation and to establish frame and byte alignment. The `gotquint` signal is a periodic pulse with 25 MHz frequency and will be used as the clock enable for the other sub-modules.

- **descrambler** - performs parallel descrambling on the data stream under **corerx** control. Upon detection of the SSD, the descrambler will be reset to a well defined initial state, after which it will start to descramble the rest of the incoming data. The SFD will be the first pattern to be descrambled. However, if no scrambling has been performed at the transmitting side the `bypass_descr` is asserted and this block will just pass the incoming data. Although this sub-module runs at 25 MHz its linear feedback shift register runs at 125 MHz.

- **fivebfourb** - converts the incoming (parallel) 5 bits quintets into corresponding (parallel) 4 bits nibbles. The use of 4B/5B coding in data transmission offers the possibility to send extra control codes along with normal data. As the code list does not contain control codes like stream delimiters, they cannot be decoded and must therefore be detected on beforehand. The full list of all data nibbles and their corresponding 5 bits quintets can be reviewed in [24]. When invalid code-groups are detected the **fivebfourb** will assert a `code_error` signal otherwise, upon detection

of the ESD code-groups, it will assert a `terminate` signal.

- **corerx** - controller of other sub-modules. As such, it is a state machine. It takes carrier detect (`CRD`) input signal from the analog part of the receiver in the PLD, along with other signals indicated from the other sub-modules, i.e., aligned signal, `code_error` signal and terminate signal.

- **nrzidec** - decodes the incoming NRZI serial data stream into NRZ format. However, if the `bypass_nrzi` is asserted, it will not perform NRZI decoding. It will just pass the data stream instead. This block runs at 125 MHz.

- **bufmuxrx** - produces the data stream that is connected to the `RXD`$\langle 3:0 \rangle$ output port. It is controlled by **corerx**.

The output signal `receiving` is to denote that carrier is sensed (detected) and this will be used for collision detection together with the `transmitting` signal from the transmitter. Both signals are brought to the input of an AND gate with the collision detection signal `COL` at its output. This is neither presented in the block scheme of the transmitter nor the receiver since it is implemented as the transceiver functionality. If both `transmitting` and `receiving` signals are high, a collision detection signal `COL` will also be high indicating that collision has occured.

6.4 Digital part design and simulation results

For the receiver digital part realization the same FPGA chip that has been used for the transmitter realization is used. Moreover, some functionality of the transceiver like carrier sensing and collision detection are also implemented. The design steps elaborated in the transmitter design are followed. To test the functionality of the design the static timing analyzer is used. Obtained values are presented in Table 6.1.

The presented response of the circuit on `CRD` signal at the input has to be taken into account when determining the total delay in the end station. The time to detect collision (`COL`) has to be taken into included in the Slot Time. A very important parameter is the slack time for the 125 MHz `CLK_IN` signal. This is the clock signal used throughout the transceiver. Slack time is the margin by which the timing requirements is met or not met. The positive slack time we

Table 6.1: Timing parameters from the static timing analyzer.

Receiver		
Timing	Signal	Value
Setup time	NRZI_IN	1.8 ns
Clock to Output time	RXD[0]	10.9 ns
Clock to Output time	RXD[1]	10.7 ns
Clock to Output time	RXD[2]	10.6 ns
Clock to Output time	RXD[3]	8.1 ns
Clock to Output time	RX_DV	10.5 ns
Clock to Output time	RX_ER	10.4 ns
Transceiver		
Shortest slack time	CLK_IN (125 MHz clock)	0.06 ns
Hold time	All inputs	≤ 0 ns
Clock to Output time	COL	11.1 ns
Clock to Output time	CRD	11.3 ns

obtained indicates that our design meets the timing requirements. A negative slack time would suggest errors in the design. The hold time is zero due to the use of the clock-lock function that transports the clock evenly over the FPGA.

Simulations of the complete receiver analog circuitry is not done due to the lack of models for the delay of integrated circuits, transimpedance amplifiers and filters. Those components have been tested separately and based on that a complete PCB is fabricated.

6.5 Experimental results

The experimental setup for the receiver is presented in Figure 6.4. The analog part of the receiver comprises separate clock and data recovery circuits and the carrier sense circuit and is realized using a PCB presented in Figure 6.5.

After passing through the transimpedance amplifier, the received signal is split in three. One part goes to the carrier sense circuit, a second part goes to the clock and data recovery circuit, where it is further split in a data and clock recovery path. Results obtained for the collision detection circuit will be presented first.

The most important issue in the carrier sensing circuit is to distinguish between situations when the medium is occupied and when it is not. To be

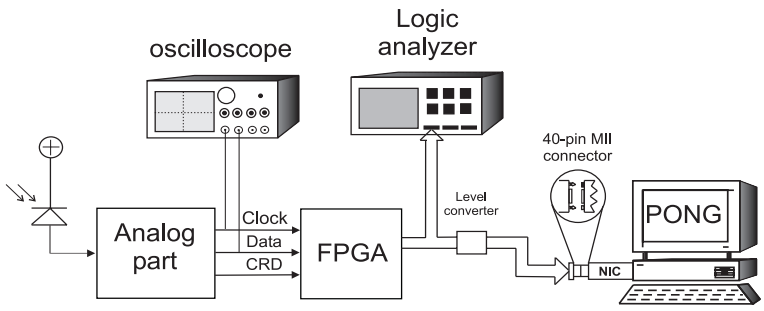

Figure 6.4: The experimental setup for the receiving part of a new PLD in FTTD network.

able to do this a threshold level has to be set-up based on measurements. If the threshold is surpassed carrier is sensed.

To determine a threshold level the received optical power levels at the receiver front-end are measured. These levels depend on the transmitted optical power and the losses in the system. The results of measurements are shown in Table 6.2.

Table 6.2: Optical power received at the PLD in one of the end nodes in the mini-star when I) no other end station is sending data, II) one out of 8 end stations is sending data, III) the router is sending data signal (only valid for the first architecture).

	I	II	III
VCSEL/LD power	-15.9 dBm	2.0 dBm	6.0 dBm
star coupler loss (8 users)	10.5 dB	10.5 dB	10.5 dB
fiber loss	1.0 dB	1.0 dB	1.0 dB
connector pairs (4×0.5) dB	2.0 dB	2.0 dB	2.0 dB
WDM losses	0.0 dB	0.0 dB	10.0 dB
power at the receiver	-29.4 dBm	-11.5 dBm	-17.5 dBm

The values presented in columns I and II of Table 6.2 apply to all the architectures while column III applies only to the first architecture since the end nodes and the router belong to the same collision domain.

The measured losses of the WDM (de)multiplexer include connector losses. Results show that we have typically 12 dB greater received power in case a packet is transmitted on the line, even when the digital data have the worst-case value, i.e. data sequence all zeros. This gives us sufficient room to place a

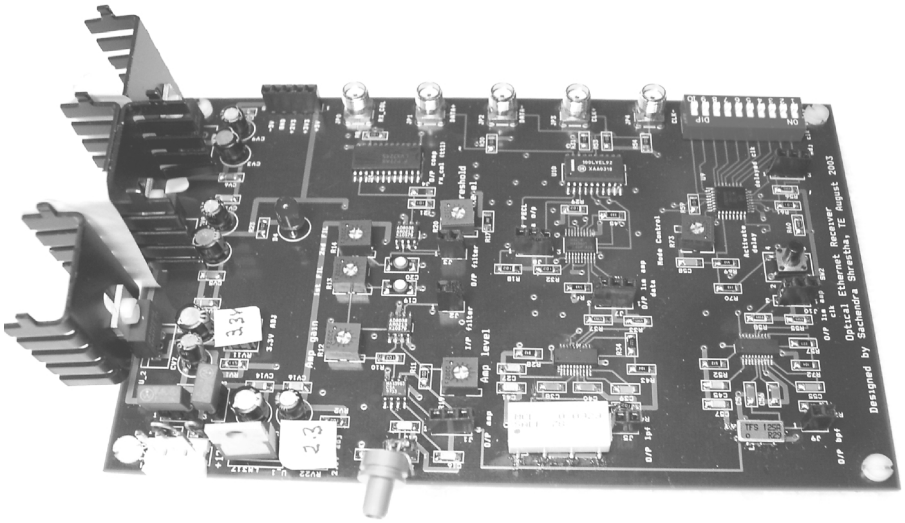

Figure 6.5: Printed circuit board of the analog part of the receiver.

threshold. The threshold range can be calculated using the responsivity of the photodetector, amplification of the transimpedance amplifier and integration constant of the integrator. Remind that a linear system is assumed. The WDM losses are rather high. To facilitate carrier sensing in the final design a WDM device with lower losses should be used.

To determine the linearity of the system we measured the dependence of the voltage at the output of the transimpedance amplifier on the received optical power. Obtained result is presented in Figure 6.6 (a). The measured responsivity curve of the photodiode is shown in part (b) of the same figure.

The received composite signal after the transimpedance amplifier will correspond to the transmitted signal. Both signals are presented in Figure 6.7.

Based on the received power, the responsivity of the photodiode and the transimpedance amplification we can determine the mean value of the signal. Based on this value a threshold can be set-up. The received optical power is measured when no data was transmitted. This corresponds to a situation when all logical zeros are transmitted assuming LVTTL signaling. In this way the worst case situation can be determined. We have also taken into account output power variation with temperature, and variation in power among different output ports in the star coupler. Using the postamplifier with small amplification to separate the filters from the transimpedance amplifier and amplify

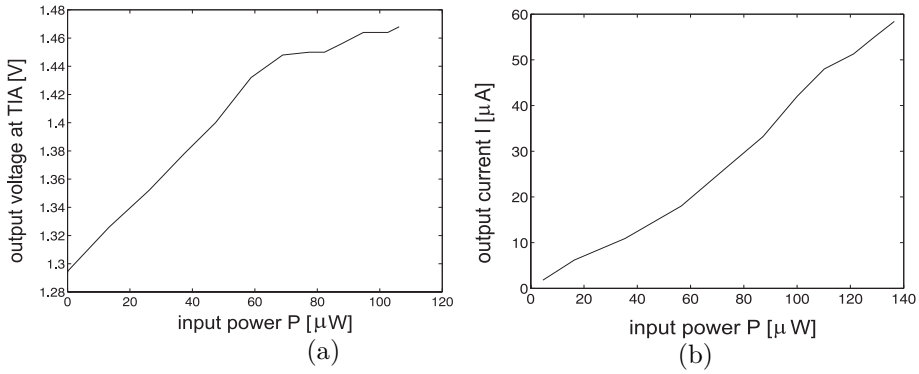

Figure 6.6: (a) A voltage at the output of the transimpedance amplifier as a function of the input power, (b) responsivity of the photodiode.

the signal further to compensate for the losses in the filters, we obtained signal levels at the comparator input that are presented in Figure 6.8.

After amplification, two copies of the incoming signal used for clock and data recovery are filtered by means of a bandpass filter with the center frequency of 125 MHz and a lowpass filter with cut-off frequency of 95 MHz, placed in the clock path and the data path, respectively. The cut-off frequency of the latter filter is chosen taking into account that 95 % of signal energy is concentrated below this frequency.

The bandpass filter used for clock recovery is a SAW filter with a 3 dB bandwidth of about 3 MHz, corresponding to the measured response time of about 400 ns. This is very important for clock extraction since we have to achieve synchronization within the first 480 ns of the data packet, according to the duration of the preamble. The measured response of the filter on the input synchronization signal is presented in Figure 6.9. The amplified 125 MHz clock signal is then brought to a decision circuit for data extraction.

Part of the signal goes through the data path and is filtered out by a passive surface mount lowpass filter of the type SCLF-95 and amplified. The clock signal is properly delayed to assure that rising edge of the clock signal will arrive at the decision circuit at the point of maximum eye opening. The delay is set manually after the difference in delays between the clock and synchronization signal in the analog part of both transmitter and receiver is determined from measurements.

Figure 6.7: Measured values of the composite modulation signal during the Fast Ethernet packet preamble (a) at the anode of the VCSEL at the transmitter side, (b) after the transimpedance amplifier at the receiver side.

To check the clock and data recovery circuit an eye pattern is made, for the data rate of 125 Mbps. For the received signal level of -17 dBm the eye pattern is shown in Figure 6.10. This signal level is taken from Table 6.2. It represents the worst case received signal power in the network architecture presented in Figure 4.1.

Recovered clock and data signals are sent to the digital part of the receiver as differential signals, but the presented eye pattern is made for positive outputs only. It can be seen that the eye is fully open which means that the analog circuitry in the receiver is working properly. The measured jitter was 589.9 ps.

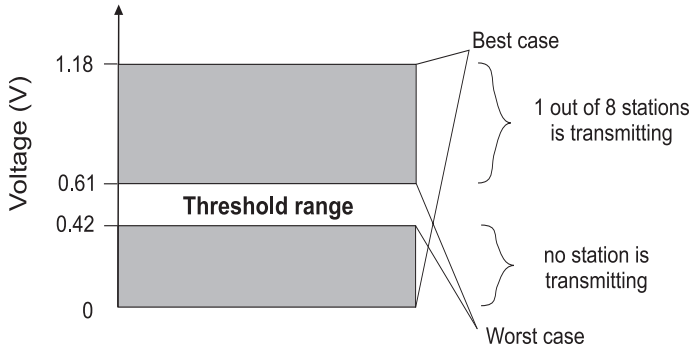

Figure 6.8: The range of threshold levels in the analog part of the PLD in the end nodes that are directly connected to the multimode star coupler.

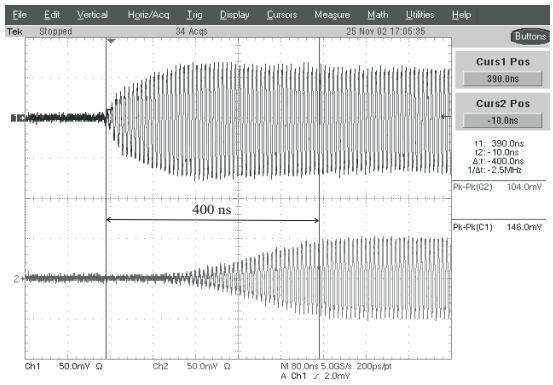

(a)

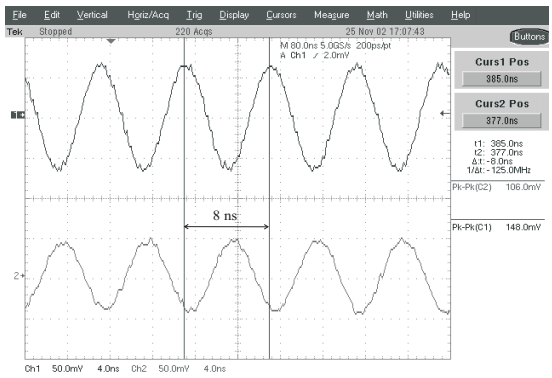

(b)

Figure 6.9: (a) The response (lower trace) of the bandpass filter on the synchronization signal (upper trace), (b) zoom-ed version of the signals at the moment the synchronization is achieved.

The clock and the extracted data signal, together with the carrier sense signal now go to the input of the FPGA chip to be processed for transmission to the MAC sublayer. A parallel signal at the FPGA output is monitored at the logic analyzer. The result is shown in Figure 6.11.

Received PONG signal on the screen of the receiving computer as a result of a PING request sent from the transmitting computer provided positive outcome of the experiments.

6.6 Conclusions

The experimental setup for testing the receiver in the PLD designed for the new NIC is given. Both digital and analog parts were tested using the PONG signal. Measurements show that both parts function according to requirements.

Measurements of the analog part of the receiver show that the threshold level for detecting both presence and absence of the carrier on the fiber medium can be set-up based on received optical power. The realization is facilitated due to fact that the voltage at the input of the comparator linearly depends on the received optical power at the input of the receiver.

The eye diagram made from the recovered data proved the correct functionality of the clock and data recovery circuit in the analog part of the receiver. This means that the ECT synchronization technique can be implemented in the proposed networks for synchronization of bursty traffic.

The PONG signal obtained on the screen in the receiving PC proved that processing the data in the FPGA has been done correctly. In the final design, the FPGA chip must be replaced by an ASIC for economical reasons.

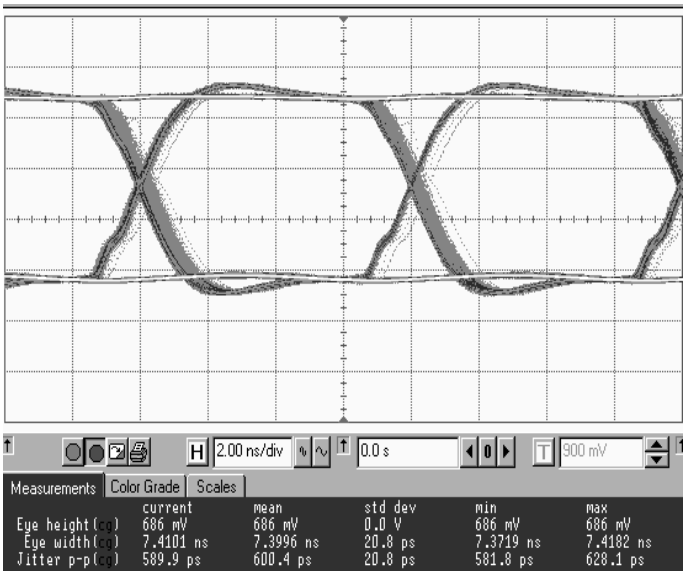

Figure 6.10: The eye patter for data rate of 125 Mbps viewed at the positive output of the decision circuit.

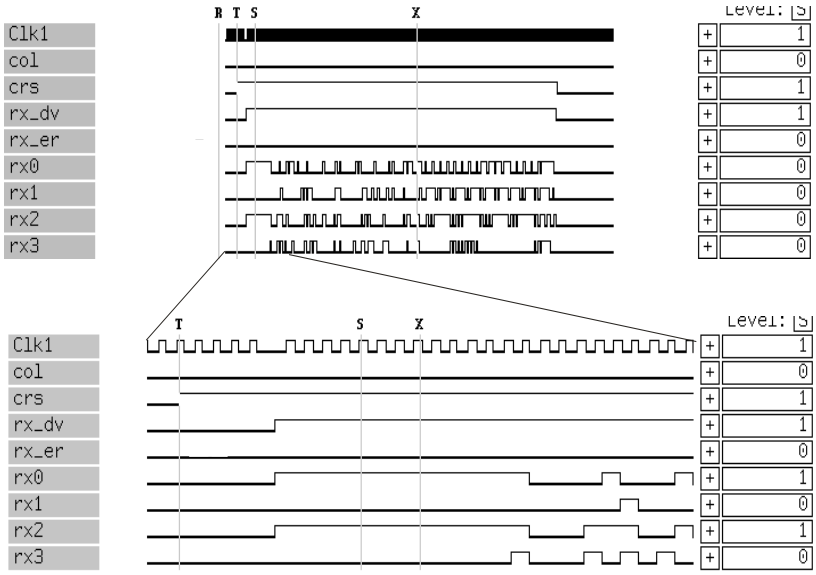

Figure 6.11: Up: Parallel signals (PONG packet) at the output of the FPGA to be transported to the MAC sublayer via the MII interface, down: zoomed preamble with SFD.

CHAPTER 7

OCDMA implementation in LANs and access networks

7.1 Introduction

In the original MOUSE project proposal, the network architectures that accommodate Asynchronous Transfer Mode (ATM) protocol were proposed since the authors of the project proposal, including many researchers, at that time believed that ATM will be the workhorse of future broadband transport service. Yet, their opinion changed over the last several years, since Ethernet became so popular that ATM is hardly implemented in LANs. The main reasons are simplicity of Ethernet implementation and its low installation cost.

Although the implementation of the ATM protocol in FTTD networks is not investigated in the project, the multiplexing techniques, an important issue in implementing ATM in optical star-shaped FTTD networks, are studied in an attempt to increase the capacity in optical FTTD networks. Remind that the multiplexing technique in ATM network would have to provide each node with a separate transmission path to the switch, since ATM is a central switching transmission technology where no common transmission path can be applied (Figure 7.1).

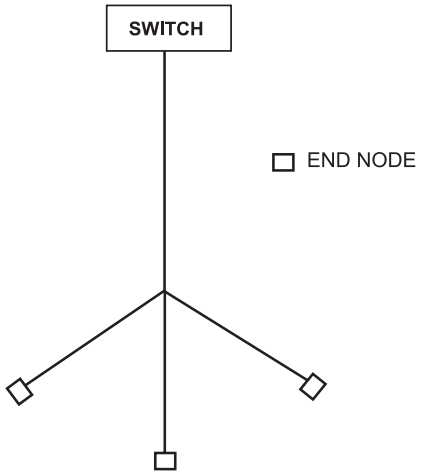

Figure 7.1: ATM network topology based on optical CDMA.

There are different multiplexing techniques that can be used. Time Division Multiple Access (TDMA) is one candidate. Since the end nodes may be situated at different distances from the star coupler, careful and flexible timing of data packets is required together with an appropriate protocol, in order to prevent collisions of packets. Another multiplexing technique that can be used is Code Division Multiple Access (CDMA). Since this technique is very suitable for bursty traffic, typical for LANs, we have investigated its implementation in FTTD applications, broadening the scope of analysis from Ethernet LANs to general passive optical LANs.

Code division multiple access (CDMA) is developed from the spread spectrum technique that was first introduced in radio communication systems in an effort to improve radio spectral usage efficiency. It is based on spreading the spectrum of narrowband messages over a much wider frequency spectrum by means of a digital code [19]. Due to the spreading action the transmitted signal arrives at the receiver as a noise-like signal and message recovery is impossible unless the original code used is known at the receiver.

With the emergence of mobile communications CDMA is used as an access technique that allows users to share a common transmission medium to transmit messages to a number of destinations. This is achieved by allocating a unique code to each individual user and distinguishing them by code division multiplexing. The use of CDMA solves the issue of efficient division of the available

transmission capacity among all the users. This technique has advantage compared to the use of other multiplexing techniques like TDMA and Frequency Division Multiple Access (FDMA) when bursty or sporadic traffic has to be supported, which is a typical behavior in LANs [47]. It is a random multiple access technique, since users can access the medium at any time. Coding allows users to share the same frequency band and to operate asynchronously. The combination of these two features makes CDMA attractive for use in optical communication systems. Another important feature of this technique is that it provides low access delay that is suited for bursty LAN traffic.

There are at least two fundamental differences in applying spread spectrum and CDMA in optical networks when compared to radio spread spectrum applications. The first difference is that optical reception is based on power rather than amplitude detection and therefore the use of radio CDMA codes which are designed for amplitude-based receivers is not straightforward in incoherent optical systems. New codes had to be invented. The second difference is that coherent reception that is commonly employed in radio CDMA systems is a nontrivial task in optical networks [48]. Additional problems include optical component performance, sensitivity to temperature variations when coherent techniques are employed, etc.

7.2 Different OCDMA techniques

All optical CDMA techniques can be distinguished into four main categories:

1. CDMA schemes that are based on suitable Pulse Positioning of the code bits according to the particular code structure. These schemes do not use spreading/despreading in a classical sense and are classified as Time Encoded techniques. Almost all the incoherent CDMA proposals fall into this category [49],[50].

2. Wavelength hopped optical CDMA schemes based on two-dimensional coding where TDMA is combined with WDM. Here the bits are transmitted in time slots at different wavelengths. More about systems that use this technique can be found in [51]-[53].

3. CDMA schemes that are based on spectral slicing of the broadband spectrum of optical sources. Here the binary code is mapped into the slices

of the broad input spectrum. This scheme can lower the bit-rate of the transmitted signal since many bits can be sent simultaneously, [54].

4. Schemes that can not be classified in any of the above categories. An example is the case of Spectral Encoding CDMA systems using spectral amplitude and spectral phase modulation with broadband optical sources [54]-[64]. The OCDMA scheme that we will concentrate on falls into this category.

The Spectral Encoding OCDMA is the technique which allows the CDMA receiver to operate at the data rate (baseband) rather than the code rate. There are two possibilities to perform coding in the spectral domain, namely spectral phase and spectral amplitude coding [48].

In our analysis we used the combination of spectral amplitude and spectral phase encoding, where encoding and decoding is performed in the optical domain by means of passive filters.

7.3 Spectrally encoded OCDMA based on cascade of MZIs

As mentioned in the introduction of this chapter, the optical CDMA technique provides random asynchronous communication access among many users and is therefore very attractive for use in the access part of the PSTN and LAN environment. In order to make the OCDMA system economically attractive and easy to implement we use spectrally encoded OCDMA based on encoding of the spectrum of broadband noncoherent optical sources, such as edge emitting LEDs or Super luminescent diodes (SLEDs). In this OCDMA system optical signal spectrum is much wider than the information bandwidth so no spreading of the information signal is required. Such a system is simple and can be realized using integrated optical components. The spectrally encoded system that we have analyzed is presented in Figure 7.2. This system has been reported for the first time in [54].

The basic elements of the system are the Mach-Zehnder (MZ) encoder and decoder. The MZ encoder and decoder reported in [54] consist of a cascade of Mach-Zehnder Interferometers (MZIs) designed in such a way that the path length difference (PLD) of each stage doubles that of the previous one. It will be shown in Subsection 7.4.1 that this is not a good choice when more than 4

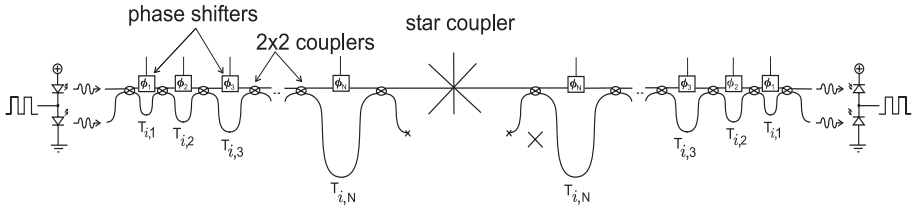

Figure 7.2: Schematic diagram of the spectrally encoded OCDMA system based on cascades of MZIs.

connections have to be supported. The PLD in the first stage has the minimal value, which is much larger than the coherence time τ_c [65] of the source.

The spectral codes in the presented system are made indirectly by phase coding, i.e. changing one or more phases in the phase shifters from 0 to $\pi/2$ and choosing the appropriate combination of PLD values in different stages of en/decoder. The index i in the delays $T_{i,k}, k = 1, ..., N$ denotes the i-th transmitter and receiver that belong to 2 different users, between which a connection is established. N denotes the total number of stages. We assume that all the delays $T_{i,k}$ are much smaller than the bit time T_b.

In presented system, like in the other systems with spectrally encoded broadband sources, a special receiver set-up is used to eliminate crosstalk, consisting of the decoding filter and differential receiver. To operate efficiently this set-up must be very well balanced [48].

When a broadband input lightwave is applied to one of the MZ encoder input ports, complementary spectral outputs are generated at the two output ports due to the phase delays in the unbalanced arms. Switching the input signal from one input port to the other, the original complementary spectral outputs will swap their positions at two output ports. Hence, by differentially modulating the input sources at the balanced transmitter, complementary spectral outputs are generated at the MZI output ports. This forms the basis of the MZ based complementary spectral encoder for bipolar optical CDMA. When a logical zero is transmitted the input data signal is low and the signal will modulate the upper light source. Similarly, when a logical one is transmitted the lower light source will be modulated. This is almost as if we have an optical switch at the output of the MZ encoder and one light source at the input. The necessary condition is that two light sources are completely uncorrelated.

Modulation in the electrical domain makes the system economically more attractive and facilitates its realization. Moreover it enables duplex transmission.

The modulator is placed in front of the encoder, so the complete structure is symmetrical, i.e. the same physical device can be used for both transmission and reception of signals. In this system we can associate each orthogonal code with a connection between two users with the same physical address (phase codes), so the maximum number of duplex connections between the two users with the same physical address equals the maximum number of orthogonal codes.

The main advantage of the architecture is that all the users use the same addressable physical device, both for transmission and reception of signals. The addresses of the users are changed by means of changing the phase shifts, thus indirectly changing the spectral intensity code of the signal that is transmitted through the passive optical star network.

This OCDMA system, like many others, is in principle a broadcast and select system. In such a system the receiver receives the signals from all the transmitters. Ideally, all the unmatched channel signals are canceled due to orthogonal encoding. Nevertheless, a receiver detects the optical power from the unmatched transmitters. This give rise to cumulative shot noise in addition to crosstalk and interference [66]. In OCDMA systems all the users occupy the same frequency band. When light waves of the same wavelength from different users fall onto the photodetector simultaneously, they will interfere with each other causing the optical beat noise [47], which is the main limiting factor in coherent OCDMA systems.

We will show in the next section that the OCDMA system, presented in Figure 7.2 can be represented as the generalized Coherence Multiplexing (CM) system presented in Figure 7.3, [41],[65]. Nevertheless, we have to stress that the main difference is that we use here a combination of amplitude and phase spectral coding of the broadband light spectrum, while in CM system only amplitude spectral coding is used with a periodic transfer function of the en/decoders, [48]. The dual coding in the cascaded system is performed using both delay lines and phase shifters. While the en/decoder transfer functions in the CM system contain only one cosine function with different periodicity depending on the delay difference in the two arms of the MZ en/decoder, the transfer function of the en/decoders in the cascaded OCDMA system contain linear combinations of both sine and cosine functions with the arguments depending on both delays and phase shifts.

Code orthogonality in the presented OCDMA system and signal-to-optical beat noise ratio are the two important issues that will be discussed next. We will first determine the code orthogonality and present the possibilities for making

different sets of orthogonal codes by using an analytical expression for the mean value of the received information-carrying signal. After that we will concentrate on the SNR of the system with respect to the beat noise, which puts the main limitation on system performance.

7.4 Performance analysis

The architecture presented in Figure 7.2 can be considered as the generalized coherence multiplexing scheme with two filters in each of the branches of one MZ interferometer [41],[67]. This is presented in Figure 7.3. Note that in the coherence multiplexing system the upper filter consist of a connection line and the lower filter of a delay line.

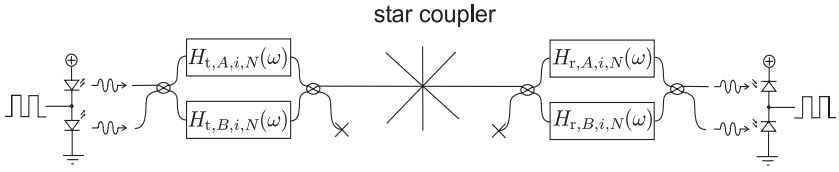

Figure 7.3: A generalized coherence multiplexing system.

$H_{\mathrm{t(r)},A,i,N}(\omega)$, $H_{\mathrm{t(r)},B,i,N}(\omega)$ are generalized field transfer functions of the filters in the transmitter (receiver). These transfer functions in turn are constituted by the delays and phase shifts from each stage of the N-stage MZ transmitter (receiver). The delays and phase shifts in each stage can be represented by the filters with transfer functions:

$$\begin{aligned} H_{\mathrm{t(r)},a,i,k}(\omega) &\triangleq e^{\mathrm{j}\phi_{i,k}} \\ H_{\mathrm{t(r)},b,i,k}(\omega) &\triangleq e^{\mathrm{j}\omega T_{i,k}} \end{aligned} \tag{7.1}$$

where $\phi_{i,k} \in \{0, \pi/2\}$ is the phase shift and $i = 1, ..., M_{\max}$ indicates the index of a particular transmitter (receiver) when cascades are made reversed to each other, $M_{\max}$ is the maximal number of orthogonal codes (connections) [69] and $k = 1, ..., N$ the index of a particular stage in the N-stage MZ en/decoder. $T_{i,k}$ denotes the delays in each stage of the MZ en/decoder.

It can be shown (see Appendix B) that the generalized transfer functions of an N-stage MZ en/decoder can be obtained from the generalized transfer function of the $(N-1)$-stage MZ en/decoder as

$$\begin{aligned} H_{A,i,N}(\omega) &= \tfrac{1}{\sqrt{2}}(H_{A,i,N-1}(\omega) - H_{B,i,N-1}(\omega))H_{a,N}(\omega), \qquad N > 2 \\ H_{B,i,N}(\omega) &= \tfrac{1}{\sqrt{2}}(H_{A,i,N-1}(\omega) + H_{B,i,N-1}(\omega))H_{b,N}(\omega), \qquad N > 2 \end{aligned} \tag{7.2}$$

where $H_{a,N}(\omega)$ and $H_{b,N}(\omega)$ are given in Equation (7.1) and the index that associates the transfer function with the transmitter or the receiver is omitted since we made this recursive formula for the receiver due to simplicity of notations.

Since OCDMA based on cascaded MZ filters can be represented as a generalized CM system we can conclude that this type of OCDMA is coherence encoded OCDMA. This technique belongs to a class of spectrally encoded OCDMA with broadband CW light sources [64]. Different phase shifts are used to modify the output spectrum of the signal and matched decoder comprises identical phase shifts and delays. The phase shifts in MZ filters modify the coherence function of the transmitted signal, hence the term coherence coding. The coherence function is here the autocorrelation function of a filtered stationary circular complex Gaussian bandpass signal, by means of which the field at the output of the encoder can be analytically represented [3]. Filtering is performed by the encoder.

Different phase shifts allows the use of identical delays for all encoders and decoders but requires differential detection to provide discrimination against crosstalk.

The system presented in Figure 7.3 can be compared to the one presented by Griffin and Sampson [58]. In that system only one delay line is used for all the encoders and decoders. This delay line is placed in one of the arms of the MZ interferometer. The dispersive element placed in the other arm of MZ interferometer was used for coding of the spectrum of the output signal by changing the phase of different parts of the spectrum of the broadband source. The difference with respect to the system analyzed here is that phase shifts here are independent of frequency and there are more delay lines.

To analyze the system presented in Figure 7.2 we have to determine the power spectral density (psd) of the encoded signal. We assume an analytic circular complex Gaussian representation of the input field $x(t)$ with the autocorrelation function [70]

$$R_{xx}(\tau) = 2P\ e^{-\pi/2(\tau/\tau_c)^2}\ e^{\mathrm{j}\omega\tau} \tag{7.3}$$

The power spectral density functions can be found from the Wiener-Khintchin relations to be

$$S_{xx}(\omega) = 2\sqrt{2}P\tau_{\mathrm{c}}\ e^{-(\omega-\omega_{\mathrm{c}})^2\tau_{\mathrm{c}}^2} \tag{7.4}$$

where P is the average power of the input optical signal and τ_{c} the coherence time of the source and ω_{c} is the center frequency of the input light spectrum.

The psd of the field at the input of the encoder (filter) can be obtained from the convolution of the psd of the optical field from the LED and the modulating bipolar NRZ signal. This follows from the product of the NRZ signal $s(t)$ and the analytical representation of optical field $x(t)$. For simplicity of calculation we assumed that psd's of the upper and the lower diode are the same, i.e. $S_{x_1x_1}(\omega) = S_{x_2x_2}(\omega) = S_{xx}(\omega)$.

Since the width of the psd of the bipolar NRZ signal is much smaller than the width of the pre-envelope of the LED field, it can be approximated by a delta function. It is known that the convolution of a signal with a delta function results in the same function centered around the position of the delta function. In our case, we are interested in the baseband representation. Such a representation of the input optical signal equals to a baseband representation of the pre-envelope of the field from the LED. This is used latter on in the calculations.

7.4.1 Code definition and orthogonality analysis

We will introduce the spectral fingerprint of the code in order to facilitate the SNR calculation. It is defined as

$$C_i^{(N)}(\omega) \triangleq H_{A,i,N}(\omega)H_{B,i,N}^*(\omega) \tag{7.5}$$

Since the recursive expressions for the generalized transfer functions $H_{A,i,N}(\omega)$ and $H_{B,i,N}(\omega)$ are known (Equation (7.2)), after lengthy but straightforward calculation (see Appendix C) we can write Equation (7.5) as [41]

$$\begin{aligned} C_i^{(N)} &= \tfrac{1}{2}[(H_{A,i,N-1}H^*_{B,i,N-1} - H^*_{A,i,N-1}H_{B,i,N-1}) \\ &\quad - (H_{A,i,N-2}H^*_{B,i,N-2} + H^*_{A,i,N-2}H_{B,i,N-2})]H_{a,i,N}H^*_{b,i,N} \\ &= [-\Re(C_i^{(N-2)}) + \mathrm{j}\Im(C_i^{(N-1)})]e^{-\mathrm{j}(\omega T_{i,N} - \phi_{i,N})}, \quad N > 2 \end{aligned} \tag{7.6}$$

where the dependence of the transfer functions on ω is omitted for the sake of simplicity of representation. The spectral intensity code is equal to the real part of the spectral fingerprint of the code. It gives shape to the power spectral density of the optical signal at the output of the encoder (see Equation (C.8)).

Based on Equations (7.2) and (7.6) it is possible to calculate the complex spectral codes for the N-stage MZ en/decoder if the complex spectral codes for $(N-1)$- and $(N-2)$-stage MZ en/decoder are known. Real and imaginary parts of the complex code can be represented as (see Appendix C)

$$\begin{aligned} \Re(C_i^{(N)}) &= -\Re(C_i^{(N-2)})\cos(\omega T_{i,N} - \phi_{i,N}) + \Im(C_i^{(N-1)})\sin(\omega T_{i,N} - \phi_{i,N}) \\ \Im(C_i^{(N)}) &= \Re(C_i^{(N-2)})\sin(\omega T_{i,N} - \phi_{i,N}) + \Im(C_i^{(N-1)})\cos(\omega T_{i,N} - \phi_{i,N}) \end{aligned} \tag{7.7}$$

In order to check the orthogonality of codes we have to prove the validity of the following expression:

$$\begin{aligned} \int_0^\infty \Re(C_{\mathrm{t},i}^{(N)})\Re(C_{\mathrm{r},j}^{(N)})S_{xx}(\omega)\ \mathrm{d}\omega &= \frac{C_1}{2\pi}\int_0^\infty S_{xx}(\omega)\,\mathrm{d}\omega \\ &= \begin{cases} 0, & i \neq j \\ C_2, & i = j, C_1, C_2 = \text{const.} \neq 0 \end{cases} \end{aligned} \tag{7.8}$$

where C_1 and C_2 are constants with respect to frequency.

In order to satisfy the orthogonality condition (7.8) the delay lines in all the stages must have different values. This can be proven by taking a different delay line value in each stage of the en/decoder and calculating (7.8). The suggestion proposed in [54] to double the delay in every consecutive stage of MZ encoder provides only 4 different orthogonal codes irrespective of the number of stages N. Since we would like to support more users by adding more stages in the encoder we had to find a proper combination of the delay lines that will provide the maximum number of orthogonal codes, such that more users can be supported.

Moreover, these delay lines must be as short as possible to facilitate the practical realization of the system using integrated optical components [69]. All the delays $T_{i,N}$ were calculated with respect to the delay in the first stage, which is multiplied by an integer $K_{i,N}$. To determine this integer a computer simulation is run where for each incremented value of $K_{i,N}$, orthogonality condition (7.8) is evaluated. Obtained values are presented in Table 7.1 for up to $N = 8$ stages.

Table 7.1: Integer values determining the path length difference in each stage of MZ en/decoder.

Number of stages (N) ↓	$K_{i,N}$							
1	1	0	0	0	0	0	0	0
2	1	2	0	0	0	0	0	0
3	1	3	5	0	0	0	0	0
4	1	3	7	12	0	0	0	0
5	1	3	7	21	33	0	0	0
6	1	3	7	21	63	96	0	0
7	1	3	7	21	63	189	285	0
8	1	3	7	21	63	189	567	852

The values presented in the Table 7.1 can be mapped into the following set of rules that provide the shortest delay lines and the maximum number of users [71]

$$\begin{aligned} T_{i,i} &= (K_{i,i-1} + K_{i-1,i-1}) \cdot T_{i,1}, && i = 2, 3, ... \\ T_{i,2} &= 3 \cdot T_{i,1}, && i = 3, 4, ... \\ T_{i,3} &= 7 \cdot T_{i,1}, && i = 4, 5, ... \\ T_{i,m} &= (7 \cdot 3^{m-3}) \cdot T_{i,1}, && \begin{cases} i = 5, 6, ... \\ m = 4, ..., i-1 \end{cases} \end{aligned} \tag{7.9}$$

Using the delays calculated in Equation (7.9) and evaluating the Equation (7.8) it can be concluded that to obtain more codes, the MZ en/decoder must have an even number of stages and the number of new code sets is doubled every time 2 new stages are added. Mathematically expressed, the total number of orthogonal codes in a set that we can get is $2^{\frac{N}{2}+1}$ for even and $2^{\frac{N-1}{2}+1}$ for odd number of stages out of 2^N possible combinations of phase shifts.

After calculating the delays we can use the Equation (7.8) to calculate the mean value of the information-carrying current at the output of the balanced

detector (Equation (C.17)), [41]:

$$\mathrm{E}[I_{\mathrm{r}}(t)] = -\frac{R_{\mathrm{pd}}}{2\pi \cdot 4\ M_{\mathrm{max}}^2} m_i \int_0^{\infty} \{\Re(C_{\mathrm{t},i}^{(N)})\}^2\ S_{xx}(\omega)\ \ \mathrm{d}\omega \qquad (7.10)$$

where m_i is the transmitted bit that can be ± 1 depending on whether the upper or lower diode is transmitting. M_{max} is the maximum number of active users and R_{pd} is the responsivity of the photodiode.

The mean value of the current is different for different number of stages. This is shown in Figure 7.4. We see that the mean value of the current is 1/4 in OCDMA system based on 1-stage MZ en/decoder, but converges to 1/6 as the number of stages increases, which is less than the mean value of the information-carrying current in the CM system by a factor of about two thirds.

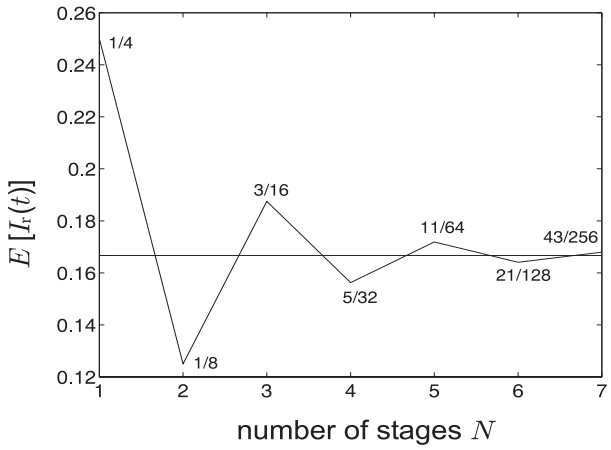

Figure 7.4: The mean value of the current at the output of the balanced detector for different number of stages.

The products of the real parts of the spectral fingerprint of the codes in Equation (7.10) will always be a sum of products of cosines [41]. After integration, only the products of cosines with the arguments $\phi_{i,k} - \phi_{j,k}, k = 1, ..., N$ will remain.

In order to achieve the orthogonality of codes, not only the delay lines but also the phase shifts have to be properly chosen. A combination of phase shifts at the transmitter and receiver (the phase code) must be chosen such that at least one of the cosines in each product in C_1 (Equation (7.8)) equals zero. For an odd number of stages ($N > 1$), there are more possibilities to choose these

combinations and the choice should be such that it gives maximum SNR at the output of the balanced detector. For example, for the 3-stage MZ en/decoder the result of Equation (7.8) is

$$C_1 = \frac{1}{4}\cos(\phi_{i,1} - \phi_{j,1})\cos(\phi_{i,3} - \phi_{j,3}) + \frac{1}{8}\cos(\phi_{i,1} - \phi_{j,1})\cos(\phi_{i,2} - \phi_{j,2})\cos(\phi_{i,3} - \phi_{j,3}) \quad (7.11)$$

We see that this expression equals zero if either $\Delta\phi_1 = \phi_{i,1} - \phi_{j,1}$ or $\Delta\phi_3 = \phi_{i,3} - \phi_{j,3}$ is $\pi/2$ and we cannot make this expression equal zero by changing $\Delta\phi_2 = \phi_{i,2} - \phi_{j,2}$. This means that we can take this value to be either zero or $\pi/2$, and change it together with either $\Delta\phi_1$ or $\Delta\phi_3$, if that will improve the SNR in the system. In this example the total number of orthogonal code sets is equal to 2, but the number will increase with the larger number of stages. Remind that the number of orthogonal codes in the set is equal to 4. For even number of stages the code sets are unique.

The orthogonal phase code set for the 1-stage MZ en/decoder is a combination of phase shifts, $(0, \pi/2)$. Since there are only two possible codes, simultaneous transmission from 2 users only can be supported.

The phase code for the OCDMA system with the 2-stage MZ en/decoder is given in Table 7.2.

Table 7.2: Orthogonal phase codes for the OCDMA system with the 2-stage MZ en/decoder.

Binary orthogonal codes	
0	0
0	$\pi/2$
$\pi/2$	0
$\pi/2$	$\pi/2$

For the 3-stage MZ en/decoder the phase codes are given in Table 7.3. Here symbol x represents either 0 or $\pi/2$, since 2 orthogonal code sets can be made for this system.

The orthogonal phase codes from the unique code in the 4-stage MZ en/decoder system are given in Table 7.4.

Table 7.3: Orthogonal phase codes for the OCDMA system with the 3-stage MZ en/decoder.

Binary orthogonal codes		
0	x	0
0	x	$\pi/2$
$\pi/2$	x	0
$\pi/2$	x	$\pi/2$

Table 7.4: Orthogonal phase codes for the OCDMA system with the 4-stage MZ en/decoder.

Binary orthogonal codes			
0	0	0	0
0	0	0	$\pi/2$
$\pi/2$	0	0	0
$\pi/2$	0	0	$\pi/2$
0	$\pi/2$	$\pi/2$	0
0	$\pi/2$	$\pi/2$	$\pi/2$
$\pi/2$	$\pi/2$	$\pi/2$	0
$\pi/2$	$\pi/2$	$\pi/2$	$\pi/2$

Finally, we present the phase codes in the 5-stage MZ en/decoder OCDMA system in Table 7.5.

Solving the equation (7.8) and analyzing C_1 we can infer the phase shifts ϕ_1 and ϕ_5 can be changed independently such that C_1 equals zero and the phase shifts ϕ_2, ϕ_3 and ϕ_4 have to be changed in the certain way. For example, we can either change phase shifts ϕ_2 and ϕ_3 together and the phase shift ϕ_4 separately, or the phase shifts ϕ_3 and ϕ_4 together and the ϕ_2 separately. We can even change all three phase shifts together. Since the phase shifts can have 2 different values, the total number of code sets is 6. The phase codes presented in Table 7.5 are from the code set obtained by changing the phase shifts ϕ_2 and ϕ_3 together and the phase shift ϕ_4 separately.

The phase codes for the spectrally encoded OCDMA system with more than 5-stages will not be presented, but they can be easily derived from Equation (7.8), by analyzing C_1.

Table 7.5: Orthogonal phase codes for the OCDMA system with the 5-stage MZ en/decoder.

Binary orthogonal codes				
0	0	0	0	0
0	0	0	0	1
1	0	0	0	0
1	0	0	0	1
0	0	0	1	0
0	0	0	1	1
1	0	0	1	0
1	0	0	1	1

7.4.2 Coding possibilities

The difference in coding schemes between the cascaded OCDMA system and CM system is that in the OCDMA system both amplitude and phase spectral encoding is performed, while in CM system only amplitude spectral encoding takes place.

It was interesting to investigate another possibility to achieve full orthogonality of codes in cascaded OCDMA systems by changing the phase shifts only, irrespective of the condition that delays must be much larger than the coherence time τ_{c} of the source and smaller than the bit time T_{b}, since this would allow larger bit-rates.

To be able to make the codes in this way, we have tried to find any value for phase shifts, not necessarily form $[0, \pi/2]$ that satisfy the conditions:

$$\begin{aligned} &\int_0^\infty \Re_0(C_{\mathrm{t},i}^{(N)})\Re_0(C_{\mathrm{r},j}^{(N)})S_{xx}(\omega)\ \ \mathrm{d}\omega = 0 \\ &\int_0^\infty \Re_0^2(C_{\mathrm{t},i}^{(N)})S_{xx}(\omega)\ \ \mathrm{d}\omega \neq 0, \quad \int_0^\infty \Re_0^2(C_{\mathrm{r},j}^{(N)})S_{xx}(\omega)\ \ \mathrm{d}\omega \neq 0 \end{aligned} \tag{7.12}$$

where subscript 0 denotes that ω=0. Trying to solve this system of equations we have found no solution. This means that we cannot achieve full orthogonality of codes by changing only the phase shifts, for any given number of stages N. This reveals the necessity of using the phase shifts in combination with delay lines for code orthogonality.

7.4.3 SNR calculation

The main limiting factor in the performance of the presented OCDMA system is the optical beat noise (OBN). We will assume in our calculations that for the N-section MZ en/decoder, all possible connections are established. In order to determine the power spectral density of OBN we will use the expression for the psd of OBN in a coherence multiplexing system [67]. Here we suppose that the psd of OBN is flat in a wide frequency range and that is the reason we will evaluate this function for $\omega = 0$:

$$S_{I_\mathrm{r}I_\mathrm{r}}(0) = \frac{R_\mathrm{pd}^2}{2\pi \cdot 256\ M_\mathrm{max}^4} \sum_{i=1}^{M}\sum_{j=1}^{M} \int_0^\infty ([H_{\mathrm{r},A,l}H_{\mathrm{r},B,l}^* + H_{\mathrm{r},A,l}^* H_{\mathrm{r},B,l}]^2 \cdot |H_{\mathrm{t},A,i} - m_i H_{\mathrm{t},B,i}|^2 |H_{\mathrm{t},A,j} - m_j H_{\mathrm{t},B,j}|^2 S_{xx}^2)\ \mathrm{d}\omega \quad (7.13)$$

We omitted here again the dependence on ω for the sake of simplicity of representation. $m_{i(j)}$ can be ± 1 depending on whether the upper or the lower diode is transmitting and M represents the number of active users. Indexes i, j, l denote different transmitters and receivers. We again assume that the bit time T_b is much larger than the delays $T_{i,k}, k = 1, ..., N$ in the MZ en/decoders.

Invoking equation (7.5) and simplifying the last expression we get

$$S_{I_\mathrm{r}I_\mathrm{r}}(0) = \frac{R_\mathrm{pd}^2}{32\pi M_\mathrm{max}^4} \int_0^\infty \left(M^2 [\Re(C_{\mathrm{r},l}^{(N)})]^2 + [\Re(C_{\mathrm{r},l}^{(N)})]^2 \sum_{i=1}^{M} [\Re(C_{\mathrm{t},i}^{(N)})]^2 \right) S_{xx}^2(\omega)\, \mathrm{d}\omega \quad (7.14)$$

Evaluating the real parts of the complex spectral codes for different number of stages N, we find that Equation (7.14) can be approximated by

$$S_{I_\mathrm{r}I_\mathrm{r}}(0) \approx \frac{R_\mathrm{pd}^2}{32\pi\ M_\mathrm{max}^4} \left(M^2 \cdot K + M \cdot K^2\right) \int_0^\infty S_{xx}^2(\omega)\ \ \mathrm{d}\omega. \quad (7.15)$$

where K is a number that converges to 1/3 for large N and is shown in Figure 7.5. The psd calculated in Equation (7.15) varies slightly for different code sets. This variation is less than 2%, so the Equation (7.15) will be used for calculating the SNR for all possible code sets.

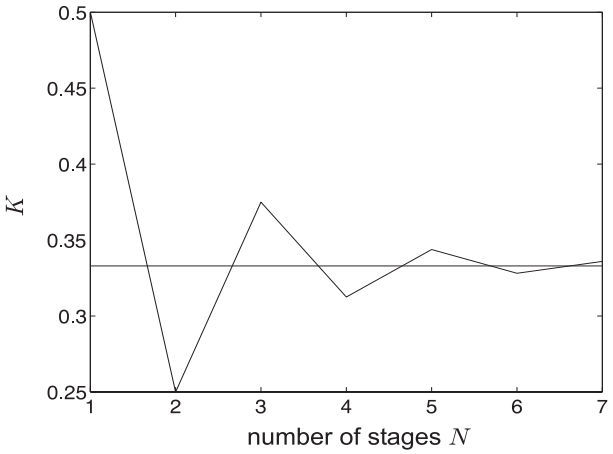

Figure 7.5: K factor representation for different number of stages N.

We see that the first term in Equation (7.15) within the brackets is the dominant one due to multiplication with the squared number of active users. We can also conclude from Equation (7.15) that the psd of the OBN stays constant for $N > 7$, no matter what the number of stages in the MZ en/decoder is, provided that the number of active users is the same.

The signal-to-beat noise ratio after the integrate-and-dump filter is given by:

$$SNR = \frac{\mathrm{E}^2[I_\mathrm{r}(t)]\ T_\mathrm{b}}{S_{I_\mathrm{r}I_\mathrm{r}}(0)} = \frac{1}{3\ M^2 + M} \cdot \frac{T_\mathrm{b}}{\tau_\mathrm{c}} \tag{7.16}$$

We see that for a large number of users the SNR decreases with three times the squared number of active users, which is two thirds worse than the SNR in the one stage coherence multiplexing system [67].

7.4.4 SNR in the OCDMA system based on multimode fibers

To simplify the analysis of the spectrally encoded OCDMA system based on multimode fibers only guided modes without mutual coupling are assumed and that the transmitted power is equally distributed among modes. As till now, the same circular complex Gaussian bandpass model has been used for the broadband light field.

Since all the modes in the fiber are actually characterized by the fields that

are spatially orthogonal to each other, interference among them will not take place. This is very important for calculating the total current at the output of the balanced detector. Although only the same modes in each of the branches in the MZ interferometer can interfere, the mean value of the output current will remain the same as in the case of the system based on a single-mode fiber. The OBN terms on the other side will reduce by the factor of n, where n is the number of modes in the multimode MZ filter, assuming that power is equally carried by all the modes in the decoder. The final result that we have obtained for SNR is

$$SNR = \frac{\mathrm{E}[I_\mathrm{r}(t)]^2 T_\mathrm{b}}{S_{I_r I_r}(0)} = \frac{n}{3M^2 + M} \cdot \frac{T_\mathrm{b}}{\tau_\mathrm{c}} \tag{7.17}$$

Comparing this result with equation (7.16) for the SNR in the system based on a single-mode fiber one can infer n times improvement in the SNR. This result favorites the realization of the system using multimode fibers and components.

7.5 System sensitivity on the phase shift drift

In this section sensitivity of the mean value of the information-carrying current on phase variations in the different phase shifters placed in each stage of MZ en/decoder will be determined. The sensitivity is very important for the performance analysis of the system since the phase variations in the phase shifters together with OBN will limit the maximal number of simultaneous users in the system.

The mean value of the information-carrying current at the output of the balanced detector in the system depends on the number of stages in MZ en/decoder [78] and is equal to the sum of cosines with different arguments. Those arguments in turn consist of a linear combination of different phase shifts applied at the phase shifters both, at the transmitter and receiver. The multiplication factors in the linear combinations of all the phase shifts at both transmitter and receiver $m_{1,2}$ can be either 0 or ± 1:

$$\mathrm{E}[I_\mathrm{r}(t)] = C \cdot \sum_i \cos_i\Big(\sum_j m_1 \phi_{\mathrm{t},j} - m_2 \phi_{\mathrm{r},j}\Big), \qquad C = \mathrm{const.} \tag{7.18}$$

This means that the number of phase shifts in different arguments of cosines will not always be the same and will depend on the number of stages, as will be shown later.

Suppose that all the delays are chosen in such a way that they provide maximal number of codes, than the average current at the output of the balanced detector, in the system with N-stage MZ en/decoder, depends only on the phase shifts in each stage of MZ en/decoder. The normalized mean value of the information-carrying current is equal to [78]:

$$\mathrm{E_n}[I_{\mathrm{r},N}(t)] = \frac{1}{2}[(\mathrm{E_n}[I_{\mathrm{r},N-1}(t)] + \mathrm{E_n}[I_{\mathrm{r},N-2}(t)]) \cdot \cos(\phi_{\mathrm{t},N} - \phi_{\mathrm{r},N})] \qquad (7.19)$$

where $\mathrm{E_n}[I_{\mathrm{r},N-1}(t)]$ and $\mathrm{E_n}[I_{\mathrm{r},N-2}(t)]$ are the normalized mean values of the currents at the output of the balanced detector of the OCDMA system with an $N-1$- and $N-2$-stage MZ en/decoder, respectively. The exact mean value of the current is obtained by multiplying Equation (7.19) by $1/2 \cdot R_{\mathrm{pd}}P$. For the trivial cases when the number of stages is 1 and 2 this values are:

$$\begin{aligned} \mathrm{E_n}[I_{\mathrm{r},1}(t)] &= \tfrac{1}{2}[\cos(\phi_{\mathrm{t},1} - \phi_{\mathrm{r},1})] \\ \mathrm{E_n}[I_{\mathrm{r},2}(t)] &= \tfrac{1}{8}[\cos(\phi_{\mathrm{t},1} + \phi_{\mathrm{t},2} - \phi_{\mathrm{r},1} - \phi_{\mathrm{r},2}) + \cos(\phi_{\mathrm{t},1} - \phi_{\mathrm{t},2} - \phi_{\mathrm{r},1} + \phi_{\mathrm{r},2})] \end{aligned} \qquad (7.20)$$

Suppose that the phase shifts $\phi_{\mathrm{t},j(\mathrm{r},j)}, j = 1, ..., N$ change from their nominal values to $\phi_{\mathrm{t},j(\mathrm{r},j)} \pm \Delta\phi_{\mathrm{t},j(\mathrm{r},j)}$ and suppose that change of this parameter does not occur fast with respect to time. If $\Delta\phi_{\mathrm{t},j(\mathrm{r},j)} \ll 1$, then we can series expand the cosine term in equation (7.18). To make the sensitivity analysis we have to find the first derivative of the mean value of the information-carrying signal with respect to the each variable (phase shift) and add them.

After calculating the first derivative we could not get a result that is unequal to zero. This means that the system will not be very sensitive to the phase drift. Consequently, the performance of the system will not be significantly degraded.

To calculate the sensitivity we have used the second derivative of the mean value of the information-carrying current $\mathrm{E}[I_{\mathrm{r}}(t)]$ with respect to the phase shifts. Suppose that deviations of all the phase shifts in the system are equal and denote this value as $\Delta\phi$. For sensitivity calculation we always choose the sign that gives the worst case deviation.

Starting from the sensitivity calculations in the OCDMA system with 1-stage

MZ en/decoder and expanding the analysis for more stages we have calculated that the sensitivity of the mean value of the information-carrying current in the OCDMA system with the N-stage MZ en/decoder equals

$$\Delta \mathrm{E}[I_{\mathrm{r}}(t)] = \frac{R_{\mathrm{pd}}P}{2^{2N}}\left[n_{N,\cos}(n_{N,\phi})\frac{(n_{N,\phi}\Delta\phi)^2}{2}\right] \tag{7.21}$$

where $n_{N,\cos}(n_{N,\phi})$ and $n_{N,\phi}$ are the number of cosines with the same number of phase shifts in their arguments and the number of phase shifts $\phi_{\mathrm{t},j(\mathrm{r},j)}$, $j = 1, ..., N$, respectively for the system with N-stage MZ en/decoder. The system sensitivity is completely determined if both $n_{N,\cos}(n_{N,\phi})$ and $n_{N,\phi}$ that depend on the number of stages in MZ en/decoder, are known.

It is obvious that the number of cosines in any N-section MZ en/decoder system is twice the value of the addition of the number of cosines in the OCDMA system with the $N-1$- and $N-2$-stage MZ en/decoder. This number will always be even. The number of phase shifts $\phi_{\mathrm{t},j(\mathrm{r},j)}, j = 1, ..., N$ in the particular argument of cosine will also be even. The number of cosines in the mean value of the information-carrying current in the OCDMA system with N-stage MZ en/decoders will be:

$$\begin{aligned} n_{N,\cos}(2\cdot l+i) = [&n_{N-2,\cos}(2\cdot(l-1)+i) \\ &+ n_{N-1,\cos}(2\cdot(l-1)+i)]\cdot 2, \begin{cases} N>2, \\ i=N-1, \quad N=\text{odd} \\ i=N, \quad N=\text{even} \\ l=1,\ldots,\lceil N/2\rceil \end{cases} \end{aligned} \tag{7.22}$$

where $n_{N-2,\cos}(2\cdot(l-1)+i)$ and $n_{N-1,\cos}(2\cdot(l-1)+i)$ are the number of cosines in the mean value of the information-carrying current in the OCDMA system with $N-1$ and $N-2$-stage MZ en/decoders, respectively. $2\cdot l+i$ is the number of phase shifts $n_{N,\phi}$ in the particular argument of cosine in the system with N-stage MZ en/decoder.

In order to give reader a feeling how large all this numbers are, a Table 7.6 is presented where the number of cosines $n_{N,\cos}(2\cdot l+i)$ with the same number of phase shifts $2\cdot l+i$ in the argument is given, provided that the number of phase shifts and total number of stages N are given.

Finally, the sensitivity of the N-stage MZ en/decoder system, for $N > 2$

Table 7.6: The number of cosines $n_{N,\cos}(2 \cdot l + i)$ with the same number of phase shifts in the argument $2 \cdot l + i$, with respect to the number of phase shifts and total number of stages.

Number of stages N	Total number of phase shifts									
	2	4	6	8	10	12	14	16	18	20
1	1	0	0	0	0	0	0	0	0	0
2	0	2	0	0	0	0	0	0	0	0
3	0	2	4	0	0	0	0	0	0	0
4	0	0	8	8	0	0	0	0	0	0
5	0	0	4	24	16	0	0	0	0	0
6	0	0	0	24	64	32	0	0	0	0
7	0	0	0	8	96	160	64	0	0	0
8	0	0	0	0	64	320	384	128	0	0
9	0	0	0	0	16	320	960	896	256	0
10	0	0	0	0	0	160	1280	2688	2048	512

reads:

$$\Delta \mathrm{E}[I_{\mathrm{r}}(t)] = \frac{R_{\mathrm{pd}} P}{2^{2N}} \left[n_{N,\cos}(2 \cdot l + i) \frac{((2 \cdot l + i)\Delta\phi)^2}{2} \right], \text{for} \begin{cases} N > 2, \\ i = N-1, N = \text{odd} \\ i = N, \quad N = \text{even} \\ l = 1, \ldots, \lceil N/2 \rceil \end{cases} \tag{7.23}$$

The variation in the mean value of the information-carrying current at the output of the balanced detector is proportional to the squared absolute value of the phase drifts. If the phase shift drifts are small variation in the mean value of the information-carrying current will be negligible.

7.6 Coherence multiplexing system with variable delays

The presented OCDMA system based on cascaded MZ en/decoders show inferior performance to a CM system with respect to the optical beat noise. Nev-

ertheless, introducing more stages in the cascaded OCDMA system, keeping the number of phase shifters the same, the coherence multiplexing system with variable delays can be designed [78]. This is presented in Figure 7.6.

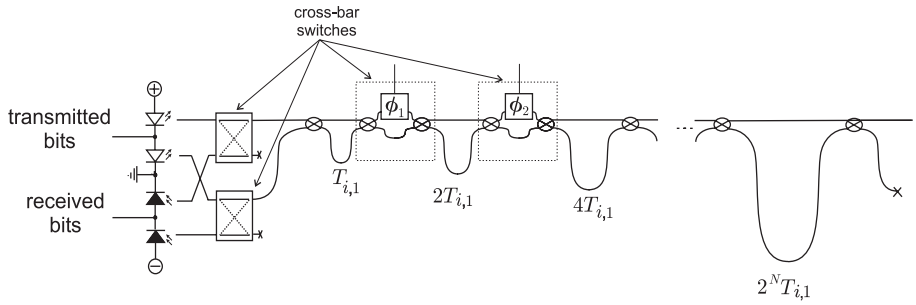

Figure 7.6: Optical encoder in the coherence multiplexing system with variable delays.

By changing different phase shifts for 0 to π using for example, the thermo-optic (TO) effect, the total path delay difference can change, since the MZIs with the phase shifters are in fact cross-bar switches. The advantage of such a system with respect to the cascaded OCDMA system is in improved signal-to-beat noise ratio which is equal to the one in a single stage CM system, [68]. Compared to the single stage CM system, all the users can use the same physical chips for the encoder and decoder, which will decrease the overall implementation cost. Moreover, modulation in the electrical domain makes such a system more attractive for practical implementation. Due to the symmetry of the encoder and decoder duplex transmission in the system can be achieved. Two switches placed in front of the encoder at the transmitting side and behind the decoder at the receiving side, are used to switch from transmission to reception of the signal and vice versa. Full-duplex transmission cannot be supported due to difficulties to isolate the transmitted from the received signal using, for example, a directional coupler and a rather strong sensitivity on reflections, which may occur at the link, at connectors etc. The disadvantage of the system is in the limited modulation speed of the SLEDs, that goes up to several hundreds of Mbps. Nevertheless, the system is still fast enough to accommodate the Fast Ethernet protocol.

7.7 Possibilities of using OCDMA in the Fast Ethernet LANs

Implementation of spectrally encoded OCDMA techniques in Fast Ethernet network can improve the performance of the network by increasing both capacity and throughput. This due to the unchanged data transmission rate in the optical domain. One possibility for implementing OCDMA technique in the LAN network is presented in Figure 7.7.

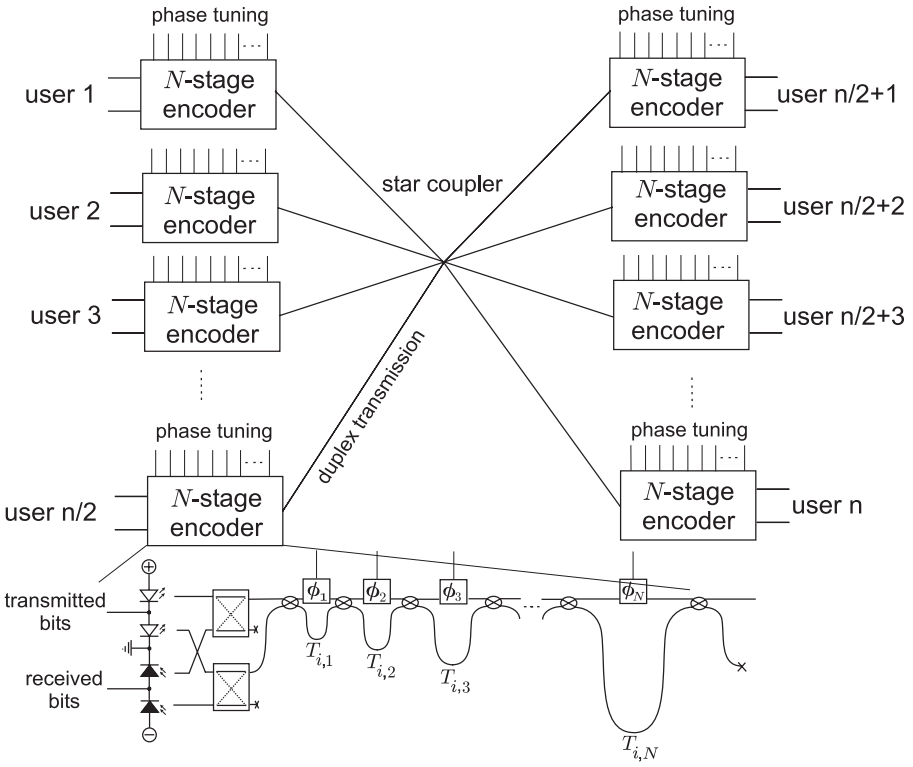

Figure 7.7: OCDMA application in optically transparent LAN.

In a LAN environment all the users are connected by means of a passive star coupler. The distance among users can be up to several kilometers when single-mode fiber is used. The bit rates the system can support depend on the electronic part since the optical part is completely passive and optically transparent. This means that upgrading the system to run on the duplex Gigabit Ethernet and 10 Gigabit Ethernet can be done by only changing the electronic

part at the users site. Since packets from different users are OCDMA encoded no collisions will take place, except for the case when two transmitters are sending to the same user. Duplex transmission is enabled due to the symmetry of encoder and decoder with respect to each other. Address changing is done by varying the phase shifts in the phase shifters placed in one of the arms in each stage of the MZ en/decoder. The performance of the system in case of half-duplex transmission is equal to performance of the Fast Ethernet networks based on switches without internal buffer. There collision occur if two or more data packets are addressed to the same destination.

When using this OCDMA technique in access networks two star couplers have to be used. One is a 1:N coupler connecting all the optical network units (ONUs) and the other one is connecting all the transceivers in an optical line terminal (OLT). This is presented in Figure 7.8. Due to the fact that larger distances have to be covered with access networks than with LANs, the presented system have to be based on single-mode fiber and components, due to the smaller attenuation and dispersion limitations.

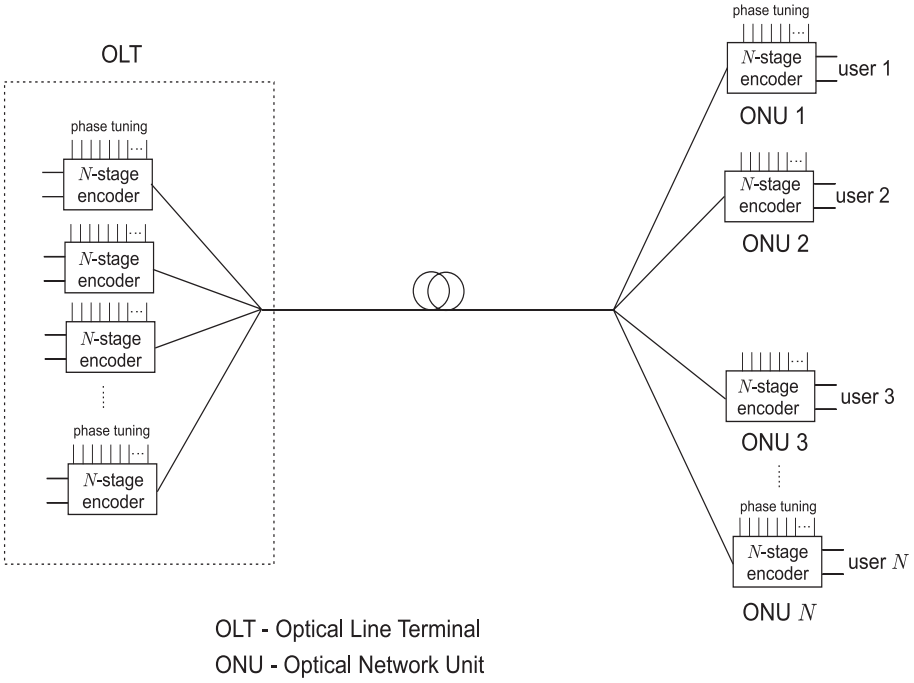

Figure 7.8: OCDMA application in a passive optical access network.

7.8 Conclusions

Two OCDMA systems based on spectral encoding are shown. Both of them are based on noncoherent light sources such as edge emitting LEDs and Super luminescent diodes. The OCDMA systems are simple and can be realized using integrated optical components. The basic elements of both systems are the MZ encoder and decoder.

The system based on cascades of MZIs performs coding of both amplitude and phase of the broadband spectrum of the source, while CM system with variable delays performs coding of spectral amplitude only. The coding is done by combination of phase shifters and appropriate delay lines in each of the stages of the MZIs. The analysis showed that the SNR in the CM system is better for about 1/3 compared to the cascaded OCDMA system, for larger number of stages.

The analysis of cascaded OCDMA systems is facilitated due to the fact that they can be represented as generalized CM systems. Based on recursive expressions for the spectral fingerprints of the codes the number of all possible sets of orthogonal codes can be determined. From SNR analysis the one that gives the best performance can be chosen for implementation. It has been calculated that the SNR is inversely proportional to three times the squared number of active users. It is important to emphasize that the obtained results are only valid if the bit time is much larger than the delays in the MZ interferometers.

The improvements with respect to the original design of cascaded OCDMA systems was in increased number of possible orthogonal codes. To obtain the maximum number of orthogonal codes a pattern was created for PLD values. This pattern provides the shortest possible PLDs in order to enable practical realization of the system using integrated-optic components. The same system can be realized using both single-mode an multimode components. It is shown that much better performance can be obtained in the multimode system with respect to OBN, compared to its single-mode counterpart. Nevertheless, the distances that can be reached among users are much shorter. This makes the multimode system more suitable for LAN networks and the single-mode system more for the access networks.

The presented CM system with variable delays offers a possibility for practical implementation of the CM system. All the users in the network can use the same physical device for en/decoding, which is the main advantage compared to the single stage CM system. To use the system in high-speed LAN environ-

ments en/decoder must be installed at the users site. Such a system offers nice upgrading possibility since the only speed limitation of the network comes from the electronic circuitry. Therefore, increasing the bit-rate requires changing of the NICs at the users site. All the optical installations may remain unaltered.

CHAPTER 8

Dispersion limitation in optical multimode systems

All the LAN architectures presented in this thesis are based on multimode fibers and short wavelength components to make the system more economically attractive. We believe that new multimode integrated optical components in combination with multimode fibers will be significant in bringing information to the user.

The dispersion restrictions on using multimode fibers in access and local area networks are usually neglected due to their relatively short span, but in order to get more accurate results, it is of importance to calculate the dispersion effect on system performance [73]-[75], especially if broadband sources are used.

In order to determine the broadening of the input pulse in the multimode fiber due to dispersion and its effect on the system performance, we will start with the analysis of the dispersion effect in the transfer function of the single-mode fiber, since we can associate each mode with the transmission channel in a single-mode fiber [4]. For the sake of simplicity, it is assumed that the modes are not mutually coupled. Therefore, the phase characteristic of an individual channel equals the phase characteristic of its corresponding mode.

We will analyze degenerate modes and consider only guided modes. The

total transfer function of the multimode fiber will be the superposition of the individual transfer functions of the single transmission channels when the transmission of each mode is considered separately, taking into account the delays between each mode due to the modal dispersion.

We will determine the effect of both chromatic and modal dispersion on pulse broadening in the multimode fiber and than calculate the dispersion penalties using two different approaches since the magnitude of the penalty depends on the type of pulse shaping performed by the optical receiver.

8.1 Chromatic dispersion

In this section we will investigate the influence of chromatic dispersion on the transfer function of the single-mode fiber, since we can approximate the transmission of the individual modes in the multimode fiber as a transmission through a single-mode fiber [4]. This type of the dispersion provokes pulse spreading since the initial pulse has a finite spectral linewidth and since group velocities are wavelength dependent [3].

Using the generalized expression for the power transfer function of the single-mode fiber [4] the impulse response of the fiber will be (see Appendix A):

$$h(t) = \frac{\sqrt{2}cPA^2\tau_c}{\pi b_0''}\; e^{-\frac{\tau_c^2(t-b_0')^2}{2\pi b_0''^2}} \tag{8.1}$$

Note that factor b_0' just shifts the impulse response. This impulse response is actually an impulse response of the single-mode fiber that can be used for the approximation of the transfer function of one particular mode in a multimode fiber. The transfer function of the single-mode fiber is now

$$H(\omega) = \mathcal{F}(h(t)) = 2cPA^2\; e^{-\frac{\omega^2\pi b_0''^2}{2\tau_c^2}}\; e^{-\mathrm{j}\omega b_0'} \tag{8.2}$$

To give an example of the shape of the impulse response in equation (8.1) we have calculated it for a silica fiber at a wavelength of $\lambda_0 = 840$ nm. Dispersion coefficient is found to be $D_\lambda = 75$ ps km^{-1}nm^{-1}. For the broadband source of $\Delta\lambda = 20$ nm and a typical fiber length for LANs of $l = 1$ km the impulse response is shown in Figure 8.1.

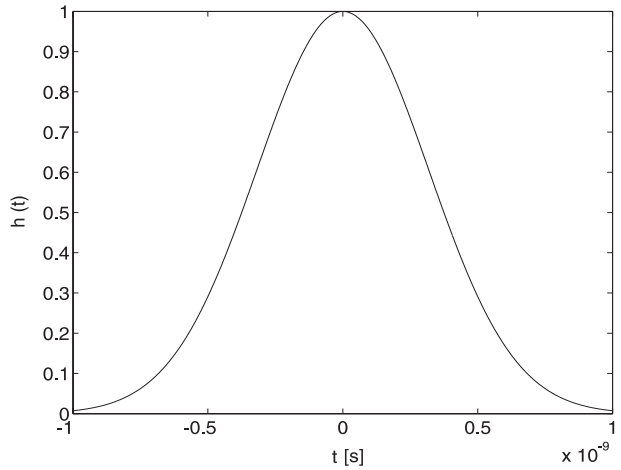

Figure 8.1: The impulse response of the single-mode fiber of length $l = 1$ km, with $D_\lambda = 75$ ps km^{-1}nm^{-1} at a wavelength of $\lambda_0 = 840$ nm and the linewidth of the source $\Delta\lambda = 20$ nm. $\tau_c = 1.563 \cdot 10^{-13}$ s.

The total impulse response of a multimode fiber can be found as a sum the impulse responses given in equation (8.1), taking into account different delays of the modes b_0' due to the modal dispersion. So, in order to calculate the total impulse response we have to determine the impact of modal dispersion on the total impulse response of the fiber.

8.2 Modal dispersion in the fiber

Group delay of the modes can be found if specific group delay for a fiber with refractive index profile is known

$$b_0' = \frac{d\beta}{d\omega} \cdot l = \tau_g \cdot l \tag{8.3}$$

where l is the length of the fiber and τ_g specific group delay in the fiber.

The specific phase shift β of the signal in a graded index fiber is given by [4]:

$$\beta = \frac{\omega}{c_0}\left[n^2(0) - \frac{2(NA)^2}{v}(2m + n + 1)\right]^{1/2} \tag{8.4}$$

where v is the normalized frequency defined as

$$v = \frac{2\pi a}{\lambda_0}(NA) = k_0(NA)a. \tag{8.5}$$

Here a is the core radius of the multimode fiber, which is in our case $a = 25$ μm and m and n are specific mode numbers. NA is the numerical aperture and c_0 the speed of light in vacuum. $n(0)$ is the refractive index of the fiber which is assumed to be frequency independent. Differentiating $\beta(\omega)$ with respect to ω gives:

$$\tau_{\mathrm{g}} = \frac{d\beta}{d\omega} = \frac{1}{c_0}\frac{v\ n^2(0) - NA^2(2m+n+1)}{\sqrt{n^2(0)v^2 - 2NA^2v(2m+n+1)}} \quad \left[\frac{\mathrm{s}}{\mathrm{m}}\right] \tag{8.6}$$

provided that the refractive index does not depend on frequency.

We see that the specific group delay differs for different group of modes with m and n such that $2m + n + 1$ gives the same value. The variation of the group delay with the mode numbers n and m can be demonstrated by the impulse response of the fiber. In Figure 8.2 an impulse response of the fiber with parabolic refractive index profile is illustrated. No material dispersion is taken into account.

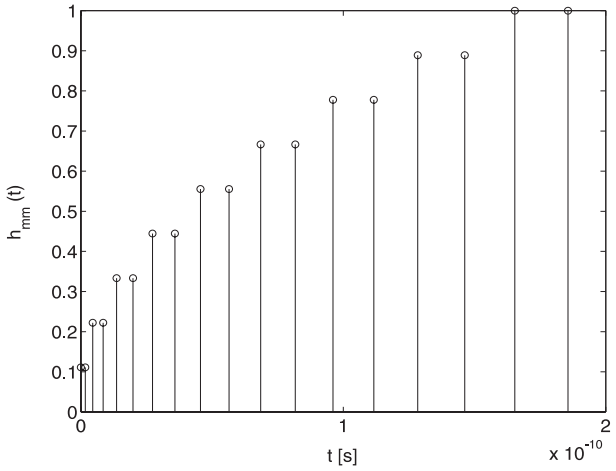

Figure 8.2: The impulse response of the multimode fiber with parabolic refractive index profile. $a = 25$ μm, $n(0) = 1.5, NA \approx 0.2$.

The normalized values along the y-axis depend on the number of modes in a mode group and delays between them are calculated using equation (8.6). In total 18 groups of guided modes are presented.

Without any material dispersion the fiber impulse response would be as in Figure 8.2, provided the total input power is equally distributed over the guided modes. The mathematical representation of the impulse response is:

$$h_{\mathrm{mm}}(t) = \sum_{i=1}^{18} a_i \ \delta(t - \tau_i) \tag{8.7}$$

where $\tau_i = b_0'(i), i = 1, ..., 18$.

8.3 Total dispersion in the multimode fiber

Based on the results obtained in the previous two subsections we can calculate the total transfer function of the multimode fiber when both group delay of different modes and material dispersion is taken into consideration. If $H_{\mathrm{c1}}(\omega)$ and $H_{\mathrm{M}}(\omega)$ denote the transfer function of the fiber for the single mode when material dispersion is taken into account and the transfer function of the multimode fiber when only modal dispersion is taken into account, respectively, then the total transfer function of the multimode fiber when both dispersions are taken into account reads [76]

$$H(\omega) = H_{\mathrm{c1}}(\omega) \ H_{\mathrm{M}}(\omega) = 2cA^2P \ e^{-\frac{(\omega b_0'')^2}{2}\frac{\pi}{\tau_c^2}} \sum_{i=1}^{18} a_i \ e^{-\mathrm{j}\omega\tau_i} \tag{8.8}$$

The impulse response of the multimode fiber is therefore:

$$h(t) = \int_{-\infty}^{\infty} h_{\mathrm{M}}(\tau) h_{\mathrm{c1}}(t - \tau) \ \mathrm{d}\tau = 2cA^2P \frac{1}{\sqrt{2\pi}\sigma_t} \sum_{i=1}^{18} a_i \ e^{-\frac{(t-\tau_i)^2}{2\sigma_t^2}} \tag{8.9}$$

where

$$\sigma_t = \frac{\sqrt{\pi} b_0''}{\tau_{\mathrm{c}}} \tag{8.10}$$

If we replace the vertical lines shown in Figure 8.2 with pulses of the same form given in Figure 8.1 and height that is proportional to the number of modes in the group concerned, and compile those we get the total impulse response of the multimode fiber that is presented in Figure 8.3.

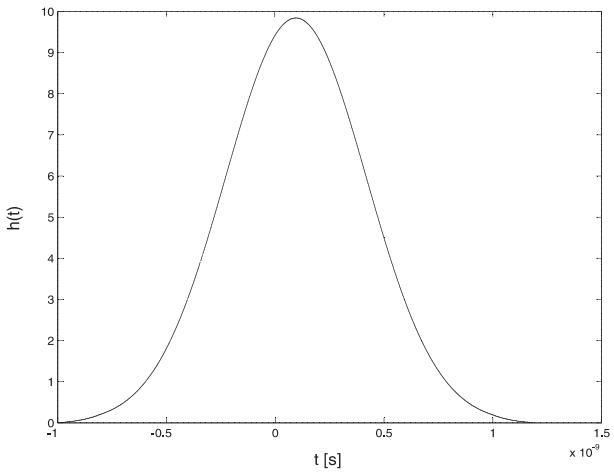

Figure 8.3: The total impulse response of the multimode fiber for $\lambda_0 = 840$ nm.

8.4 Calculation of dispersion penalties

The magnitude of the penalty will depend upon the type of pulse shaping performed by the optical receiver. Two different possibilities will be considered [74]:

1. The receiver transfer function is matched to the input signal format and fiber span length so that a raised-cosine output waveform is maintained after transmission through the fiber. A power penalty is incurred owing to the larger noise bandwidth of the equalized receiver.

2. The receiver is designed to produce a raised-cosine output waveform given an undistorted NRZ input signal. No equalization is performed to compensate for pulse broadening due to fiber dispersion. For this case a power penalty results from the eye closure caused by ISI.

8.4.1 The first possibility

In this analysis the power penalty incurred in equalized receivers is dependent on the receiver noise spectral density.

As an input signal to the LED, let us consider a NRZ signal format, which has a signal spectrum:

$$H_{\mathrm{s}}(\omega) = 2\frac{\sin \omega/2B}{\omega} \tag{8.11}$$

where $B = 1/T_{\mathrm{b}}$ is the signal bit rate and T_{b} is the bit time.

For the output waveform we take the commonly used raised-cosine pulse:

$$h_{\mathrm{out}}(t) = \frac{\sin \pi Bt}{\pi Bt}\frac{\cos \pi Bt}{1-(2Bt)^2} \tag{8.12}$$

with the spectrum

$$H_{\mathrm{out}}(\omega) = \begin{cases} \frac{1}{B}\cos^2 \frac{\omega}{4B}, & |\omega| \leq B/2\pi \\ 0, & |\omega| > B/2\pi \end{cases} \tag{8.13}$$

In the case of a distortionless transmitter and a dispersionless channel, the receiver transfer function $H_{\mathrm{r}}(\omega)$ required to produce the output of equation (8.12) may be determined from

$$H_{\mathrm{r}}(\omega) = \frac{H_{\mathrm{out}}(\omega)}{H_{\mathrm{s}}(\omega)} = \begin{cases} \frac{\omega}{4B}\cot \frac{\omega}{4B}, & |\omega| \leq B/2\pi \\ 0, & |\omega| > B/2\pi \end{cases} \tag{8.14}$$

The effect of propagation through the fiber is represented by the transfer function $H(\omega)$. In order to maintain the raised-cosine output the receiver must be equalized, requiring a new response $H'_{\mathrm{r}}(\omega)$ given by

$$H'_{\mathrm{r}}(\omega) = \frac{H_{\mathrm{out}}(\omega)}{H_{\mathrm{s}}(\omega)H(\omega)} = \frac{H_{\mathrm{r}}(\omega)}{H(\omega)} \tag{8.15}$$

Given a receiver noise spectral density $G(\omega)$, an optical power penalty P_{d} may be computed from the increased noise bandwidth [74]

$$P_{\mathrm{d}} = 5\ \log\left[\frac{\int G(\omega)|H_{\mathrm{r}}(\omega)|^2|H(\omega)|^{-2}\ \mathrm{d}\omega}{\int G(\omega)|H_{\mathrm{r}}(\omega)|^2\ \mathrm{d}\omega}\right] \tag{8.16}$$

Since the total noise power spectral density (shot noise psd+thermal psd) does not depend on frequency we can write that

$$P_{\mathrm{d}} = 5\ \log\left[\frac{\int |H_{\mathrm{r}}(\omega)|^2|H(\omega)|^{-2}\ \mathrm{d}\omega}{\int |H_{\mathrm{r}}(\omega)|^2\ \mathrm{d}\omega}\right] \tag{8.17}$$

In order to find the solution for equation (8.17) we have to expand $|H(\omega)|^{-2}$, from equation (8.8), into a Taylor series. Taking the first three terms from the series and invoking equation (8.10), the power penalty reads

$$P_{\mathrm{d}} = 5\log \frac{1}{(2cPA^2\sum_{i=1}^{18} a_i)^2}\left(1+6.07\frac{b_0''^2\pi}{\tau_c^2}B^2+42\frac{b_0''^4\pi^2}{\tau_c^4}B^4\right) \tag{8.18}$$

This power penalty is shown in Figure 8.4 in terms of the signal bit rate. Note that this is only valid for $2\pi B\sigma_t \leq 1$.

8.4.2 The second possibility

In this case no equalization is performed at the receiver to compensate for the fiber transfer function. The output signal pulse will be distorted due to the dispersion, with waveform given by

$$h_{\mathrm{out}}(t) = \frac{1}{2\pi}\int_{-\infty}^{+\infty} H_{\mathrm{s}}(\omega)H(\omega)H_{\mathrm{r}}(\omega)\ e^{\mathrm{j}\omega t}\ \mathrm{d}\omega \tag{8.19}$$

where $H_{\mathrm{s}}(\omega), H(\omega)$ and $H_{\mathrm{r}}(\omega)$ are defined in (8.11), (8.8) and (8.14), respectively.

Solving this integral we get:

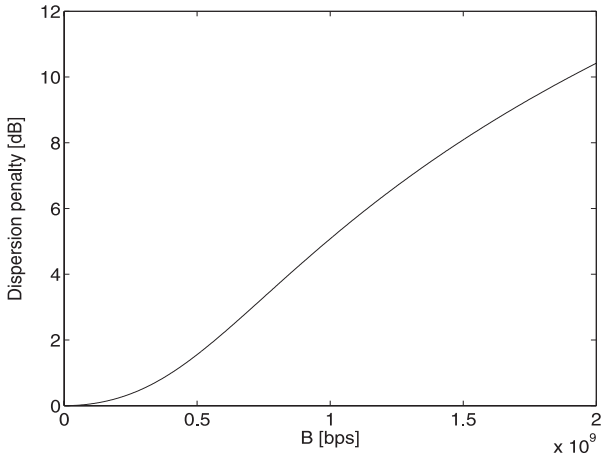

Figure 8.4: Dispersion penalties for an equalized receiver versus bit-rate. The light source is an LED with $\lambda_c = 840$ nm, $\Delta\lambda = 20$ nm, coherence time $\tau_c = 1.563 \cdot 10^{-13}$ s, $b_0'' = 2.807 \cdot 10^{-23}$ s^2/m, $P = 1$ mW, $A = 0.1689$ ($\alpha = 2.5$ dB/km). The length of the fiber is $l = 1$ km. For these parameters the condition $2\pi B\sigma_t \leq 1$ is met.

$$
\begin{aligned}
h_{\text{out}}(t) = \frac{cPA^2}{B}\frac{1}{\sqrt{2\pi}\sigma}\sum_{i=1}^{18} e^{-\frac{(t-\tau_i)^2}{2\sigma^2}} \\
\cdot \Big\{ \operatorname{erf}(\sqrt{2}\pi\sigma B + \mathrm{j}\frac{t-\tau_i}{\sqrt{2}\sigma}) + \operatorname{erf}(\sqrt{2}\pi\sigma B - \mathrm{j}\frac{t-\tau_i}{\sqrt{2}\sigma}) \\
+ e^{-\frac{4B^2(t-\tau_i)+1}{8B\sigma^2}} \cdot \Big[\operatorname{erf}(\sqrt{2}\pi\sigma B + \mathrm{j}\frac{t-\tau_i+\frac{1}{2B}}{\sqrt{2}\sigma}) + \operatorname{erf}(\sqrt{2}\pi\sigma B - \mathrm{j}\frac{t-\tau_i+\frac{1}{2B}}{\sqrt{2}\sigma}) \\
+ \operatorname{erf}(\sqrt{2}\pi\sigma B + \mathrm{j}\frac{t-\tau_i-\frac{1}{2B}}{\sqrt{2}\sigma}) + \operatorname{erf}(\sqrt{2}\pi\sigma B - \mathrm{j}\frac{t-\tau_i-\frac{1}{2B}}{\sqrt{2}\sigma}) \Big] \Big\} \quad (8.20)
\end{aligned}
$$

To ascertain the effect of intersymbol interference (ISI) on system performance, let us consider an input signal consisting of an arbitrarily sequence of $(2K+1)$ bits

$$b_{-K}b_{-K+1}\cdots b_{-1}b_0b_1\cdots b_{K-1}b_K \quad (8.21)$$

with bit b_0 occuring at time $t = 0$, bit b_K at time $t = K/B$, where B is the transmission rate. There are 2^{2K+1} possible sequences, each equally probable

for a random signal. Neglecting noise, the output at time t for a sequence labeled M is a superposition of the input pulses from each of the $2K+1$ input bits

$$h_M(t) = \sum_{n=-K}^{K} b_n^M h_{\text{out}}\left(t + \frac{n}{B}\right) \tag{8.22}$$

An eye pattern may be constructed from the superposition of the 2^{2K+1} possible output waveforms $h_M(t)$.

The performance of data transmission system can be determined by examining the eye diagram [77]. The maximum opening of the eye pattern shows clearly the minimum margin that the system has against noise at its best sampling point. We will normalize the eye opening such that the eye opening that is equal to unity is perfect and an eye opening of zero indicates that the eye is closed. We assume detection of bit b_0.

The peak eye closure is defined as the maximal amount that intersymbol interference can perturb a given signal level

$$D = \frac{1}{h_{\text{out}}(t_0)} \sum_{\substack{n=-K \\ n\neq 0}}^{K} |h_{\text{out}}(t_0 + \frac{n}{B})| \tag{8.23}$$

The eye opening is now [77]:

$$E_O = 1 - D = 1 - \frac{1}{h_{\text{out}}(t_0)} \sum_{\substack{n=-K \\ n\neq 0}}^{K} |h_{\text{out}}(t_0 + \frac{n}{B})| \tag{8.24}$$

It will be most convenient to compute the eye opening as unity minus the peak eye closure for binary PAM signals. The received sample $h_M(t_0)$, where t_0 is the optimal sampling point, in the absence of noise is given by

$$h_M(t_0) = b_0 h_{\text{out}}(t_0) + \sum_{\substack{n=-K \\ n\neq 0}}^{K} b_n h_{\text{out}}(t_0 + \frac{n}{B}) \tag{8.25}$$

The maximal value of the summation in equation (8.25), indicating the inter-

symbol interference, occurs when that data sequence $\{b_n\}$ is transmitted which utilizes for each symbol b_n the maximum signal level of the same algebraic sign as $h_{\text{out}}(t_0 + n/B)$.

By noting that [74]

$$\lim_{K\to\infty} \sum_{n=-K}^{K} e^{\mathrm{j}\omega n/B} = B\delta(\omega), \qquad |\omega| < B/2\pi \tag{8.26}$$

after lengthy but straightforward calculation it can be shown that

$$\sum_{n=-K}^{K} h_{\text{out}}\left(t = t_0 + \frac{n}{B}\right) = 1 \tag{8.27}$$

This expression can be written in a different form as

$$\sum_{\substack{n=-K \\ n\neq 0}}^{K} h_{\text{out}}\left(t = t_0 + \frac{n}{B}\right) = 1 - h_{\text{out}}(t = t_0) \tag{8.28}$$

for arbitrarily long sequences.

Eye opening now reads

$$E_O = 1 - D = 1 - \frac{1 - h_{\text{out}}(t_0)}{h_{\text{out}}(t_0)} = \frac{2h_{\text{out}}(t_0) - 1}{h_{\text{out}}(t_0)} \tag{8.29}$$

For a receiver for which signal-dependent shot noise has a negligible contribution to the total noise the dispersion penalty, in decibels, may be calculated by simply considering the additional optical signal power required to achieve the same worst-case detection level as of the full open eye (E_O=1)

$$P_{\text{d}} = 10\log\left(\frac{1}{E_O}\right) = -10\log(E_O) \tag{8.30}$$

We observe that for a receiver, which has not be equalized, the derived power penalty requires no assumption about he noise spectral density of the receiver. We have assumed, however, that the entire contribution to the bit-error rate

comes from the worst case isolated "1" and isolated "0". Actually we should consider the contribution of all possible bit sequences to the total BER. This has been done by producing the eye diagram from all the sequences $h_M(t)$ for different bit rates. However, the bit sequences which define the eye closure are in fact the dominant contributors to the BER.

In order to calculate P_{d} we first have to determine the Equation (8.20) for $t = t_0$. To determine the optimum decision point t_0 we had to make the eye diagram of the signal $h_{\mathrm{out}}(t)$ for different bit rates. Changing the bit rates from 0 to 2 GHz we have determined the optimum decision point to be $t_0 = 1.5 \cdot 10^{-10}$ s. It is obvious from (8.30) that $0 < E_O < 1$.

The values of P_{d} versus bit-rate, for a fiber length of 1 km, are presented in Figure 8.5.

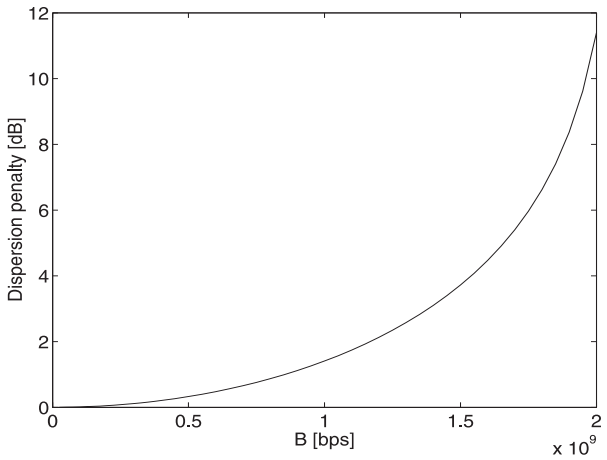

Figure 8.5: Dispersion penalty versus bit-rate. The light source is an LED with $\lambda_{\mathrm{c}} = 840$ nm, $\Delta\lambda = 20$ nm, coherence time $\tau_{\mathrm{c}} = 1.563 \cdot 10^{-13}$ s, $b_0'' = 2.807 \cdot 10^{-23}$ s^2/m, $P = 1$ mW, $A = 0.1689$ ($\alpha = 2.5$ dB/km). The length of the fiber is $l = 1$ km.

Comparing dispersion penalties presented in Figures 8.4 and 8.5, obtained from two different cases, we can conclude that smaller BER can be achieved in the system where no equalization is performed for fiber dispersion, for the same bit-rates of the transmitted signal as in the case of equalization. Practical implication of this result is that this will facilitate receiver realization, since dispersion compensation in the receiver requires more complicated design. For the bit-rates larger than 2 Gbps smaller BER can be achieved in the system with equalization for fiber dispersion.

8.5 Conclusions

In this chapter dispersion analysis in the optical system based on broadband light sources and multimode fibers and components, is presented. Obtained results show that distances between two users can be up to 1 km, if the bit-rate of the transmitted signal does not exceed 1 Gbps. For larger bit-rates, shorter fiber lengths must be used.

The power penalty analysis for two different cases, when the compensation circuitry in the receiver is implemented and when is not, shows that better performance can be obtained in the latter system, which will also lead to a simpler realization of the receiver and possibly lower implementation cost.

CHAPTER 9

Conclusions and directions for further research

9.1 Conclusions

The future of high-speed computer networks will be optical. The number of advantages of the optical fiber medium with respect to UTP is so large that even the most "hard-liners" committed to copper-based medium, admit that combination of copper and fiber will interconnect our PCs in the near future, leaving the room for the wireless as the coming technology. Wireless connections are nowadays specific for mobile applications and have always limited use. The "only" barrage, yet a huge one, is the cost that is associated with optical fiber LAN implementations. The obvious willingness for having computers interconnected by means of fibers and lack of veritable ideas how to make that real, are the two facts that became foundation for the work presented in this thesis. Innovation as the ultimate goal within the affordable cost framework was the keynote of the presented work.

Having in mind the already existing solutions for computer networks we have suggested both technology and architectures for the future optical networks with strong commitment to push the optical fiber even closer to the everyday user,

bridging the gap that separates him now from the "highway of information".

Our basic idea was to combine opto-electronic and optical components, fibers and network architectures to come to the design that will brake the price barrier for having optical LAN interconnecting PCs. Although cost analysis has not been elaborated, we strongly believe that presented solutions in combination with mass production can set the path for installing the future optical computer network, or at least will be incentives for the new solutions to come. Moreover, bringing the flavor of how the proposed solutions for accommodating the Fast Ethernet protocol can easily be adapted for their natural upgrades the Gigabit Ethernet and 10 Gigabit Ethernet, sets a solid basis for making the proposed technology mature.

We expect that the new Fast Ethernet networks presented will first find their application in the environments like power plants, airport buildings and military facilities, where strong electromagnetic radiation seriously affects data transmission resulting in decrease of network throughput. Further consumers could be the big movie companies with requirements of exchanging huge movie materials via computer network or accessing large video databases. The reasons are mainly economical. The users in these companies are willing to have fast and reliable computer networks and are able to afford more money for their installations. Finally, by getting the technology mature and thus lower instalation costs, we can expect penetration of the proposed networks in small business offices and homes.

In Chapter 4 we have presented fiber-optic LAN architectures for FTTD application suited for lowering the cost of bringing optical fiber all the way to the user. To achieve this we have based our designs primarily on the most widely used Ethernet protocol. Moreover, we have used multimode fibers together with multimode polymer-based integrated star couplers and coarse WDM (de)multiplexers and short wavelength lasers and detectors. Using short wavelengths offers the possibility for integrating Si photodiodes with the receiver front-end using straightforward CMOS technology, something that will decrease overall implementation cost of the networks. Further decrease in costs is achieved through the low downtime of the network, low maintenance cost and the possibility for future upgrade since optical fibers offer large bandwidth.

The architectures presented can possibly accommodate the Gigabit Ethernet protocol. To achieve this only NICs at the user's site and NICs in the router have to be replaced. It would appear that solutions for synchronization of burst traffic and collision detection can be scaled to the Gigabit Ethernet signaling

rate of 1.25 Gbps facilitating a new Gigabit Ethernet NIC realization.

Depending on demands the user can choose among the architectures presented. The passive optically transparent architectures are cheaper to implement and they are specially suitable for applications where no extra power can be supplied outside of the router cabinet and where maintenance costs are high. The architectures that comprise active elements should be used in situations where Ethernet switches have already been installed.

The difference between our architectures and already existing Fast Ethernet ones is that we use point-to-multipoint connection. Another difference is that our new Fast Ethernet proposals are using burst traffic transmission with the necessity for the end stations to synchronize on each incoming packet. For this a preamble of the Ethernet packet specified by the IEEE 802.3 standard is used, in contrast to all the other Fast Ethernet standards that do not require a preamble for synchronization due to their constant signaling transmission.

Comparing our proposals with the other Fast Ethernet network proposals many advantages can be marked off. The variety of optical fiber advantages compared to the twisted pair wires that distinguish all the fiber-based network standards from the massively deployed twisted-pair ones holds for our proposals. What makes them prominent with respect to existing fiber standards is the lower overall cost, increased span, slightly improved performance and possibility for easy upgrade.

The 100BASE-FX standard is based on long-wavelength optical light sources that are much more expensive than the short-wavelength light sources used in our networks, which will eventually lead to decrease in network implementation cost. Nevertheless, the distances that can be bridged with the long wavelength light sources in combination with single-mode fibers are much larger. The cost advantage of using short wavelength is used in the latest Fast Ethernet optical fiber standard, 100BASE-SX, but to make our proposals even more attractive for practical implementation we cut the costs even further. By keeping the network passive we decrease the maintenence cost and upgrade cost which are high over the longer time span. Another advantage is that our networks can have more than 100 m larger span, with extra cabling savings by introducing coarse WDM.

Two stumbling blocks, namely synchronization of bursty traffic and collision detection had to be resolved such that the presented networks can accommodate the Fast Ethernet protocol. Solutions for the problems are given in Chapters 5 and 6. Synchronization of bursty traffic is solved by introducing a sinusoidal

synchronization carrier that is sent through the fiber together with the data packet and switched on and off with it. The solution for collision detection is found in using the Directional Coupling method in combination with Average Power Sensing due to simplicity of their implementation. Proposed synchronization technique is not the most optimal one with respect to power consumption, dynamic range and temperature variations but still helped us to prove the functionality of proposed networks and moreover can scale well with the data rate.

To facilitate the network interface card realization a new physical layer device has been realized that can be attached to already existing NICs with an MII interface. To design a PLD a transmitter and receiver had to be designed, which in turn consist of digital and analog circuitry, as described in details in Chapters 5 and 6. Both transmitter and receiver realizations proved the functionality of the design.

The last two chapters cover a subject different from the rest of the thesis. Chapter 7 describes the optical code division multiple access technique in the system based on cascades of Mach-Zehnder interferometers and possibility of its implementation in the future optical LANs and access networks. Chapter 8 includes dispersion analysis in the optical communication system based on broadband sources and multimode fibers.

In the OCDMA system presented in Chapter 7 each orthogonal code can be assigned to a connection between two users, so the maximal number of duplex connections between the two users equals maximal number of orthogonal codes. The duplex tranmission is enabled by placing the modulator in front of the encoder, so the complete structure is symmetrical, i.e. the same physical device can be used for transmitting and receiving signals. Modulation in the electrical domain makes the system economically more attractive and facilitates its realization. The disadvantage is that bit-rates of modulating signals that directly modulate the LED can go up to several hundreds of megabits-per-second only. The greatest advantage of the architecture is that all the users use the same addressable physical device, both for transmission and reception of signals. The addresses of the users are changed by means of changing the phase shifts, thus indirectly changing the spectral intensity code of the signal that is transmitted through the passive optical star network.

Based on recursive expressions for the spectral fingerprints of the codes one can easily determine the number and all possible sets of orthogonal codes and based on SNR analysis determine which one gives the best performance. We calculated that the SNR is inversely proportional to three times the squared

number of active users. It is important to emphasize that the obtained results are only valid if the bit time is much larger than the delays in the MZ interferometers, which is the case in most practical realizations.

We have shown that OCDMA system based on multimode fibers and components has much better performance with respect to OBN compared with its single-mode counterpart, but the distances that can be bridged between the end users are much shorter.

At the end of the Chapter 7 a coder/decoder design is given, also based on cascades of MZIs, which is basically a generalized coherence multiplexing (CM) system with a possibility to change the address of users by changing the phase shifts in particular stages of cascaded system. It gives strong contribution to CM practical implementation.

The power penalty analysis, given in Chapter 8 for two different cases, when the equalization circuitry in the receiver is implemented and when is not, show that better performance can be obtained in the latter system for the bit-rates up to 2 Gbps, which will also lead to a simpler realization of the receiver and possibly lower implementation cost. To achieve smaller BER at higher bit-rates, equalization circuit in the receiver that compensates for fiber dispersion have to be used.

9.2 Directions for further research

Integration of the transceiver analog circuitry on a single chip is certainly a very important issue in translating the proposed designs into commercially available products. The FPGA should be replaced by a single ASIC. To improve the design other synchronization techniques for bursty traffic synchronization in PONs have to be studied in order to find the most optimal solution with respect to optical power budget, dynamic range of the receiver and simplicity of design.

To make the proposed networks widely accepted, a field trial should be made to test the system in practice and the complete proposal has to be submitted to the standardization body. A field trial can help making a thorough analysis of both performance and cost. To make the technology mature further research must be done to allow easy upgrade of the networks, such that they can accommodate both Gigabit and 10 Gigabit Ethernet.

Since the 10 Gigabit Ethernet protocol has mainly been made for application in the wide area networks (WANs), careful analysis must be made to implement

it in the LAN environment all the way to the end stations and terminals where implementation cost is an important issue.

Further research can be made in providing compatibility among all the presented networks accommodating Ethernet protocols up to the 10 Gigabit Ethernet one as this enables gradual system upgrade with minimum investments and promises high utilization.

Another important issue to explore is the application of the proposed LAN/access network architectures in both Fiber-to-the-Home (FTTH) and Fiber-to-the-Desk (FTTD) applications.

List of Acronyms

ANSI	American National Standard Institute
APC	Automatic Power Control
ASIC	Application Specific Integrated Circuit
ATM	Asynchronous Transfer Mode
AUI	Attachment Unit Interface
BER	Bit Error Rate
CATV	Cable Television
CD	Collision Detection
CDMA	Code Division Multiple Access
CSMA	Carrier Sense Multiple Access
CM	Coherence Multiplexing
CRC	Cyclic Redundancy Check
CRS	Carrier Sense
CW	Continuous Wavelength
ECT	Embedded Clock Transport
E/O	Electro Optical
EPON	Ethernet Passive Optical Network
ESD	End of Stream Delimiter
F-P	Fabry-Perot
FCS	Frame Check Sequence
FDDI	Fiber Distribution Data Interface

FDMA	Frequency Division Multiple Access
FPGA	Field Programmable Gate Array
FTP	File Transfer Protocol
FTTD	Fiber to the Desk
FTTH	Fiber to the Home
GMII	Gigabit Medium Independent Interface
HTTP	Hyper Text Transfer Protocol
ICMP	Internet Control Message Protocol
IEEE	Institute of Electrical and Electronic Engineers
IFG	Inter Frame Gap
IP	Internet Protocol
ISI	Inter Symbol Interference
ISO	International Organization for Standardization
JFET	Junction Field Effect Transistor
LAN	Local Area Network
LD	Laser Diode
LED	Light Emitting Diode
LLC	Logical Link Control
LVDS	Low Voltage Differential Signal
LVTTL	Low Voltage Transistor-Transistor Logic
MAC	Medium Access Protocol
MAN	Metropolitan Area Network
MAU	Media Attachment Unit
MDI	Medium Dependent Interface
MII	Media Independent Interface
MLT	MultiLevel Threshold
MZI	Mach-Zehnder Interferometer
NRZI	Non-Return-to-Zero, Invert-on-ones
OBN	Optical Beat Noise
OCDMA	Optical Code Division Multiple Access
O/E	Opto Electrical
OLT	Optical Line Terminal
ONT	Optical Network Terminal
OSI	Open System Interconnect
OOK	On Off Keying
PC	Personal Computer
PCB	Printed Circuit Board

PCS	Physical Encoding Sublayer
PECL	Positive Emitter Coupled Logic
PLD	Physical Layer Device; Path Length Difference
PLL	Phase Locked Loop
PMA	Physical Medium Attachment sublayer
PMD	Physical Medium Dependant
PON	Passive Optical Network
PSTN	Public Switched Telephony Network
QoS	Quality of Service
SC	Subscriber Connector
SFD	Start of Frame Delimiter
SDH	Synchronous Digital Hierarchy
SDU	Service Data Unit
SNR	Signal to Noise Ratio
SMTP	Simple Mail Transfer Protocol
SONET	Synchronous Optical Network
SSD	Start of Stream Delimiter
ST	Straight Tip
STA	Station Management
TCP	Transmission Control Protocol
TTL	Transistor-Transistor Logic
TDMA	Time Division Multiple Access
UDP	User Datagram Protocol
UTP	Unshielded Twisted Pair
VHDL	Very High Speed Integrated Circuit Hardware Description Language
VCSEL	Vertical Cavity Surface Emitting Laser
WAN	Wide Area Network
WDM	Wavelength Division Multiplexing

Bibliography

[1] A. Savvas, "Fiber Networks: coming to a premises near you," *Lightwave Europe*, pp. 27–28, Oct. 2002.

[2] M. Norris, *Gigabit Ethernet, Technology and Application*, Artech House, 2003.

[3] B. E. A. Saleh, M. C. Teich, *Fundamentals of Photonics*. Wiley, 1991.

[4] W. van Etten, J. van der Plaats, *Fundamentals of Optical Fiber Communications*, Prentice Hall, 1991.

[5] J. Genoe, D. Coppée, J. H. Stiens, R. A. Vounckx, M. Kuijk, "Calculation of the current response of the spatially modulated light CMOS detector," *IEEE Transactions on Electron. Devices*, Vol. 48, pp. 1892–1902, Sep. 2001.

[6] S. Radovanović, A. J. Annema, B. Nauta, "Monolithically Integrated Photo-Diodes in Standard CMOS Technology for High Speed Optical Communication: General Consideration and Analysis," in *Program for Research on Integrated Systems and Circuits 2002*, Veldhoven, Netherlands, Nov. 2002.

[7] S. Musa, A. Borreman, G. Pandraud, P. Knijn, G. Sengo, M. B. J. Diemeer, A. Driessen, "Multimode fiber matched arrayed

waveguides grating-based (de-)multiplexer for short distance communications," in *European Conference on Optical Communication*, Copenhagen, Denmark, PLC 6.2.1, Sep. 2002.

[8] S. Musa, N. S. Lagali, B. Docter, G. Sengo, G. J. M. Krijnen, A. Driessen, "Design and fabrication of low-cost, ultra-compact polymer based multimode 4 x 4 star couplers," in *10th European Conference on Integrated Optics (ECIO)*, Paderborn, Germany, pp. 248–251, Sep. 2001.

[9] P. W. Shumate, "Passive Optical Networks and FTTX," in *Short course notes, European Conference on Optical Communication*, Copenhagen, Denmark, SC-2, Sep. 2002.

[10] C. E. Spurgeon, *Ethernet, The Definitive Guide*, O'Reilly and Associates, Inc., 2000.

[11] L. B. Quinn, R. G. Russsell, *Fast Ethernet*, Wiley, 1997.

[12] G. Held, *Ethernet Networks*, Wiley, 1998.

[13] L. Kazovsky, S. Benedetto, A. Willner, *Optical Fiber Communication Systems*, Artech House, 1996.

[14] B. O'Hara, A. Petrick, *The IEEE 802.11 Handbook: A Designer's Companion*, Standards Information Network IEEE Press, 1999.

[15] G. Held, *Data Communications Networking Devices*, fourth edition, Wiley, 1999.

[16] J. Hecht, *Understanding Fiber Optics*, third edition, Prentice Hall, 1999.

[17] D. Hanson, "Local-area networks," *FiberSystems*, pp. 26–28, Nov. 1998.

[18] M. Molle, G. Watson, "100Base-T/IEEE802.12/Packet Switching," *IEEE Commun. Mag.*, pp. 64–73, Aug. 1996.

[19] W. Stallings, *Data & Computer Communications*, sixth edition, Prentice Hall, 2000.

[20] A. S. Tanenbaum, *Computer Networks*, third edition, Prentice Hall, 1996.

[21] J. W. Reedy, J. R. Jones, "Methods of Collision Detection in Fiber Optic CSMA/CD Networks," *IEEE Journal on Selected Areas in Communications*, Vol. Sac3, pp. 890–896, Nov. 1985.

[22] "Measured attenuation of the 4 pair twisted-pair cable," [Online]. Available: http://www.computernessos.it/cabling/belden3.htm

[23] "Optical Fiber Cabling Components Standard (ANSI/TIA-455-78B-2002)," [Online]. Available: http://www.tiaonline.org/ standards/

[24] IEEE Std 802.3, *Carrier Sense Multiple Access with Collision Detection (CSMA/CD) access method and physical layer specification.* Institute of Electrical and Electronic Engineering Press, 1998.

[25] F. Halsall, *Data Communications, Computer Networks and Open Systems*, Prentice Hall, 1996.

[26] K. Oshima, T. Kitayama, M. Yamaki, T. Matsui, K. Ito, "Fiber-Optic Local Area Passive Network Using Burst TDMA scheme," *J. Lightwave Technol.*, Vol. LT-3, pp. 502–509, June 1985.

[27] T. Tamura, M. Nakamura, S. Ohshima, T. Ito, T. Ozeki, "Optical Cascade Star Network-A New Configuration for a Passive Distribution System with Optical Collision Detection Capability," *J. Lightwave Technol*, Vol. LT-2, pp. 61–66, Feb. 1984.

[28] M. Kavehrad, C. E. W. Sundberg, "A Passive Star-Configured Optical Local Area Network Using Carrier Sense Multiple Access with Novel Collision Detection," *J. Lightwave Technol.*, Vol. LT-5, pp. 1549–1563, Nov. 1987.

[29] C. J. Chae, E. Wong, R. S. Tucker, "Optical CSMA/CD Media Access Scheme for Ethernet Over Passive Optical Network," *IEEE Photon. Technol. Lett.*, Vol. 14, pp. 711–713, May 2002.

[30] S. Y. Suh, S. W. Granlund, S. S. Hegde, "Fiber-Optic Local Area Network Topology," *IEEE Commun. Mag.*, pp. 26–32, Aug. 1986.

[31] L. Peterson, B. S. Davie, *Computer Networks, a System approach*, Morgan Kaufmann, 1996.

[32] R. M. Metcalfe, D. R. Boggs, "Ethernet: Distributed Packet Switching for Local Computer Networks," *Communications of the ACM*, Vol. 19, July 1976.

[33] Optical Fiber Cabling Components Standard (ANSI/TIA/EIA-568-B.3-2000). [Online]. Available: http://www.tiaonline.org/ standards/

[34] White paper, "10/100BASE-SX: Lowering the Cost of Fiber Migration," *Transition Networks*, [Online]. Available: http://www.transition.com

[35] I. Radovanović, W. van Etten, "New Ethernet Based Optically Transparent Network for Fiber-to-the-Desk Application," in *Proceedings of 5th IEEE International Conference on Transparent Optical Networks (ICTON 2003)*, Warsaw, Poland, Vol. 2, pp. 189–192, June 2003.

[36] I. Radovanović, W. van Etten, "Ethernet Based Passive Optical Local Area Networks for Fiber-to-the-Desk Application," *J. Lightwave Techn.*, Special issue on optical networks, Nov. 2003.

[37] G. Kramer, G. Pesavento, "Ethernet Passive Optical Network (EPON): Building a Next-Generation Optical Access Network," *IEEE Communications Magazine*, Vol. 40, pp. 66–73, Feb. 2002.

[38] G. Kramer, B. Mukherjee, G. Pesavento, "IPACT: A Dynamic Protocol for an Ethernet PON (EPON)," *IEEE Communications Magazine*, Vol. 40, pp. 74–80, Feb. 2002.

[39] I. Radovanović, W. van Etten, W. Beuwer, "New passive optical network architectures for fiber-to-the-desk application," in *Proc. IEEE/LEOS Symposium (Benelux Chapter)*, Delft, The Netherlands, pp. 259–262, Oct. 2000.

[40] I. Radovanović, W. van Etten, R. O. Taniman, R. Kleinkiskamp, "Novel Ethernet Based Optical Local Area Networks for Computer Interconnection," in *Proc. IEEE Conference on Local Computer Networks 2003, (LCN 2003)*, Bonn/Königswinter, Germany, Oct. 2003.

[41] I. Radovanović, G. Heideman, H. Siasi, A. Meijerink, W. van Etten, "Addressable Spectrally Encoded Optical CDMA System for Application in Access and Local Area Networks," in *Proc. URSI XXVII General Assembly*, Maastricht, The Netherlands, pp. 1047–1051, Aug. 2002.

[42] T. Hermes, "New Reflective Type Star Coupler for Full Duplex Channels," *Electron. Lett.*, Vol. 27, pp. 2136–2138, Nov. 1991.

[43] T. Ota, "Four-port Multimode Interconnectable Star Coupler," *Electron. Lett.*, Vol. 29, pp. 919–920, May 1993.

[44] T. Ota, M. Arii, Y. Kawabata, "Eight-port Multimode Interconnectable Star Coupler Adopting Intersected Optical Waveguide Circuits," *Electron. Lett.*, Vol. 32, pp. 320–321, Feb. 1996.

[45] A. Borreman, A. A. M. Kok, M. B. J. Diemeer, A. Driessen, "Low-cost polymeric multimode optical devices," in *Proceedings of IEEE/LEOS Benelux Chapter Workshop on Low-Cost Photonics*, Mons, Belgium, June 2003.

[46] B. Tian, *All-Optical Fast Packet Switch Based on Self Electro-optic Effect Devices*, Ph.D. thesis, Twente University Press, 2002.

[47] D. J. G. Mestdagh, *Fundamentals of Multiaccess Optical Fiber Networks*, Artech House, 1995.

[48] T. Pfeiffer, "OCDM(A) Networks- Will They Become Competitive?," in *Proceedings of the European Conference on Optical Communication, ECOC 2002*, Copenhagen, Denmark, ANT 11.5.1, Sep. 2003.

[49] P. Prucnal, M. Santoro, T. Fan, "Spread spectrum fiber optic local area network using optical processing," *J. Lightwave Techn.*, Vol. 4, pp. 547–554, May 1986.

[50] W. Kwong, P. Prucnal, "Performance comparison of asynchronous and synchronous code-division multiple-access techniques for fiber optic local area networks," *IEEE Trans. Commun.*, Vol. 39, pp. 1625–1632, 1991.

[51] C. Yegnanarayanan, A. S. Bhushan, B. Jalali, "Fast Wavelength-Hopping Time-Spreading Encoding/Decoding for Optical CDMA," *IEEE Photon. Technol. Lett.*, Vol. 12, pp. 573–575, May 2002.

[52] H. Fathallah, P.-Y. Corts, L. A. Rusch, S. LaRochelle, L. Pujol, "Experimental Demonstration of Optical Fast Frequency Hopping-CDMA Communications," in *European Conference on Optical Communication*, Nice, France, TuB2.4, Sep. 1999.

[53] R. M. H. Yim, L. R. Chen, J. Bajcsy, "Design and Performance of 2-D Codes for Wavelength-Time Optical CDMA," *IEEE Photon. Technol. Lett.*, Vol. 14, pp. 714–716, May 2002.

[54] C. F. Lam, *Multi-wavelength Optical Code-Division-Multiple-Access Communication Systems*, Ph.D. thesis, UCLA, 1999.

[55] M. E. Mahric, "Coherent Optical CDMA Networks," *J. Lightwave Technol.*, Vol. 11, pp. 854–863, May/June 1993.

[56] R. A. Griffin, D. A. Sampson, D. A. Jackson, "Optical Phase Coding for Code-Division Multiple Access Networks," *IEEE Photon. Technol. Lett.*, Vol. 4, pp. 1401–1404, Dec. 1992.

[57] R. A. Griffin, D. A. Sampson, D. A. Jackson, "Modification of optical coherence using spectral phase coding for use in photonic code-division multiple access systems," *Electron. Lett.*, Vol. 29, pp. 1469–1470, Dec. 1993.

[58] R. A. Griffin, D. A. Sampson, D. A. Jackson, "Coherence Coding for Photonic Code-Division Multiple Access Networks," *J. Lightwave Technol.*, Vol. 13, pp. 1826–1837, Sep. 1995.

[59] T. Pfeiffer, B. Deppisch, M. Kaiser and R. Heidemann, "High speed optical network for asynchronous multiuser access applying periodic spectral coding of broadband sources," *Electron. Lett.*, Vol. 33, pp. 2141–2142, 1997.

[60] M. Kavehrad, D. Zaccarin, "Optical Code-Division-Multiplexed System Based on Spectral Encoding of Noncoherent Sources," *J. Lightwave Technol.*, Vol. 13, pp. 534–545, Mar. 1995.

[61] L. Nguyen, B. Aazhang, J. F. Young, "All-optical CDMA with bipolar codes," *Electron. Lett.*, Vol. 31, pp. 469–470, Mar. 1995.

[62] I. Andonovic, "Experimental Demonstration of the (De)Coding of Hybrid Phase and Frequency Codes Using a Pseudolocal Oscillator for Optical Code Division Multiplexing," *IEEE Photon. Technol. Lett.*, Vol. 10, pp. 887–889, Sep. 1998.

[63] G. C. Gupta, D. Uttamchadani, "Coherent Optical Code Division Multiple Access System for LANs," *Optical Fiber Technology*, Vol. 2, pp. 191–194, 1996.

[64] N. Karafolas, D. Uttamchandani, "Optical Fiber Code Division Multiple Access Networks: A review," *Optical Fiber Technology*, Vol. 2, pp. 149–168, 1996.

[65] R. H. Wentworth, "Theoretical Noise Performance of Coherence-Multiplexed Interferometric Sensors," *J. Lightwave Technol.*, Vol. 7, pp. 941–956, June 1989.

[66] E. D. J. Smith, P. T. Gough, D. P. Taylor, "Noise Limits of Spectral-Encoding CDMA Systems," *Electron. Lett.*, Vol. 31, pp. 1469–1470, Aug. 1995.

[67] A. Meijerink, "Performance Improvement of a Generalized Coherence Multiplexing System," in *Proceedings of the IEEE Region 8 EUROCON'2001*, Bratislava, Slovakia, pp. XXXII–XXXV, 2001.

[68] G. J. Pendock, D. D. Sampson, "Capacity of Coherence-Multiplexed CDMA Networks," *Optics Communications*, Vol. 143, pp. 109–117, Nov. 1997.

[69] I. Radovanović, L. Bakker, W. van Etten, "Improvement in design of Mach- Zehnder en/decoder for implementing new orthogonal codes in OCDMA systems," in *Proc. of the Symposium on Communications and Vehicular Technology'01*, Delft, The Netherlands, pp. 234–236, Oct. 2001.

[70] J. W. Goodman, *Statistical Optics*, Wiley, 2000.

[71] I. Radovanović, L. Bakker, W. van Etten, "Cascaded Mach-Zehnder encoder for spectrally encoded optical CDMA systems," in *Proc. IEEE/LEOS Symposium (Benelux Chapter)*, Brussels, Belgium, pp. 213–216, Dec. 2001.

[72] I. Radovanović, W. van Etten, "Performance comparison of the cascaded MZI based OCDMA system using multimode and singlemode fibers," in *Proc. IEEE/LEOS Symposium (Benelux chapter)*, Amsterdam, The Netherlands, pp. 238–241, Dec. 2002.

[73] A. F. Elrefaie, R. E. Wagner, D. A. Atlas, D. G. Daut, "Chromatic Dispersion Limitations in Coherent Lightwave Transmission Systems," *J. Lightwave Technol.*, Vol. 6, pp. 704–709, May 1988.

[74] J. L. Gimlett, "Dispersion Penalty Analysis for LED/Single-Mode Fiber Transmission Systems," *J. Lightwave Technol.*, Vol. LT-4, pp. 1381–1392, 1986.

[75] G. P. Agrawal, P. J. Anthony, T. M. Shen, "Dispersion Penalty for 1.3-μm Lightwave Systems with Multimode Semiconductor Laser, " *J. Lightwave Technol.*, Vol. 6, pp. 620–625, May 1988.

[76] I. Radovanović, W. van Etten, "Dispersion Penalties in Optical Access and Local Area Networks based on MM Fibers," in *Proc. of 9th Symposium on Communications and Vehicular Technology in the Benelux, SCVT 2002*, Louvain-la-Neuve, Belgium, pp. 65–72, Oct. 2002.

[77] R. W. Lucky, J. Salz, E. J. Weldon Jr., *Principles of data communication.* McGraw-Hill Book Company, 1968.

[78] L. Bakker, *Analysis of Optical CDMA Techniques for Application in an Optical LAN*, M.Sc. thesis, University of Twente, The Netherlands, 2001.

APPENDIX **A**

Optical fiber power transfer function

In this appendix we derive the impulse response of a single-mode fiber when the factor b_0' is taken into account for calculating the baseband model of the power transfer function of single-mode fiber, $G_1(\omega)$.

The single-mode fiber can be considered as a bandpass system with the field transfer function [4]:

$$G(\omega) = G_1(\omega - \omega_c) + G_1^*(-\omega - \omega_c) \tag{A.1}$$

where $G_1(\omega)$ is the equivalent baseband transfer characteristic.

Using the propagation constant, this field transfer function can be represented as:

$$G(\omega) = e^{-\gamma(\omega)l} = e^{-\alpha(\omega)l - j\beta(\omega)l} \tag{A.2}$$

where $\alpha(\omega)$ and $\beta(\omega)$ are attenuation and specific phase shift, respectively, and l is the fiber length.

In order to solve the bandpass transmission problem we will formulate the equivalent low-pass transmission model, since bandpass to lowpass transformation completely retains the essence of the filtering process. We already have

a baseband model for the broadband source, and we will now try to find a baseband model for the fiber.

Expanding (A.1) into a Taylor series about ω_c and supposing that the attenuation of the fiber is constant in the region of interest, then the equivalent baseband characteristic reads

$$G_1(\omega) \approx Ae^{-\mathrm{j}b_0-\mathrm{j}b_0'\omega-\mathrm{j}\frac{b_0''}{2}\omega^2} \tag{A.3}$$

with

$$b_0 \triangleq \beta(\omega_\mathrm{c})l,\ b_0' \triangleq \beta'(\omega_\mathrm{c})l,\ b_0'' \triangleq \beta''(\omega_\mathrm{c})l,\ A \triangleq e^{-\alpha l} \tag{A.4}$$

In (A.3) we assumed that $\beta^{(m)}(\omega_\mathrm{c}) = 0$ for $m \geq 3$.

Using Equation (A.3) it can be shown that the transfer of the single-mode fiber equals

$$\begin{aligned} H_{\mathrm{c}1}(\omega) &= \frac{1}{2\pi}G_1(\omega) * [G_1^*(-\omega)S_{xx}] = \\ &= \frac{2\sqrt{2}P\tau_\mathrm{c}A^2}{2\pi}\ G_1(\omega) * \left[e^{\mathrm{j}(b_0-b_0'\omega+\frac{\omega^2}{2}b_0'')}e^{-\frac{\omega^2\tau_\mathrm{c}^2}{2\pi}}\right] \\ &= \frac{\sqrt{2}P\tau_\mathrm{c}A^2}{\pi}\ e^{-\mathrm{j}b_0'\omega}e^{-\mathrm{j}b_0''\frac{\omega^2}{2}}\int_{-\infty}^{\infty} e^{-\left[\frac{\Omega^2}{2}\frac{\tau_\mathrm{c}^2}{\pi}-\mathrm{j}\Omega\omega b_0''\right]}\ \mathrm{d}\Omega \\ &= 2PA^2\ e^{-\frac{\pi}{2\tau_\mathrm{c}^2}(\omega b_0'')^2}\ e^{-\mathrm{j}(b_0'\omega+b_0''\frac{\omega^2}{2})} \end{aligned} \tag{A.5}$$

where $*$ denotes convolution.

As a general property of the Fourier transform we have [4]:

$$\Re\{f(t)\} = \frac{1}{2}\mathcal{F}^{-1}\{F(\omega) + F^*(-\omega)\} \tag{A.6}$$

so that the transfer function of the optical fiber communication system under

consideration becomes

$$\begin{aligned} H(\omega) &= \frac{c}{2}(H_{\mathrm{c1}}(\omega) + H_{\mathrm{c2}}(\omega)) = \frac{c}{2}(H_{\mathrm{c1}}(\omega) + H^*_{\mathrm{c1}}(-\omega)) \\ &= cPA^2\ e^{-\frac{\pi}{2\tau_c^2}\omega b_0''^2}\ e^{-\mathrm{j}(b_0'\omega + b_0''\frac{\omega^2}{2})} + cPA^2\ e^{-\frac{\pi}{2\tau_c^2}\omega b_0''^2}\ e^{-\mathrm{j}(b_0'\omega - b_0''\frac{\omega^2}{2})} \\ &= 2cPA^2\ e^{-\frac{\pi}{2\tau_c^2}\omega b_0''^2}\cos\left(\frac{\omega^2}{2}b_0''\right)\ e^{-\mathrm{j}\omega b_0'} \end{aligned} \quad \text{(A.7)}$$

The impulse response of the fiber now becomes:

$$\begin{aligned} h(t) &= \frac{1}{2\pi}\int_{-\infty}^{\infty} H_{\mathrm{c}}(\omega)\ e^{\mathrm{j}\omega t}\,\mathrm{d}\omega \\ &= \frac{cPA^2}{\pi}\int_{-\infty}^{\infty} e^{-\frac{2\pi}{\tau_c^2}\omega b_0''^2}\cos\left(\frac{\omega^2}{2}b_0''\right)\ e^{-\mathrm{j}\omega b_0'}\ e^{\mathrm{j}\omega t}\,\mathrm{d}\omega \\ &= \frac{cPA^2}{2\pi}\int_{-\infty}^{\infty} e^{-\frac{2\pi}{\tau_c^2}\frac{\omega}{2}b_0''^2}\left[e^{\mathrm{j}\frac{\omega^2}{2}b_0''} + e^{-\mathrm{j}\frac{\omega^2}{2}b_0''}\right]\ e^{\mathrm{j}\omega(t-b_0')}\,\mathrm{d}\omega \\ &= h_1(t) + h_2(t) \end{aligned} \quad \text{(A.8)}$$

Solving for $h_1(t)$ and $h_2(t)$ we get

$$\begin{aligned} h_1(t) &= \frac{cPA^2\tau_{\mathrm{c}}}{\sqrt{2\pi b_0''(\pi b_0'' - \mathrm{j}\tau_{\mathrm{c}}^2)}}\ e^{-\frac{\tau_c^2(t-b_0')^2}{2\pi b_0''(\pi b_0'' - \mathrm{j}\tau_c^2)}} \\ h_2(t) &= \frac{cPA^2\tau_{\mathrm{c}}}{\sqrt{2\pi b_0''(\pi b_0'' + \mathrm{j}\tau_{\mathrm{c}}^2)}}\ e^{-\frac{\tau_c^2(t-b_0')^2}{2\pi b_0''(\pi b_0'' + \mathrm{j}\tau_c^2)}} \end{aligned} \quad \text{(A.9)}$$

The total impulse response is now

$$\begin{aligned} h(t) = h_1(t) + h_2(t) = \\ = \frac{cPA^2\tau_{\mathrm{c}}}{\sqrt{2\pi b_0''}\sqrt{(\pi^2 b_0''^2 + \tau_{\mathrm{c}}^2)}}\ e^{-\frac{\pi\tau_c^2(t-b_0')^2}{2(\pi^2 b_0''^2 + \tau_c^4)}}\ \cdot \\ \cdot\left[\sqrt{(\pi b_0'' + \mathrm{j}\tau_{\mathrm{c}}^2)}\ e^{-\mathrm{j}\frac{\tau_c^4(t-b_0')^2}{2b_0''(\pi^2 b_0''^2 + \tau_c^4)}} + \sqrt{(\pi b_0'' - \mathrm{j}\tau_{\mathrm{c}}^2)}\ e^{\mathrm{j}\frac{\tau_c^4(t-b_0')^2}{2b_0''(\pi^2 b_0''^2 + \tau_c^4)}}\right] \end{aligned} \quad \text{(A.10)}$$

Before we proceed we now have to find an analytical expression for the following

$$\sqrt{x - \mathrm{j}y}\ e^{\mathrm{j}z} + \sqrt{x + \mathrm{j}y}\ e^{-\mathrm{j}z} = 2(x^2 + y^2)^{1/4}\cos\left(z - \frac{1}{2}\arctan\frac{y}{x}\right) \quad \text{(A.11)}$$

The final expression for the impulse response is

$$h(t) = \frac{\sqrt{2}cPA^2\tau_c}{\sqrt{\pi b_0''\sqrt{\pi^2 b_0''^2 + \tau_c^4}}}\; e^{-\frac{\pi\tau_c^2(t-b_0')^2}{2(\pi^2 b_0''^2+\tau_c^4)}} \cdot \cos\left(\frac{\tau_c^4(t-b_0')^2}{2b_0''(\pi^2 b_0''^2+\tau_c^4)} - \frac{1}{2}\arctan\frac{\tau_c^2}{\pi b_0''}\right) \quad \text{(A.12)}$$

For $\pi b_0'' \gg \tau_c^2$ we get

$$h(t) = \frac{\sqrt{2}cPA^2\tau_c}{\pi b_0''}\; e^{-\frac{\tau_c^2(t-b_0')^2}{2\pi b_0''^2}} \quad \text{(A.13)}$$

APPENDIX B

OCDMA system as the generalized CM system

In this appendix we will present how OCDMA system based on cascades of N MZIs, shown in Figure B.1 can be represented as the generalized CM system, presented in Figure B.2. Moreover, we will derive the recursive expression for calculating the transfer functions of two filters in the generalized CM system, representing the N-stage OCDMA system, based on the transfer functions of the filters in the generalized CM system obtained from the $N-1$-stage OCDMA system.

We will begin with the analysis of the 1-stage MZ de/encoder, presented in Figure B.3.

Let us denote the complex broadband optical fields at the input and the output of the encoder as $x(t)$ and $y(t)$ respectively, and let us denote the general transfer functions of the filters in two branches of the MZ interferometer as the transfer functions of the phase shift and the delay line

$$H_{a,1}(\omega) \stackrel{\triangle}{=} e^{\mathrm{j}\phi_1} \qquad \text{and} \qquad H_{b,1}(\omega) \stackrel{\triangle}{=} e^{\mathrm{j}\omega T_1} \tag{B.1}$$

and appropriate impulse responses of the filters as $h_{a,1}(t)$ and $h_{a,2}(t)$.

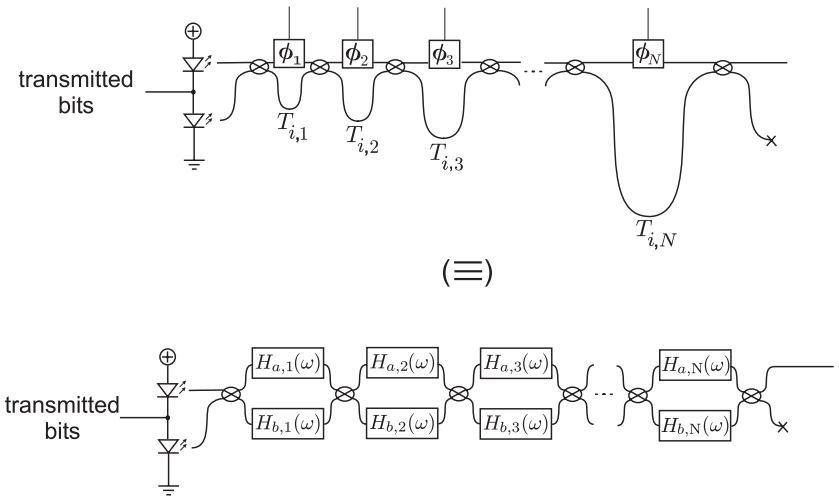

Figure B.1: The encoder of the spectrally encoded OCDMA system based on cascades of MZIs where phase shift and the delay line in each stage of the encoder are represented as the filters.

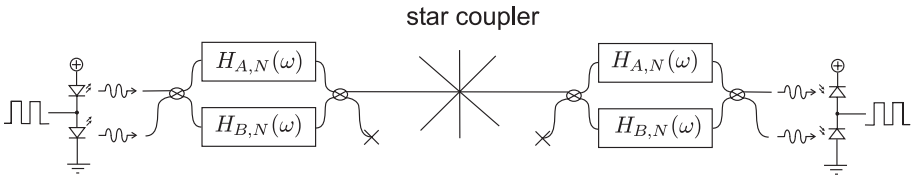

Figure B.2: Generalized coherence multiplexing system.

The optical fields at the upper and the lower outputs of the encoder will be [47]

$$\begin{aligned} y_{1,1}(t) &= \tfrac{1}{2}[h_{a,1}(t) \otimes x(t) - h_{b,1}(t) \otimes x(t)] \\ y_{2,1}(t) &= \tfrac{\mathrm{j}}{2}[h_{a,1}(t) \otimes x(t) + h_{b,1}(t) \otimes x(t)] \end{aligned} \tag{B.2}$$

where operator $\otimes$ denotes the convolution. The first number in the subscript of the output field denotes the output and the second one the number of stages. For the trivial case of the OCDMA system with the 1-stage MZ en/decoder, it can be seen from Figures B.2 and B.3 that the transfer functions in two branches of MZ interferometers in the generalized CM system will be equal to the general transfer functions of the filters in two branches of the OCDMA system 1-stage

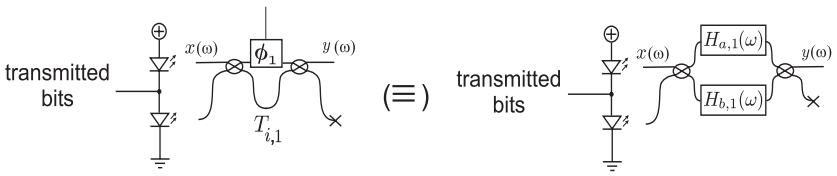

Figure B.3: The 1-stage encoder of the spectrally encoded OCDMA system based on cascades of MZIs where both the phase shift and delay line are represented as filters.

MZ en/decoder, i.e.

$$H_{A,1}(\omega) = H_{a,1}(\omega) \qquad \text{and} \qquad H_{B,1}(\omega) = H_{b,1}(\omega) \tag{B.3}$$

Adding one more stage to the encoder, the optical fields at the output of the encoder reads

$$\begin{aligned} y_{1,2}(t) &= \frac{1}{2\sqrt{2}}[(h_{a,1}(t) - h_{b,1}(t)) \otimes h_{a,2}(t) \otimes x(t) \\ &\quad -(h_{a,1}(t) + h_{b,1}(t)) \otimes h_{b,2}(t) \otimes x(t)] \\ y_{2,2}(t) &= \frac{\mathrm{j}}{2\sqrt{2}}[(h_{a,1}(t) - h_{b,1}(t)) \otimes h_{a,2}(t) \otimes x(t) \\ &\quad -(h_{a,1}(t) + h_{b,1}(t)) \otimes h_{b,2}(t) \otimes x(t)] \end{aligned} \tag{B.4}$$

In the generalized CM system the optical fields at the outputs of the encoder can be calculated as

$$\begin{aligned} y_{1,2}(t) &= \tfrac{1}{2}[h_{A,2}(t) \otimes x(t) - h_{B,2}(t) \otimes x(t)] \\ y_{2,2}(t) &= \tfrac{\mathrm{j}}{2}[h_{A,2}(t) \otimes x(t) + h_{B,2}(t) \otimes x(t)] \end{aligned} \tag{B.5}$$

Here the second number in the subscripts denote that we are deriving the transfer functions of the generalized CM system from the transfer functions in the OCDMA system with the 2-stage MZ en/decoder.

Comparing Equations (B.4) and (B.5) we can write

$$\begin{aligned} h_{A,2}(t) &= \frac{1}{\sqrt{2}}(h_{a,1}(t) - h_{b,1}(t)) \otimes h_{a,2}(t) \\ h_{B,2}(t) &= \frac{1}{\sqrt{2}}(h_{a,1}(t) + h_{b,1}(t)) \otimes h_{b,2}(t) \end{aligned} \tag{B.6}$$

From Equation (B.6) it is obvious that

$$\begin{aligned} H_{A,2}(\omega) &= \frac{1}{\sqrt{2}}(H_{a,1}(\omega) - H_{b,1}(\omega))H_{a,2}(\omega) \\ &= \frac{1}{\sqrt{2}}(H_{A,1}(\omega) - H_{B,1}(\omega))H_{a,2}(\omega) \\ H_{B,2}(\omega) &= \frac{1}{\sqrt{2}}(H_{a,1}(\omega) + H_{b,1}(\omega))H_{b,2}(\omega) \\ &= \frac{1}{\sqrt{2}}(H_{A,1}(\omega) + H_{B,1}(\omega))H_{b,2}(\omega) \end{aligned} \tag{B.7}$$

The last two equations show how to calculate the transfer functions $H_{A,2}$ and $H_{B,2}$ of the generalized CM system placed in the two arms of the MZ interferometer from the transfer functions of the filters in each stage of the cascaded 2-stage OCDMA system.

Adding more stages to the decoder and following the procedure above it can easily be derived that

$$\begin{aligned} H_{A,N}(\omega) &= \frac{1}{\sqrt{2}}[H_{A,N-1}(\omega) - H_{B,N-1}(\omega)]H_{a,N}(\omega) \\ H_{B,N}(\omega) &= \frac{1}{\sqrt{2}}[H_{A,N-1}(\omega) + H_{B,N-1}(\omega)]H_{b,N}(\omega) \end{aligned} \tag{B.8}$$

APPENDIX C

Spectral codes

Spectral fingerprint of the code in a system with the N-stage MZ en/decoder is defined as

$$C^{(N)}(\omega) \triangleq H_{A,N}(\omega)H^*_{B,N}(\omega) \tag{C.1}$$

Invoking Equation (B.8) we obtain

$$C^{(N)} = \frac{1}{2}[|H_{A,N-1}|^2 - |H_{B,N-1}|^2 + (H_{A,N-1}H^*_{B,N-1} - H^*_{A,N-1}H_{B,N-1})]H_{a,N}H^*_{b,N} \tag{C.2}$$

Substituting Equation (B.8) once more into Equation (C.2), and simplifying the expression we get

$$C^{(N)} = \frac{1}{2}[-(H_{A,N-2}H^*_{B,N-2} + H^*_{A,N-2}H_{B,N-2}) + (H_{A,N-1}H^*_{B,N-1} + H^*_{A,N-1}H_{B,N-1})]H_{a,N}H^*_{b,N} \tag{C.3}$$

We omitted here the dependence on ω for the sake of simplicity of representation. This equation can be written in terms of spectral fingerprints of the codes for

the OCDMA systems with $N-1$ and $N-2$ stages as

$$\begin{aligned} C^{(N)}(\omega) = \frac{1}{2}[&-(C^{(N-2)}(\omega) + C^{*(N-2)}(\omega)) \\ &+ (C^{(N-1)}(\omega) - C^{*(N-1)}(\omega))\ e^{-\mathrm{j}(\omega T_N - \phi_N)} \\ &= [-\Re\{C^{(N-2)}(\omega)\} + \mathrm{j}\Im\{C^{(N-1)}(\omega)]\ e^{-\mathrm{j}(\omega T_N - \phi_N)} \end{aligned} \quad \text{(C.4)}$$

Finally we get

$$\begin{aligned} C^{(N)}(\omega) &= \Re\{C^{(N)}(\omega)\} + \mathrm{j}\ \Im\{C^{(N)}(\omega)\} \\ &= -\Re\{C^{(N-2)}(\omega)\}\cos(\omega T_N - \phi_N) + \Im\{C^{(N-1)}(\omega)\}\sin(\omega T_N - \phi_N) \\ &+ \mathrm{j}\ \Re\{C^{(N-2)}(\omega)\}\sin(\omega T_N - \phi_N) + \mathrm{j}\Im\{C^{(N-1)}(\omega)\}\cos(\omega T_N - \phi_N) \end{aligned} \quad \text{(C.5)}$$

where

$$\begin{aligned} \Re\{C^{(N)}(\omega)\} &= -\Re\{C^{(N-2)}(\omega)\}\cos(\omega T_N - \phi_N) \\ &\quad + \Im\{C^{(N-1)}(\omega)\}\sin(\omega T_N - \phi_N) \\ \Im\{C^{(N)}(\omega)\} &= \Re\{C^{(N-1)}(\omega)\}\sin(\omega T_N - \phi_N) \\ &\quad + \Im\{C^{(N-1)}(\omega)\}\cos(\omega T_N - \phi_N) \end{aligned} \quad \text{(C.6)}$$

The real part of the spectral fingerprint of the code is the spectral intensity code, which determines the shape of the power spectral density of the optical signal at the output of the MZ encoder. This can be proven writing the Equation (B.5) for the generalized CM system obtained from the N-stage OCDMA system

$$\begin{aligned} y_{1,N}(t) &= \tfrac{1}{2}[h_{A,N}(t) \otimes x(t) - h_{B,N}(t) \otimes x(t)] \\ y_{2,N}(t) &= \tfrac{\mathrm{j}}{2}[h_{A,N}(t) \otimes x(t) + h_{B,N}(t) \otimes x(t)] \end{aligned} \quad \text{(C.7)}$$

Calculating the autocorrelation function of $y_{1,N}(t)$ and using the Wiener-Khinchin theorem we finally get

$$\begin{aligned} S_{yy}(\omega) &= \frac{1}{4}[(H_{A,N}(\omega) - H_{B,N}(\omega))(H_{A,N}(\omega) - H_{B,N}(\omega))^*]\ S_{xx}(\omega) \\ &= \frac{1}{4}[2 - [H_{A,N}(\omega)H_{B,N}(\omega)^* + H_{A,N}(\omega)^* H_{B,N}(\omega)]\ S_{xx}(\omega) \\ &= \frac{1}{2}[1 - \Re\{C^{(N)}(\omega)\}]\ S_{xx}(\omega) \end{aligned} \quad \text{(C.8)}$$

The spectral intensity code is determined by the phase shift combinations in the phase shifters in the MZ encoder. This phase shift combination consists

of the sequence of zeros and half-pi's and can be denoted as the phase code. Finally, this phase code can be mapped into the sequence of zeros and ones, with 1 representing the phase shift of $\pi/2$. In this way, we obtain the binary code that can eventually be used to control the phase shifters.

Here we present expressions for both real and imaginary part of the spectral fingerprint of the code for up to 5-stage en/decoder. Moreover, we give a graphical representation of the spectral intensity codes, as an example, from one code set. Remind that for an even number of stages this code set is unique. For the OCDMA system with more than one code set, the presented codes are arbitrarily chosen.

Starting conditions for calculating the codes are

$$\begin{aligned} C^{(0)}(\omega) &= 0 \\ \Re\{C^{(1)}(\omega)\} &= \cos(\omega T_1 - \phi_1) \\ \Im\{C^{(1)}(\omega)\} &= -\sin(\omega T_1 - \phi_1) \end{aligned} \tag{C.9}$$

The spectral intensity code for 1-stage MZ en/decoder is presented in Figure C.1 for two different phase shifts, $\phi_1 \in \{0, \pi/2\}$. This combination of phase shifts, $(0, \pi/2)$, represents the phase code set for the 1-stage MZ en/decoder. Since there are only two possible codes, simultaneous transmission from 2 users only can be supported.

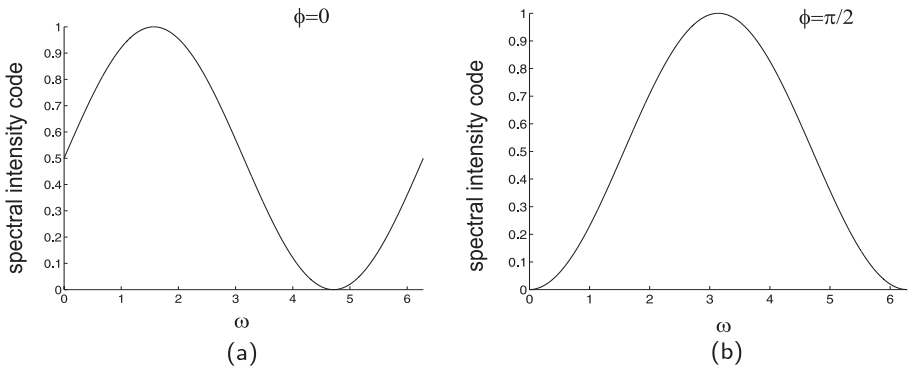

Figure C.1: Spectral intensity codes for the OCDMA system with the 1-stage MZ en/decoder when the phase shift ϕ_1 equals 0 (a), and $\pi/2$ (b).

The spectral intensity code and the imaginary part of the spectral fingerprint of the code for the OCDMA system with the 2-stage en/decoder are given in

Equation (C.10). For this system only one orthogonal set of codes is possible.

$$\begin{aligned} \Re\{C^{(2)}(\omega)\} &= -\sin(\omega T_1 - \phi_1)\sin(\omega T_2 - \phi_2) \\ \Im\{C^{(2)}(\omega)\} &= -\sin(\omega T_1 - \phi_1)\cos(\omega T_2 - \phi_2) \end{aligned} \tag{C.10}$$

The spectral intensity codes for 4 different transmitters (receivers) are illustrated in Figure C.2. For the 3-stage MZ en/decoder the expression for spectral intensity code is given in Equation (C.11) and the graphical representation of one spectral intensity code set, with 4 orthogonal codes is given in Figure C.3.

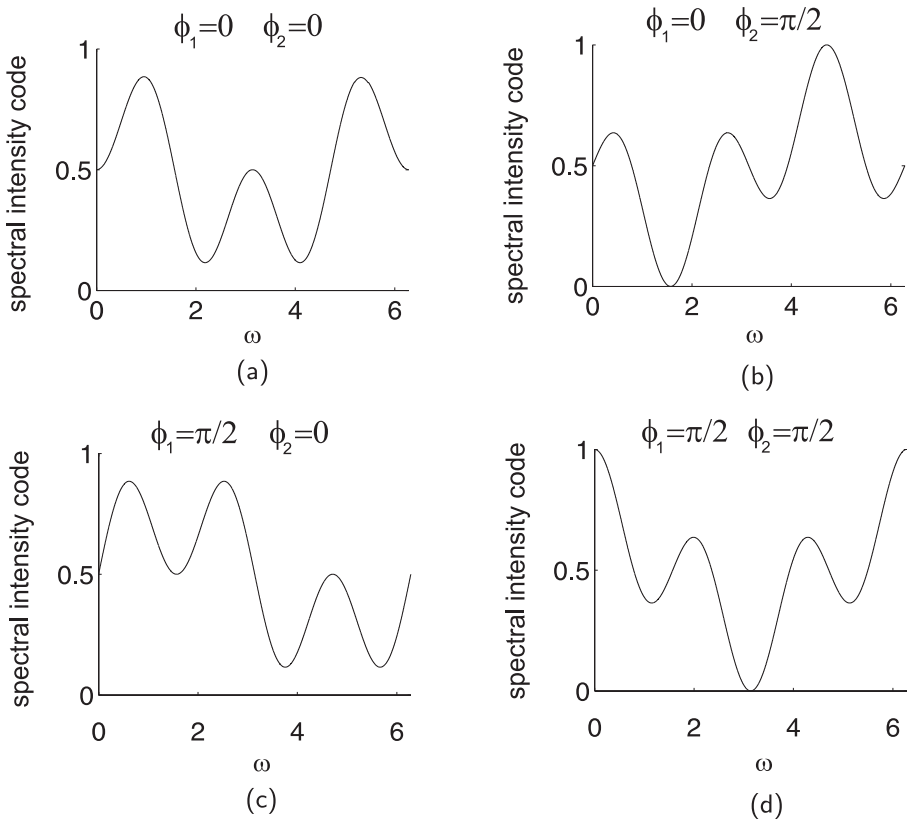

Figure C.2: Spectral intensity codes for the OCDMA system with the 2-stage MZ en/decoder when the phase code equals 0,0 (a), 0,$\pi/2$ (b), $\pi/2$,0 (c) and $\pi/2$,$\pi/2$ (d).

$$\begin{aligned}\Re\{C^{(3)}(\omega)\} &= -\cos(\omega T_1-\phi_1)\cos(\omega T_3-\phi_3)\\ &\quad +\sin(\omega T_1-\phi_1)\cos(\omega T_2-\phi_2)\sin(\omega T_3-\phi_3)\\ \Im\{C^{(3)}(\omega)\} &= \cos(\omega T_1-\phi_1)\sin(\omega T_3-\phi_3)\\ &\quad -\sin(\omega T_1-\phi_1)\cos(\omega T_2-\phi_2)\cos(\omega T_3-\phi_3)\end{aligned} \tag{C.11}$$

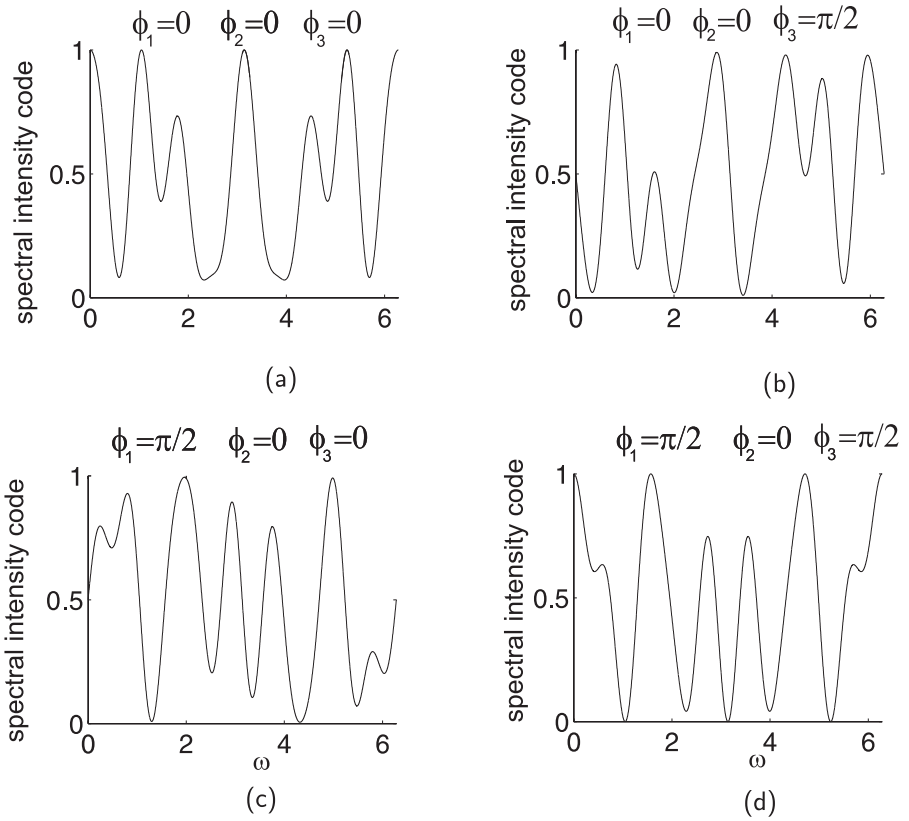

Figure C.3: Spectral intensity codes for the OCDMA system with the 3-stage MZ en/decoder for the one orthogonal code set, when the phase code equals 0,0,0 (a), 0,0,$\pi/2$ (b), $\pi/2$,0,0 (c) and $\pi/2$,0,$\pi/2$ (d).

For 4 and more stages in the encoder, the graphical representation of spectral intensity codes look more complicated. This is the reason we only give the expressions for their calculation. For the OCDMA system with 4-stage MZ

en/decoder this expression reads

$$\begin{aligned}\Re\{C^{(4)}(\omega)\} &= \sin(\omega T_1-\phi_1)\sin(\omega T_2-\phi_2)\cos(\omega T_4-\phi_4)\\ &\quad+\cos(\omega T_1-\phi_1)\sin(\omega T_3-\phi_3)\sin(\omega T_4-\phi_4)\\ &\quad-\sin(\omega T_1-\phi_1)\cos(\omega T_2-\phi_2)\cos(\omega T_3-\phi_3)\sin(\omega T_4-\phi_4)\\ \Im\{C^{(4)}(\omega)\} &= -\sin(\omega T_1-\phi_1)\sin(\omega T_2-\phi_2)\sin(\omega T_4-\phi_4)\\ &\quad+\cos(\omega T_1-\phi_1)\sin(\omega T_3-\phi_3)\cos(\omega T_4-\phi_4)\\ &\quad-\sin(\omega T_1-\phi_1)\cos(\omega T_2-\phi_2)\cos(\omega T_3-\phi_3)\cos(\omega T_4-\phi_4)\end{aligned} \tag{C.12}$$

The spectral intensity code for the OCDMA system with the 5-stage MZ en/decoder is given in Equation (C.13).

$$\begin{aligned}\Re\{C^{(5)}(\omega)\} &= \cos(\omega T_1-\phi_1)\cos(\omega T_3-\phi_3)\cos(\omega T_5-\phi_5)\\ &\quad-\sin(\omega T_1-\phi_1)\cos(\omega T_2-\phi_2)\sin(\omega T_3-\phi_3)\cos(\omega T_5-\phi_5)\\ &\quad-\sin(\omega T_1-\phi_1)\sin(\omega T_2-\phi_2)\sin(\omega T_4-\phi_4)\sin(\omega T_5-\phi_5)\\ &\quad+\cos(\omega T_1-\phi_1)\sin(\omega T_3-\phi_3)\cos(\omega T_4-\phi_4)\sin(\omega T_5-\phi_5)\\ &\quad-\sin(\omega T_1-\phi_1)\cos(\omega T_2-\phi_2)\cos(\omega T_3-\phi_3)\cos(\omega T_4-\phi_4)\\ &\quad\cdot\sin(\omega T_5-\phi_5)\end{aligned} \tag{C.13}$$

The expressions for the spectral intensity codes for the OCDMA systems with more than 5-stage MZ en/decoders are lengthy and will not be presented here. Nevertheless, they can be easily calculated using the Equations (C.6) and (7.18).

C.1 Mean value of the current and code orthogonality

In an ideal case, the mean value of the information-carrying current at the output of the balanced detector in a receiver should contain the signal only from the transmitter that has the same phase code as this particular receiver. In case that two phase codes differ, this current should be equal to zero. The mean value of the information-carrying current equals the difference between the mean values of currents obtained from the two photodiodes, which in turn depend on the optical power impinging on the photodiodes. These powers can be calculated by integrating the psd's of optical signals at two outputs of the

decoder. Taking all these into account, the mean value for the information-carrying current reads:

$$\mathrm{E}[I_{\mathrm{r}}(t)] = \frac{1}{2\pi}\int_0^\infty [(1-\Re\{C_{\mathrm{r},j}^{(N)}(\omega)\}) - (1+\Re\{C_{\mathrm{r},j}^{(N)}(\omega)\})]\ S_{yy}(\omega)\ \ \mathrm{d}\omega \quad \text{(C.14)}$$

where $S_{yy}(\omega)$ is the psd of optical signal at the output of the encoder. Here we have neither taken into account the transmission loss nor the dispersion in the fiber. Invoking Equation (C.8) into Equation (C.14) and simplifying we get

$$\mathrm{E}[I_{\mathrm{r}}(t)] = \frac{1}{2\pi}\int_0^\infty \Re\{C_{\mathrm{r},j}^{(N)}(\omega)\}[1-\Re\{C_{\mathrm{t},i}^{(N)}(\omega)\}]\ S_{xx}(\omega)\ \ \mathrm{d}\omega \quad \text{(C.15)}$$

The value of the integral

$$\int_0^\infty \Re\{C_{\mathrm{r},j}^{(N)}(\omega)\}\ S_{xx}(\omega)\ \ \mathrm{d}\omega \quad \text{(C.16)}$$

is always zero since the spectral intensity code $\Re\{C_{\mathrm{r},j}^{(N)}(\omega)\}$ is periodic.

Finally, the mean value of the information-carrying current reads

$$\mathrm{E}[I_{\mathrm{r}}(t)] = \frac{1}{2\pi}\int_0^\infty \Re\{C_{\mathrm{r},j}^{(N)}(\omega)\}\Re\{C_{\mathrm{t},i}^{(N)}(\omega)\}\ S_{xx}(\omega)\ \ \mathrm{d}\omega \quad \text{(C.17)}$$

This value should be different from zero only for $i = j$, i.e. when the spectral codes of both the transmitter and receiver are the same. The integral represents the inner product of the two spectral intensities codes, which is used in determining the orthogonality of two signals. This is the reason we have used this integral for calculating the orthogonality of the codes (see Equation (7.8)).

.

Index